AD-A148 758 RADIATION/CATALYTIC AUGMENTED COMBUSTION(U) EXXON 1/2
RESEARCH AND ENGINEERING CO LINDEN NJ CORPORATE RESEARC
.. A E CERKANOWICZ ET AL. MAY 84 AFOSR-TR-84-1129
UNCLASSIFIED F49620-81-C-0028 F/G 21/5 NL

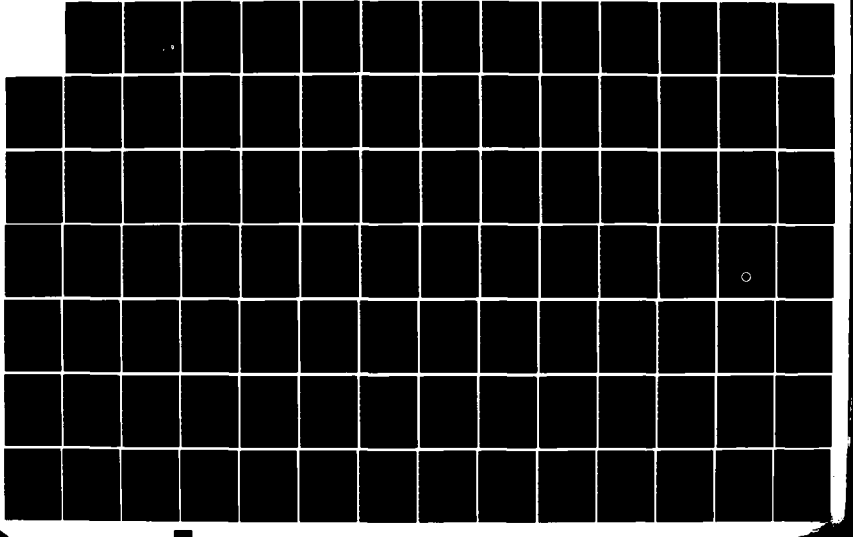

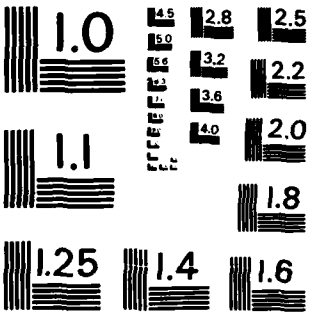

AFOSR-TR- 84-1129

(14)

RADIATION/CATALYTIC AUGMENTED COMBUSTION

A. E. CERKANOWICZ
I. D. CRANE
CORPORATE RESEARCH-TECHNOLOGY FEASIBILITY CENTER
EXXON RESEARCH AND ENGINEERING COMPANY
CLINTON TOWNSHIP, ROUTE 22 EAST, ANNANDALE, NEW JERSEY 08801

MAY 1984

FINAL SCIENTIFIC REPORT
CONTRACT NUMBER F49620-81-C-0028

Approved for public release; distribution unlimited

AIR FORCE OFFICE OF SCIENTIFIC RESEARCH
BLDG. 410
BOLLING AIR FORCE BASE
WASHINGTON, D.C. 20332

THIS REPORT HAS BEEN RELEASED BY

I. S. PASTERNAK
MANAGER
SYSTEMS ADVANCEMENT AND TRANSFER

UNCLASSIFIED
SECURITY CLASSIFICATION OF THIS PAGE (When Data Entered)

REPORT DOCUMENTATION PAGE	READ INSTRUCTIONS BEFORE COMPLETING FORM
1. REPORT NUMBER: AFOSR-TR- 84-1129	2. GOVT ACCESSION NO. / 3. RECIPIENT'S CATALOG NUMBER
4. TITLE (and Subtitle): RADIATION/CATALYTIC AUGMENTED COMBUSTION	5. TYPE OF REPORT & PERIOD COVERED: Final, 1 April 1981 - 31 March 1983 / 6. PERFORMING ORG. REPORT NUMBER
7. AUTHOR(s): A. E. Cerkanowicz, I. D. Crane	8. CONTRACT OR GRANT NUMBER(s): F49620-81-C-0023
9. PERFORMING ORGANIZATION NAME AND ADDRESS: Exxon Research and Engineering Company, Corporate Research-Technology Feasibility Ctr., Rt. 22 East, Clinton Twsp., Annandale, NJ 08801	10. PROGRAM ELEMENT, PROJECT, TASK AREA & WORK UNIT NUMBERS: 2308A2, 61102F
11. CONTROLLING OFFICE NAME AND ADDRESS: Air Force Office of Scientific Research/NA, Building 410, Bolling Air Force Base, D.C. 20332	12. REPORT DATE: May 1984 / 13. NUMBER OF PAGES
14. MONITORING AGENCY NAME & ADDRESS (if different from Controlling Office)	15. SECURITY CLASS. (of this report): Unclassified / 15a. DECLASSIFICATION/DOWNGRADING SCHEDULE

16. DISTRIBUTION STATEMENT (of this Report)

Approved for public release; distribution unlimited

17. DISTRIBUTION STATEMENT (of the abstract entered in Block 20, if different from Report)

18. SUPPLEMENTARY NOTES

19. KEY WORDS (Continue on reverse side if necessary and identify by block number)

Photochemical Ignition	Photodissociation	Flameholder
Enhanced Combustion	Flame Propagation	Stability Limits
Vacuum Ultraviolet Radiation	Spark Ignition	Flame Propagation
Ultraviolet Radiation	Catalytic Combustion	

20. ABSTRACT (Continue on reverse side if necessary and identify by block number)

Two novel concepts for extending aircraft operational range have been researched under this contract. They are radiative and catalytic augmentation techniques. The feasibility of utilizing these techniques to alter (augment) combustion initiation and reaction kinetics which restrict combustor operation via limits on flammability, flame propagation, ignition and stability has been investigated. Both techniques have demonstrated the potential to improve combustion processes. The radiative technique under laboratory static conditions has successfully ignited fuel-air mixtures, and has enhanced combustion processes, utilizing

DD FORM 1 JAN 73 1473 EDITION OF 1 NOV 65 IS OBSOLETE

UNCLASSIFIED
SECURITY CLASSIFICATION OF THIS PAGE (When Data Entered)

20. ABSTRACT (Cont'd.)
pulsed and continuous vacuum ultraviolet light sources. Similarly, the catalytic technique has broadened stability limits under normally difficult fuel lean, low temperature conditions. Complementary efforts have focused on the development of analytical capabilities required for modeling the radiative and catalytic techniques.

TABLE OF CONTENTS

FOREWARD

This is the final report on research in Radiation/Catalytic Augmented Combustion conducted with partial support of the Air Force Office of Scientific Research under Contract No. F49620-81-C-0028. The research under this contract continues the work performed under previous Contract No. F49260-77-C-0085 and described by Final Technical Report (AFOSR-TR-82-0132).

This final report covers the progress of research since its inception on April 1, 1981 through March 31, 1983. The work was performed under the direction of Exxon Research and Engineering Company (ER&E), Linden, New Jersey. Dr. M. Lavid was Principal Investigator until August 30, 1982, when Mr. I. D. Crane assumed responsibility through completion. Dr. A. E. Cerkanowicz assisted in writing this final report. Experimental studies on catalytic augmented combustion were performed by Drs. R. J. Gill and D. B. Olson under a subcontract at AeroChem Research Laboratories, Inc., Princeton, New Jersey.

No further research on augmented combustion is being undertaken at ER&E. Therefore, to provide a perspective on the total effort, this report also includes highlights of portions of the work done previously.

ABSTRACT

Two novel concepts for extending aircraft operational range have been researched under this contract. They are radiative and catalytic augmentation techniques. The objective has been to investigate the feasibility of utilizing these techniques to alter (augment) combustion initiation and reaction kinetics which restrict combustor operation via limits on flammability, flame propagation, ignition and stability. Both techniques have demonstrated the potential to improve combustion processes. The radiative technique under laboratory static conditions has successfully ignited fuel-air mixtures, and has enhanced combustion processes, utilizing pulsed and continuous vacuum ultraviolet (VUV) light sources. Similarly, the catalytic technique has broadened stability limits under normally difficult fuel lean, low temperature conditions. Complementary efforts have focused on the development of analytical capabilities required for modeling the radiative and catalytic techniques.

The radiative technique is an original approach which can influence combustion processes by the employment of a non-physically intrusive beam of light. This technique utilizes selected wavelengths in the VUV region to produce oxygen atoms by photodissociating molecular oxygen. When a critical concentration of atomic oxygen is achieved (about 10^{22} atoms/m^3), combustion initiation occurs. Subsequent reactions of atomic oxygen with fuel molecules, as well as with other combustion species, lead to ignition and sustained combustion via chain reactions. Simple combustion enhancement without initiation can be achieved at lower oxygen atom concentration levels. Radiative ignition and combustion enhancement tests have been conducted under various static conditions. This work included VUV excimer laser ignition tests, and additional ignition and enhancement experiments employing a continuous light source (EIMAC). The VUV output of the continuous light source was found to be marginal for ignition as well as for enhancement. However, it was successfully used to demonstrate the feasibility of igniting fuel-oxidant mixtures (propane/02) using continuous or steady-state light sources.

Catalytic combustion is a concept wherein combustion reactions initiated by a heterogeneous catalyst play an important role in the energy release process of a reacting fuel-air system. This part of the program has been primarily aimed at determining the feasibility of improving flame stabilization and reducing pressure loss in aircraft afterburner systems by replacing the conventional bluff-body by a porous catalytic flameholder. The bluff-body stabilizes the combustion by forming a recirculation zone which, in turn, enhances mixing and heat transfer. However, it also causes a substantial pressure loss. By using a porous, catalytic flameholder the temperature and concentration of reactive species in the flameholder wake can be "forced" to levels favorable for stable and efficient combustion. Experiments in a continous flow combustion test facility have shown that a porous catalytic flameholder can provide more stable combustion and a lower pressure drop than a bluff-body ... ...der. This indicates that catalytically coated flameholders may be a promising approach to enhanced stabilization of highly diluted partially combusted gas streams such as those exiting the main burner section of a gas turbine engine.

SUMMARY

Aircraft operation is limited by combustion associated phenomena involving ignition, flammability, flame propagation, and stable combustion. Recent combustion research has identified a number of potentially promising techniques for rectifying combustion-associated aircraft limitations. The objective of this work is to develop an understanding of basic mechanisms and processes associated with two new techniques which effect combustion augmentation by ultraviolet irradiation or catalytic surfaces.

Both the radiative and catalytic augmented combustion concepts have been demonstrated to favorably alter combustion processes. The radiative technique offers the potential for dynamically controlling ignition and flame propagation through non-physically intrusive means. The catalytic technique is a physically intrusive but passive approach which can broaden flame stability limits. Additionally, analytical tools have been developed to aid in the effective transfer of these concepts to practical (nonlaboratory) combustion systems.

- Radiative Augmented Combustion

The ignition and combustion enhancement of typical gaseous and liquid fuel-air mixtures used in air-breathing propulsion engines by vacuum ultraviolet (VUV) irradiation and by ultraviolet (UV) irradiation have been the principal focus of the radiative augmented combustion concept. Ignition and/or enhancement of combustion is achieved by selectively producing reactive combustion intermediary species via a photodissociative mechanism or combined photo-thermal methods (1-3). Implementation of the technique is via the use of a non-intrusive (zero fluid dynamic drag) beam of light in a selected wavelength region.

Figure 1 illustrates one possible application configuration where a non-physical flameholder is generated in a high velocity flow by focusing the continuous radiation output from a VUV light source at some point within the fuel-air flow field. A "zero pressure drop" flameholder is thus established since no physical obstruction to the flow exists. Feasibility of this concept has been established in the laboratory by ignition of a stationary propane-oxygen mixture using a continuously operated light source. Previously (1-3), only pulsed light sources were sufficiently powerful in VUV radiation to ignite fuel-air mixtures.

The combustion intermediate species of major importance in this approach is atomic oxygen. The photochemical initiation mechanism specifically utilizes the efficient photodissociation of oxygen which occurs for radiant energy below 180 nm. Subsequent reaction of atomic oxygen with fuel molecules (as well as other combustion species) leads to sustained combustion (initiation) when oxygen atom concentrations on the order of 10^{3} atoms/m^3, or greater, are generated. Oxygen atom concentrations below the critical level will not result in combustion initiation but can lead to combustion enhancement. By photochemically providing an excess of oxygen atoms above a typical level of about 10^{12} atoms/m^3, the thermal reactivity of a fuel-air mixture can be altered leading to a change in flame propagation rate. Further, since reduced amounts of oxygen atoms are effective for enhancement, the usable radiant wavelength range can be extended to about 200 nm.

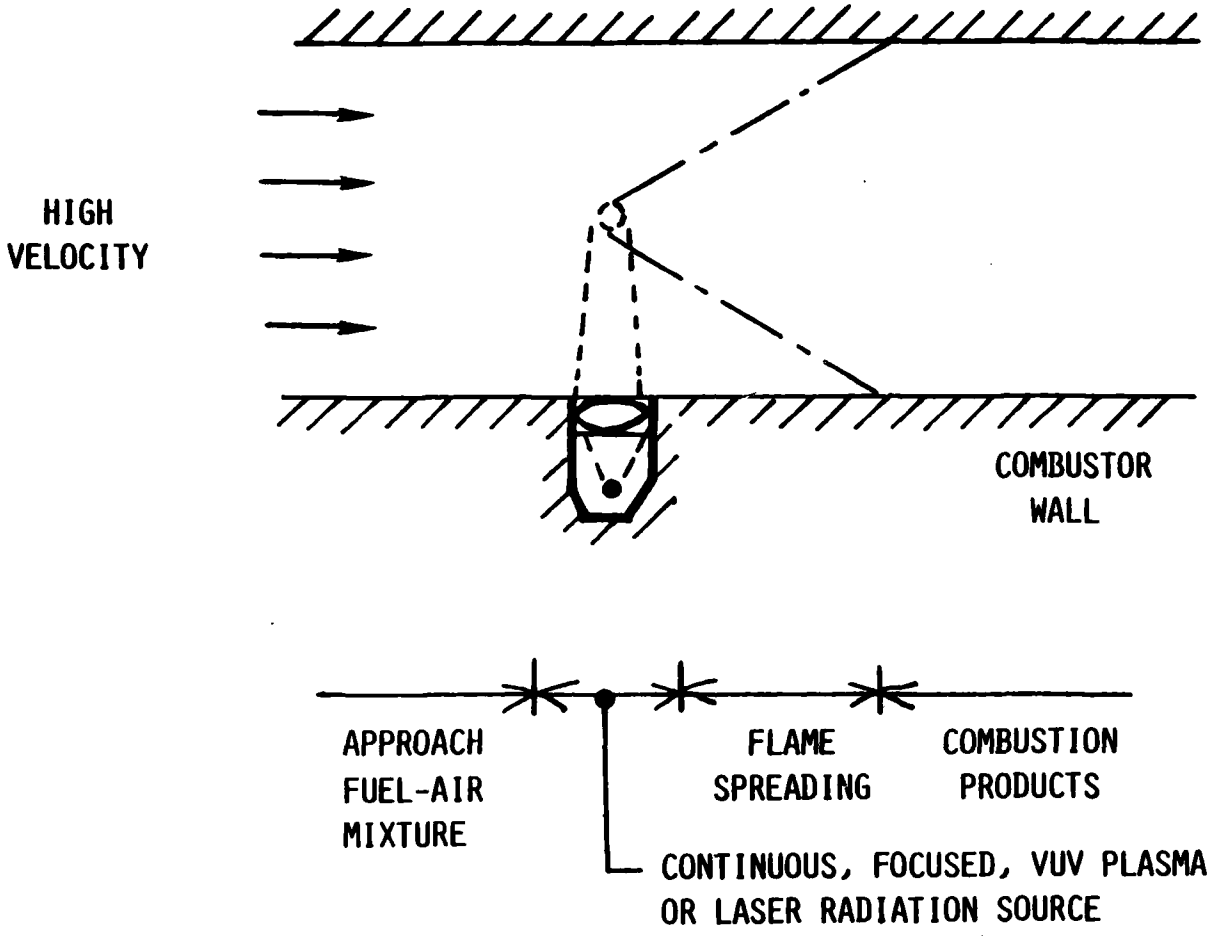

Figure 1. Radiative Flame-Stabilization Geometry (zero pressure drop flame-holder)

Previous research (1-3) used specially designed pulsed plasma short arcs to provide necessary VUV radiant energy for initiation studies. These earlier studies explored the influence of radiation wavelength, fuel type, fuel-oxygen-nitrogen mixture ratios, pressure, temperature, and mixture velocity on the radiative initiation process. More recent work (10) confirmed the results of the previous work with respect to the radiative initiation mechanism and extended light source considerations. The successful ignition with a continuous light source was reported for the first time.

In the most recent research, new ignition experiments with pulsed VUV laser sources and additional continuous light source (EIMAC) ignition tests have been undertaken. The VUV laser ignition work was conducted by employing an excimer laser at two VUV wavelengths; 157 nm (F_2) and 193 nm (ArF). Radiative ignitions were achieved with the fluorine laser and not with the argon fluoride laser, even though the latter has about 20 fold greater fluence. This result demonstrates the important role of the spectral selectivity of the absorption coefficient of molecular oxygen. Successful radiative ignitions with a continuous light source (EIMAC) were achieved on only two occasions and only after many attempts due to the marginal VUV output of this xenon lamp.

In the previous efforts a comprehensive computer model of the photochemical initiation mechanism was formulated. This model includes extensive kinetics for photon absorption, molecular dissociation and reactant mixture kinetics. This model has confirmed and guided experimental effort and provides a base for the designer to examine new ignition methods and applications. In the most recent research, this model has demonstrated good phenomenological agreement with the observed ignition behavior. In particular it has shown good quantitative agreement with the laser ignition results. This reinforces the adequacy of the model for elucidation of photon-radical interaction in combustion initiation.

Experiments exploring the radiative enhancement of combustion were conducted with propane-air mixtures and a continuous UV source. Scoping studies of radiative effects on flame propagation velocity, extinction distance, and extinction time indicated that extension of the normal flammability limit should be possible. If successful, the use of continuous VUV/UV light sources would offer a potential opportunity to broaden the current flammability envelope, extending aircraft operational range beyond presently available flight corridor.

Although its VUV output is marginal, EIMAC is currently the best available continuous VUV light source and therefore it was used for the most recent combustion enhancement work. A large number of tests investigating propane-air flames were conducted. Due to experimental difficulties and the marginal VUV output, the data obtained were limited and not conclusive. Nevertheless, the observation of some dramatic changes did indicate an effect of irradiation on the combustion process. Considerably more work is required to elucidate the processes involved.

- Catalytic Augmented Combustion

In comparison with the radiative technique, catalytic combustion augmentation is physically intrusive on the fuel-air flow field but does not

require a direct energy supply. Combustion is promoted by use of a solid catalytic surface which accelerates the fuel-air reaction through physical contact. The catalyst is deposited on the surface of a high-temperature ceramic substrate which is in the form of a honeycomb placed in the reactant flow stream in the manner of a conventional flameholder. In contrast to solid conventional bluff-body flameholders, however, a portion of the reactive mixture will pass through the catalytic unit. Oxidation of the fuel, and energy release is promoted in this portion of the mixture due to surface activated reaction. The increased temperature and concentration of reactive combustion intermediaries provided by the flow exiting the catalytic unit is favorable to stable, efficient gas phase combustion of the bulk of the reactant mixture.

Figure 2 illustrates one possible catalytic flame-stabilization geometry. Only a portion of the reactant mixture flows through the catalytic flameholder thereby avoiding the concommitant energy loss due to a high pressure drop. This approach represents a significant departure from other catalytic combustion techniques where the catalytic monolith occupies the full flow path.

Flame stabilization tests by AeroChem Research Laboratories (Appendix I) in a continuous flow combustion facility have demonstrated that porous catalytic flameholders may be a promising approach to augment combustion stability limits. During the contract period, three flameholders of the same cross sectional area - a solid bluff body, a porous catalytic structure, and a porous noncatalytic structure - were characterized experimentally. Results at low reactant velocity (below 13 m/s) show conclusively that the fuel lean blowoff limits are wider with a catalytic flameholder than with noncatalytic but otherwise identical flameholders. More importantly, for velocities above 11 m/s, the porous catalytic flameholder exhibited a wider lean blowoff limit than a solid flameholder. Additionally, the porous catalytic flameholder exhibited a lower pressure drop. High output combustors or afterburners require flame stabilization in a high velocity fuel-air mixture and their performance would benefit from the increased blowoff limit. Extension of the experimental data for velocities up to 200 m/s is needed, however, to verify and quantify the departure in blowoff limit.

Two models have been developed for specific aspects of the catalytic flame stabilization concept. The first provides for description of the aerothermochemistry within the catalytic unit and has been demonstrated to correctly predict the catalytic performance. The second deals with the flow split through and bypassing the catalytic unit and the wake mixing region downstream of the catalytic unit. A first order description of catalytic flameholding is possible using a combination of these models. Comparison with experimental data is required to establish the model parameters.

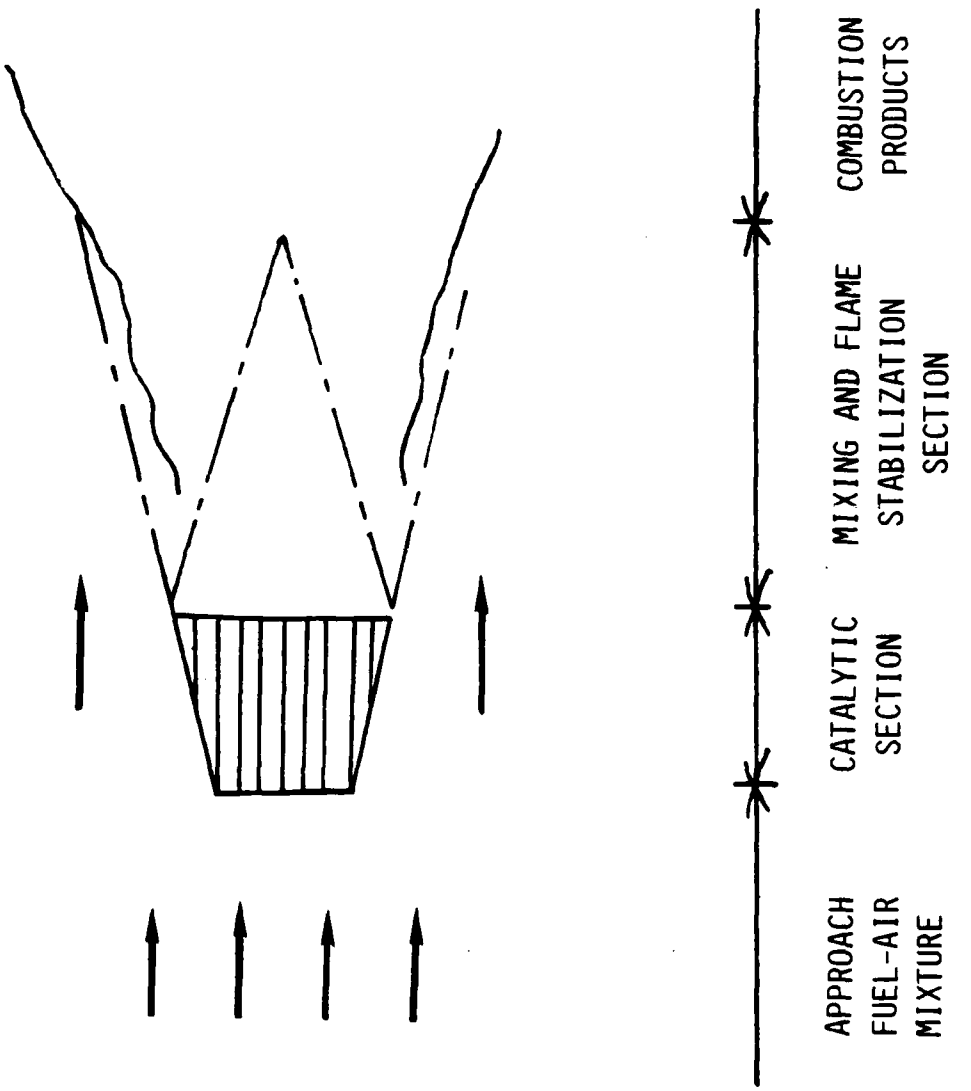

Figure 2. Catalytic Flame-Stabilization Geometry.

DISCUSSION

RADIATION AUGMENTED COMBUSTION

Various radiative sources were experimentally characterized or evaluated with regard to photochemical combustion initiation and enhancement over a wide range of operating conditions. Three different types of vacuum ultraviolet (VUV) igniters were effectively utilized: (1) pulsed plasma short arcs, (2) focused continuous short arcs, and (3) pulsed lasers. Table I lists the optical features of these light sources. A continuous ultraviolet (UV) short arc source was also employed in combustion enhancement experiments. Photochemical mitigations were evaluated by measuring the stored energy required for successful combustion initiation. Measurements of flame velocity and reactant burn-out time were used to characterize photochemical enhancement.

- Photochemical Ignition Experiments

Detailed spectroscopic data was obtained on the pulsed, plasma short arc in the vacuum ultraviolet and ultraviolet wavelength regions (5). This particular source has been used for the majority of the photochemical ignition parameterization experiments. Figure 3 illustrates the spectral distribution of intensity for this source which exhibits pronounced peaks in the 145 to 175 nm wavelength region. This is a region of photon energy which is extremely efficient in initiating combustion reactions. Spectral data also indicated that the temporal behavior of the light pulse can be effectively modeled as a critically damped pulsed of the form

$$I/Imax = (t/t^*)\exp(1-t/t^*)$$

where I = pulse intensity, Imax = maximum intensity, t = time, and t* = time to peak intensity. Propane-air ignition experiments with this radiation source reconfirmed the previously observed photochemical ignition characteristics.

The second type of light source successfully employed in radiative augmented combustion experiments was a commercially available EIMAC lamp. This was a continuous xenon point source with a low grade sapphire window and an elliptical reflector. Blackbody radiant energy output in the 150-400 nm spectral region was developed at input power levels of up to 600 watts. Ignition of propane-oxygen mixtures at ambient temperature and atmospheric pressure was achieved at equivalence ratios of 0.8 and 1.0 with power inputs of 615 watts and 500 watts. Although the light source was destroyed in each case, this represents the first demonstrations of radiative ignition using continuous light source irradiation. Continued development of this capability would provide the option of designing an optical-radiative flameholder with zero pressure drop due to physical obstruction.

Laser ignition experiments were conducted by the principal investigator (Dr. Lavid) at Los Alamos Scientific Lab/Applied Photochemistry Division using their Lumonics TE861 laser facility. The lasers were used at two wavelengths; 193 nm (ArF) and 157 nm (F_2) with measured fluence at about 300 to 400 mJ/cm^2 and 20 to 40 mJ/cm^2 respectively. Hydrogen-oxygen-nitrogen mixtures at varying equivalence ratio and subatmospheric pressure were used.

TABLE I

OPTICAL FEATURES OF VUV/UV LIGHT SOURCES

SOURCE	WAVELENGTH RANGE (nm)	WINDOW	MODE	OPTICS	OPTICAL PATH	ENERGY/ FLUENCE	RESEARCH APPLICATION
ILC	140-400	UV Grade Sapphire	Pulsed	Point Source	Vacuum	0.5-50 J	Ignition
ORC	200-400	High Grade Quartz	Continuous	Focused/ Parallel	Air	1 kW	Enhancement
EIMAC	150-400	Normal Sapphire	Continuous	Focused	Vacuum/ Air	0.5-0.6 kW	Enhancement/ Ignition
LUMONICS TE861	193	MgF_2	Pulsed	Focused	Ar/He	50 mJ 350 mJ/cm^2	Ignition
LUMONICS TE861	157	MgF_2	Pulsed	Focused	Ar/He	6 mJ 30 mJ/cm^2	Ignition

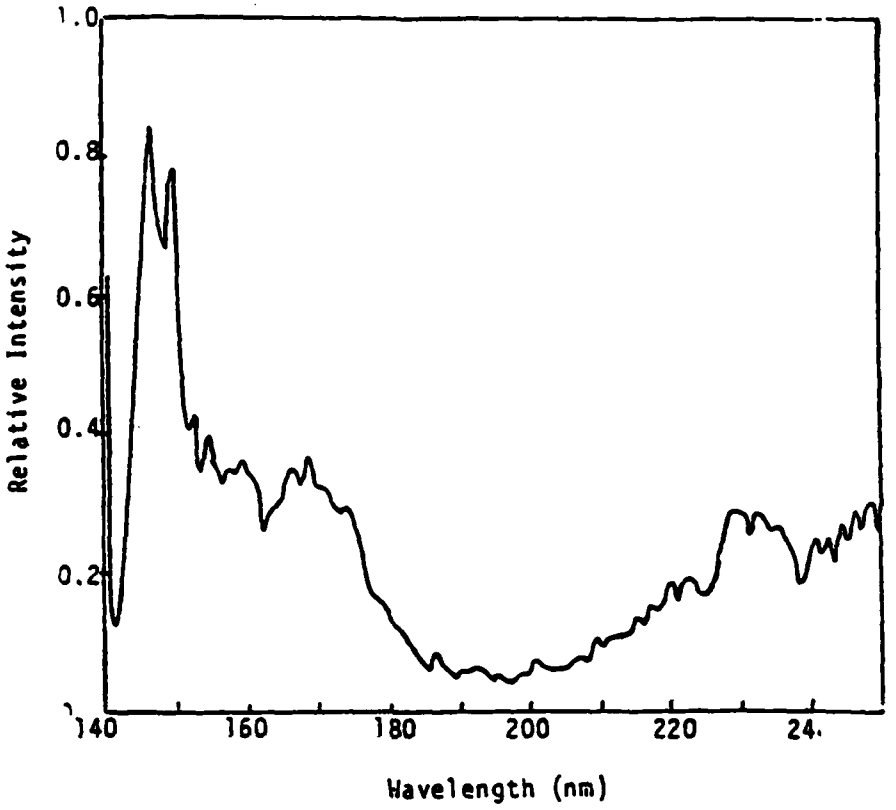

Figure 3 - Spectral Distribution of Intensity
for Pulsed VUV Light Source

Photochemical ignition was not achieved using the ArF laser. This is consistent with previous results (1) which indicated that wavelengths below 160 to 170 nm were the most effective in producing radiative ignition. Use of the F_2 laser proved successful although the fluence was about 1/20 that of the ArF laser.

Two characteristics of the F_2 laser need to be discussed before the results of ignition experiments can be understood. First, laser pulse energy decreases with use as shown in Figure 4, necessitating that the F_2-He mixture in the laser chamber be refreshed on a regular basis. More importantly, the focal length of the laser-optical system is wavelength dependent. This is clearly illustrated by the results in Figure 5, which show relative pulse energy vs. focal distance. Exclusion of VUV irradiation is achieved by purging the optical path with oxygen. The focal point when the total energy flux is present is about 24.6 cm while the optimum focal point for the VUV occurs at about 19.7 cm. When operated properly, laser ignition of hydrogen-oxidant mixtures were achieved on a regular basis. These results confirm the radiative ignition concept and extend the repertoire of available light sources usable for photochemical combustion initiation.

- Combustion Enhancement Experiments

The ultraviolet capabilities of the EIMAC source were also utilized in exploring combustion enhancement. In these experiments, propane/air mixtures at various equivalence ratios and pressure were subjected to UV irradiation simultaneous with flame propagation (9,11). The effect of propagation toward and away from the light source was studied. Since comparison with literature quoted flame speeds is highly dependent on specific conditions such as direction of gravity, heat loss, confinement, etc., complementary tests in the absence of light were also performed. The cinemagraphic technique employed precluded accurate measurement at near stoichiometric onditions due to intense light from the combustion reactions. Tables II and III highlight some of the results of this work. A more comprehensive treatment of the results is given in Refs. 9 and 11.

Table II indicates that a substantially positive effect on both extinction time and distance occurs due to light irradiation in front of a propagating flame. This effect was most pronounced for fuel lean mixtures where up to an 81% increase in extinction time and 25% increase in extinction distance were measured. These measurements were only taken with the light passing through the unburned mixture toward the propagating flame.

Additional, more extensive enhancement experiments have been done investigating propane-air flames using the EIMAC light source. Although its output is marginal, the EIMAC is currently the best available continuous light source. Emphasis was placed on measuring flame propagation velocity to evaluate combustion enhancement. While no extinction distances or times were recorded in these more recent experiments, the scope of the work was broadened to include two different optical paths between the flame front and the light source. Flame propagation velocities were primarily affected when the source was behind the flame front and irradiation was passing through the combustion products. Due to experimental difficulties and the marginal VUV output, the data obtained were not conclusive. As indicated in Table III, some conditions lead to inhibition rather than enhancement. However the observation of some

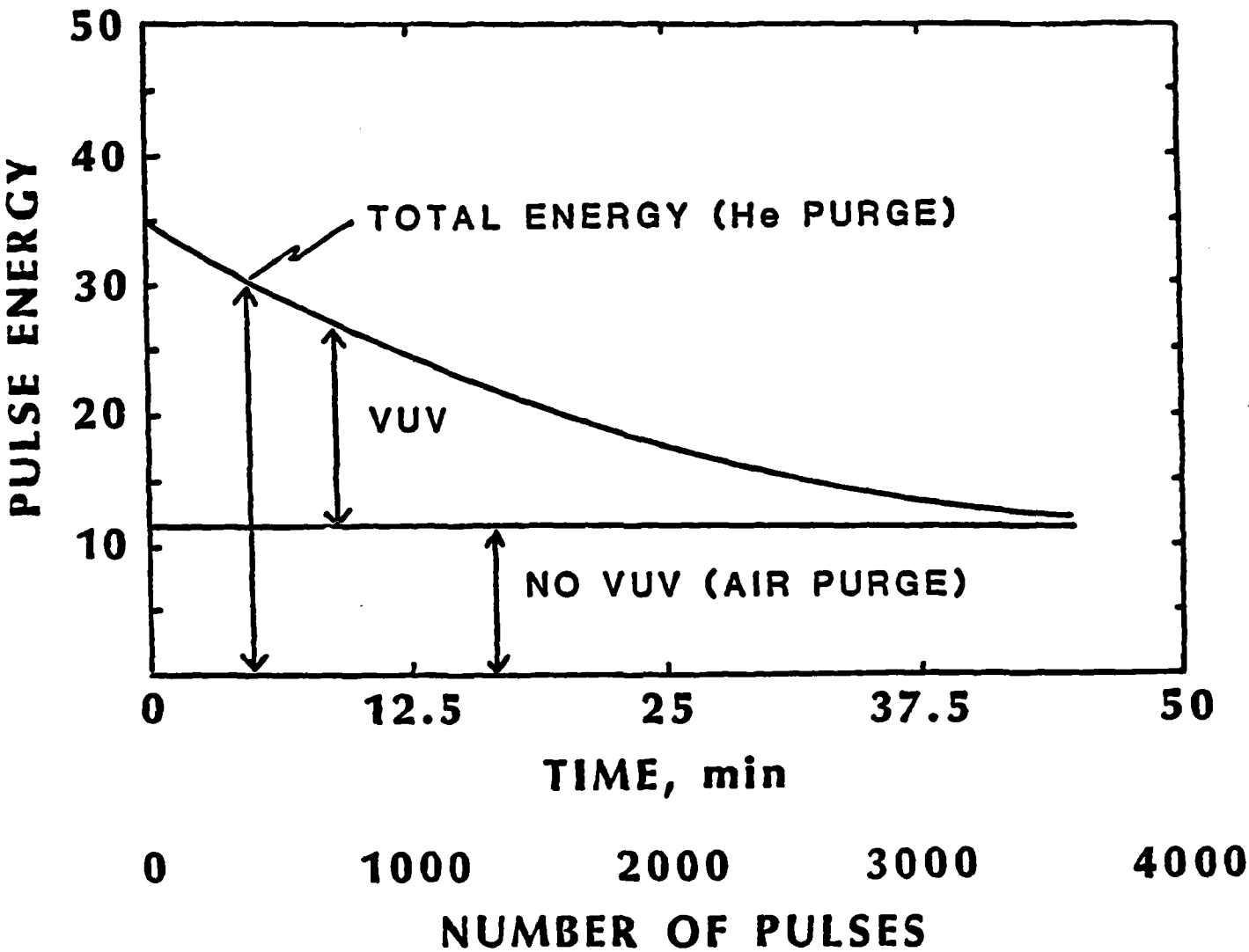

Figure 4. PULSE ENERGY (NO TRANSMITTANCE LOSS) VS. TIME (NUMBER OF PULSES)

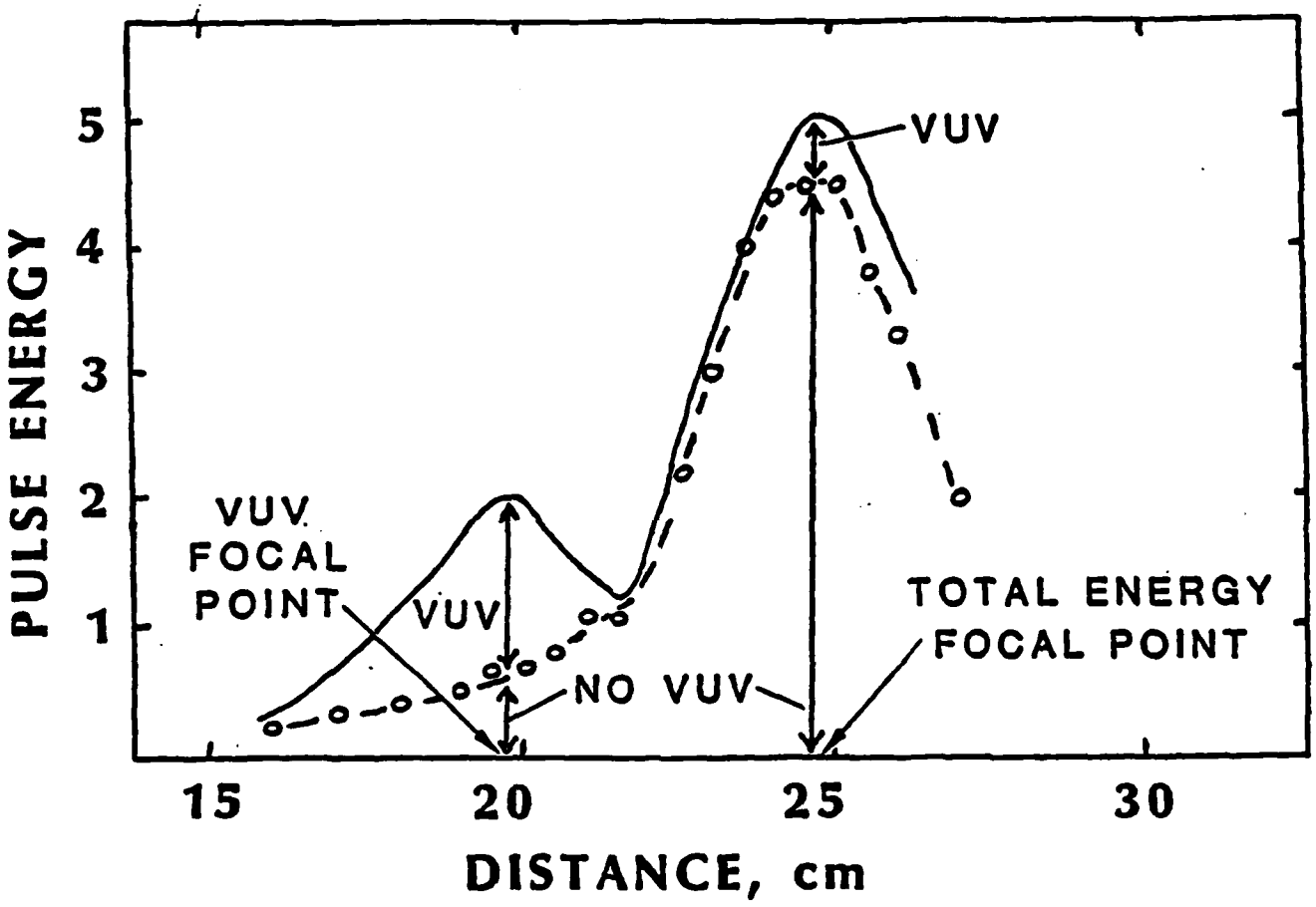

Figure 5. PULSE ENERGY (WITH LENS AND WINDOW LOSSES) VS. DISTANCE

TABLE II

EXTINCTION TIMES AND DISTANCES
FOR PROPANE-AIR FLAMES
IRRADIATED FROM THE REACTANT SIDE

Equivalence Ratio	Pressure	Dark/Light	Extinction Time (frames)*	Change %	Extinction Distance (cm)	Change %
.82	1 atm	Dark	20.0		13.9	
		Light	36.3	+81	17.4	+25
.82	400 torr	Dark	18.0		17.3	
		Light	30.0	+67	21.0	+21
.78	607 torr	Dark	41.5		24.2	
		Light	50.0	+20	28.0	+15

* 64 frames = 1 sec

TABLE III

FLAME PROPAGATION VELOCITIES FOR PROPANE-AIR FLAMES IRRADIATED FROM THE PRODUCT SIDE

Equivalence Ratio	Pressure	Dark/Light	Flame Velocity (cm/s)	Change (%)
0.79	1 atm	Dark	217	-46
		Light	116	
0.79	400 torr	Dark	89	+21
		Light	108	
1.50	1 atm	Dark	76	+112
		Light	161	

dramatic changes does indicate an effect of irradiation on the combustion process. Considerably more work needs to be done to define the processes involved.

- Analytical Modelling

Analytical work was directed toward elucidating the fundamental interaction of photon absorption, subsequent dissociation, the chemical kinetics of the reactant mixtures, and possible heat loss to the surroundings. Preliminary modelling results discussed in Ref. 4 and Appendix II are summarized with additional details here. Currently, the chemical kinetics included allow treatment of hydrogen-oxygen-mixtures with the possible presence of an inert diluent. The reactant species which are considered are presented in Table IV. The presence of electronically excited state species, not typical of most hydrogen-oxygen schemes, is dictated by their photochemical production, and although their inclusion is not indispensible, $O(^1D)$ will be seen to play a detectable role. Some 90 chemical reactions which occur between these species are included in the model. Rate constants in the form AT^{-B} exp (-C/T) were obtained from the extensive literature on the subject, with emphasis on data in the initiation and early ignition temperature range (300-1200 K). The rate data tabulated in Ref. 1 were used, with some values updated to reflect those used in recent reviews (7,15).

Radiant absorption is assumed to follow a Beer-Lambert law. The absorbing species include O_2, O_3, H_2O, HO_2 and H_2O_2. Upon absorbing a photon, these species are assumed to dissociate to products which depend on the energy of the photon. Thus, quantum yields as a function of wavelength have been taken to be one over a given interval and zero otherwise. The photodissociation reactions considered are given in Table IV, together with the relevant wavelength intervals. Photodissociation can thus be handled as a uni-molecular reaction in which the dissociation rate is obtained as the product of the concentration of the absorbing species and a pseudo-first-order rate constant, which depends on the incident spectral irradiance, $I(x,t,\gamma)$, at a given point in the mixture and at a given time. Because the objective is to gauge the robustness of the ignition kernel, which lies close to the combustor window, the spatial dependence is not considered and the spectral irradiance used is that which would be measured at the mixture side of the window. The number of incident photons of wavelength λ to $\lambda+d\gamma$ per unit area time is thus $I(\lambda/hc)I(t,\lambda)$. When multiplied by the wavelength-dependent cross-section of the absorber and integrated over the relevant wavelengths, we thus obtain the desired rate constant for photodissociation is obtained. The integral is, in fact, approximated as a sum with one nanometer wavelength increments. Unlike the chemical rate constants, it is time-dependent through the temporal dependence of $I(t,\lambda)$. This dependence was taken to be of the form $I(t,\lambda) = Imax(\lambda)P(t)$; where P (t) is the pulse shape function, generally taken to be that of a critically damped pulse. Tabulated absorption coefficients for all absorbing species are used; absorption of O_2 in the Schumann-Runge bands follows the treatment of G. Kocharts (7). For each species, a rate balance was formed by consideration of all chemical and photochemical reactions in which it participates (4).

A heat balance equation accounts for heat liberated or removed by chemical reaction and possible heat loss to surroundings. The heat loss has

TABLE IV

HYDROGEN-OXYGEN PHOTOCHEMICAL SYSTEM

REACTANT SPECIES

O (^1D)	O_2	OH
O	O_3	H_2O
O_2 ($^1\Sigma_g^+$)	H	HO_2
O_2 ($^1\Delta_g$)	H_2	H_2O_2

PHOTODISSOCIATION REACTIONS

Absorber → Products					Wavelength Region (nm)
O_2	→	O	+	O	175 - 245
O_2	→	O	+	O (^1D)	134 - 175
O_3	→	O_2	+	O	>310
O_3	→	O_2 ($^1\Delta g$)	+	O (^1D)	260 - 310
O_3	→	O_2 ($^1\Sigma_g^+$)	+	O (^1D)	<260
H_2O	→	OH	+	H	<242
HO_2	→	OH	+	O	<456
H_2O_2	→	OH	+	OH	<365

been taken proportional to the difference between gas and ambient temperatures, with heat loss coefficient calculated from $hc = 16\ k/SC_p d^2$; k = thermal conductivity. The diameter (d) is estimated for the ignition kernel by using the irradiated cross-sectional area. The model is finally constituted as an initial value problem for the resulting system of nonlinear ordinary differential equations. Solution techniques are documented in Ref. 4. Diffusion and convective effects have been neglected.

The resulting system of differential equations is autonomous and, as recognized by Yang and Gray (6), it is profitable to consider the trajectories determined by the solutions in phase space and the singular points of the system. Reference to multi-dimensional phase space is cumbersome, and for combustion initiation in the H_2/O_2 system, largely unnecessary. It suffices to present the results in the temperature vs. oxygen atom concentration plane, with the oxygen radical acting as a surrogate for the other radicals. When so done, the trajectories reveal a phase plane typical of a simple critical chain branching system, as shown in Figure 6. The unlabeled solid trajectories represent solutions for varying initial temperature and oxygen atom concentration. The dashed line indicates the separatrix between the fast-reaction region, C, and the noncombusting region, N. This separatrix is, of course, composed of the two trajectories which lead to the saddle point, S, heuristically the critical point arising from the balance of chain branching and chain termination. Trajectories which lie below this separatrix lead to the stable node, A, at ambient temperature. Trajectories which lie above the separatrix are characterized by rapid chain-branching and increase in temperature and thereby indicate ignition.

Thus, in the absence of irradiation, the reactant mixture which begins at a point on a given trajectory will tend by chemical action to follow that trajectory. Consider now the effect of irradiation and the consequent production of oxygen atoms. The resulting solution curve is no longer one of the reaction-determined trajectories but departs from these trajectories in the direction of increasing oxygen atom concentration. Such a path is shown as curve 1 in Fig. 6. It is the resultant of oxygen atom increase due to photodissociation and temperature increase due to chemical reaction. In this case, the separatrix is crossed and ignition results. Curve 2, however, represents a solution in which a radiant pulse has effectively ceased before the separatrix has been crossed; the curve thus rejoins a trajectory leading back to the stable node and no ignition results. In contrast, other ignition approaches (e.g., "pure" thermal, spark) rely significantly on departure from the trajectories in the direction of increasing temperature and follow paths which can be expected to differ from that of radiative initiation. This analysis provides a qualitative framework for understanding photochemical initiation and indicates the value of the phase plane for presenting the quantitative modeling results to be discussed.

• Comparison of Model and Experiment

Application of the model to pulsed plasma short arc initiated reactions has been extensively discussed before (Refs. 1, 4, and Appendix II). The model has proved particularly useful in understanding the laser ignition experiments. Analysis of laser ignition characteristics indicates that with the currently available fluences the shorter wavelength laser (F_2) is capable of achieving photochemical ignitions, while the ArF laser is not.

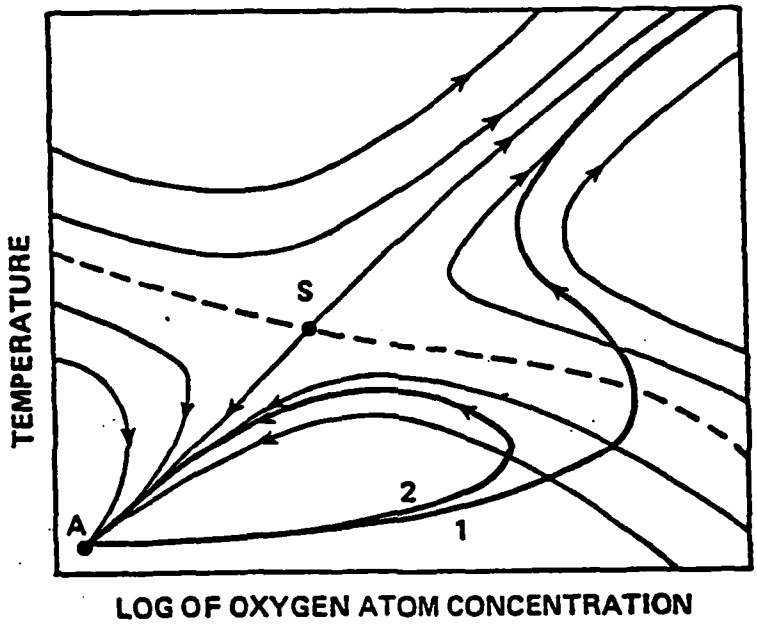

FIGURE 6. REPRESENTATIVE PHASE PLANE FOR PHOTOCHEMICAL INITIATION OF COMBUSION.

S: SADDLE POINT
A: NODAL POINT AT AMBIENT TEMPERATURE
——: TRAJECTORIES IN THE ABSENCE OF IRRADIATION
---: SEPARATRIX OF COMBUSTING AND NON-COMBUSTING REGIONS
——1: SOLUTION CURVE FOR IRRADIATION LEADING TO IGNITION
——2: SOLUTION CURVE FOR IRRADIATION WITHOUT IGNITION

This finding is in agreement with our numerical predictions, as depicted in Fig. 7. The bars shown indicate the minimum fluence predicted to photochemically ignite a premixed hydrogen-oxygen mixture at an equivalence ratio of 0.6 and at 20 kPa for the wavelengths of the F_2 (157 nm) and ArF (193 nm) lasers. These values were calculated from the radiative ignition model by increasing the value for the fluence (i.e. irradiance, as the pulse width remains the same) until a solution indicating ignition was obtained. The resulting fluences are 36 and 2.7 x 10^5 mJ/cm^2, respectively. This significant difference in fluences (and therefore energies) is primarily due to the spectral selectivity of the absorption coefficient of the oxygen molecule. At 157 nm, which is in the Schumann-Runge continuum, the absorption coefficient is 167 cm^{-1}, and at 193 nm, which is in the S-R bands, it is 0.027 cm^{-1}, about four orders of magnitude lower (7). Experimental results indicated by the symbols for ignition and no-ignition events agree with these predictions. Although the fluence of the F_2 laser is considerably smaller than that of the ArF laser, it successfully achieved ignition, while the ArF failed in photochemically igniting the same gaseous mixtures.

Minimum ignition energies for combustible gaseous mixtures are typically given as a function of equivalence ratios at various pressures. Since it was very difficult experimentally to vary accurately the energy emitted by the laser and absorbed by the mixture, this was kept constant and the pressure of the mixture was varied instead. Figure 8 depicts the minimum pressure at which the mixture is photochemically ignitable by the F_2 laser vs. equivalence ratio for hydrogen-oxygen and hydrogen-air mixtures. The curves in the figure are derived from analytical predictions for minimum ignition pressures which were obtained by fixing other model inputs to values corresponding to those of the experimental conditions. In particular, the value used for the heat loss coefficient was based on the irradiated cross-section; it was then varied only according to its pressure dependence. A search was performed until two pressures were obtained which differed by 1 kPa, with ignition indicated for the higher and not the lower. For H_2/O_2 and equivalence ratio of 0.6, such solution curves are displayed on the phase plane in Fig. 9. It is interesting to compare this figure to Fig. 6 and to observe the expected cusp-like behavior in the neighborhood of the saddle point. This procedure was carried out for a sufficient number of equivalence ratios to allow the curves to be drawn accurately.

The experimental results in Fig. 8 are indicated with bars to represent the uncertainty in the results obtained due to fluctuations in laser output. The agreement between analytical predictions represented by the solid lines and experimental results shown as data points is very satisfactory. As expected, the results show that it is easier to ignite H_2/O_2 than H_2 air mixtures. The primary reason for the increase in pressure needed for the air system to ignite is the necessity to increase molecular oxygen concentration so as to achieve the required production of oxygen atoms upon irradiation. Indeed, the critical O_2 concentration somewhat exceeds that for the corresponding H_2/O_2 mixture due to the presence of the diluent, N_2, resulting in an increase in thermal inertia, and to the deleterious effects of increasing pressure, e.g. increased rate for certain chain termination paths. Also, it is important to note that experimental and numerical results indicate that fuel-lean mixtures with some excess oxygen are more favorable for photochemical ignitions than other mixtures, with the most favorable mixture at an equivalence ratio of 0.6. This finding is quite different from

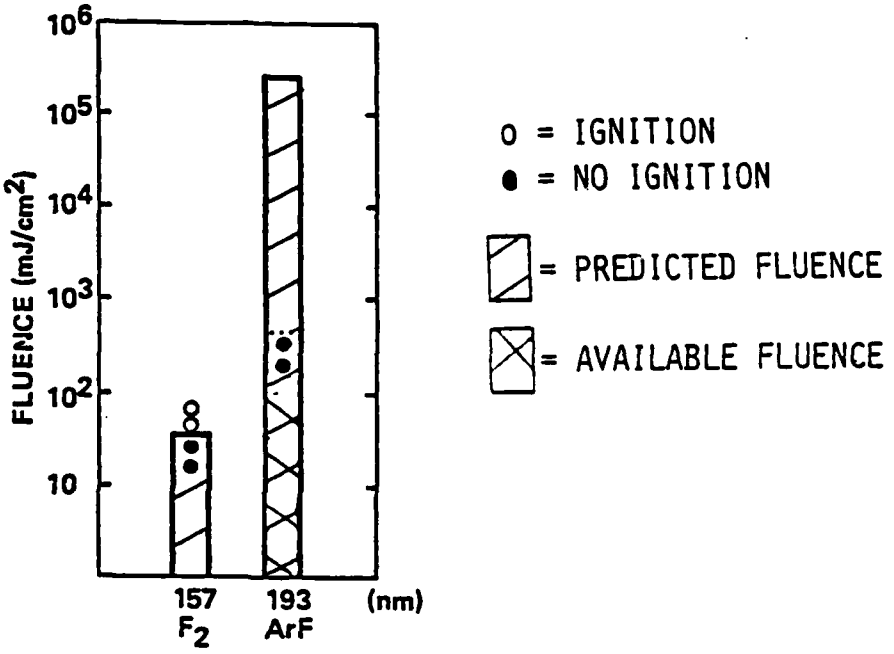

CONDITIONS: H_2/O_2, Ø = 0.6, P = 20 kPA

FIGURE 7. COMPARISON OF FLUORINE (F_2) AND ARGON-FLUORIDE (ArF) LASERS AS IGNITORS

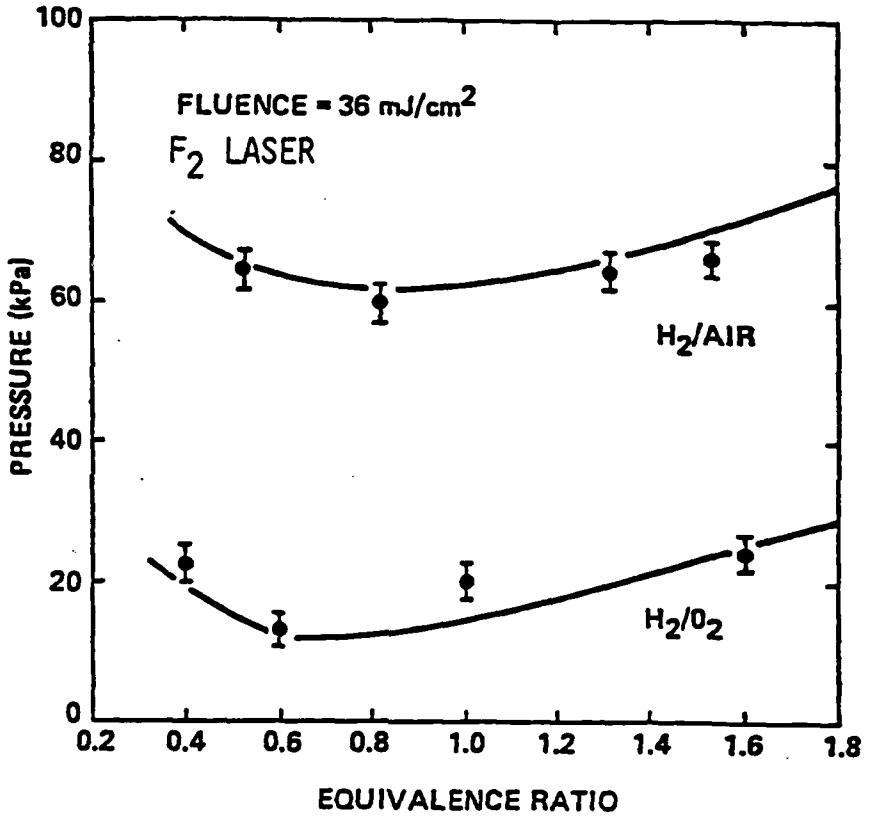

FIGURE 8. MINIMUM IGNITION PRESSURE; COMPARISON OF THEORETICAL PREDICTION WITH EXPERIMENTAL DATA.

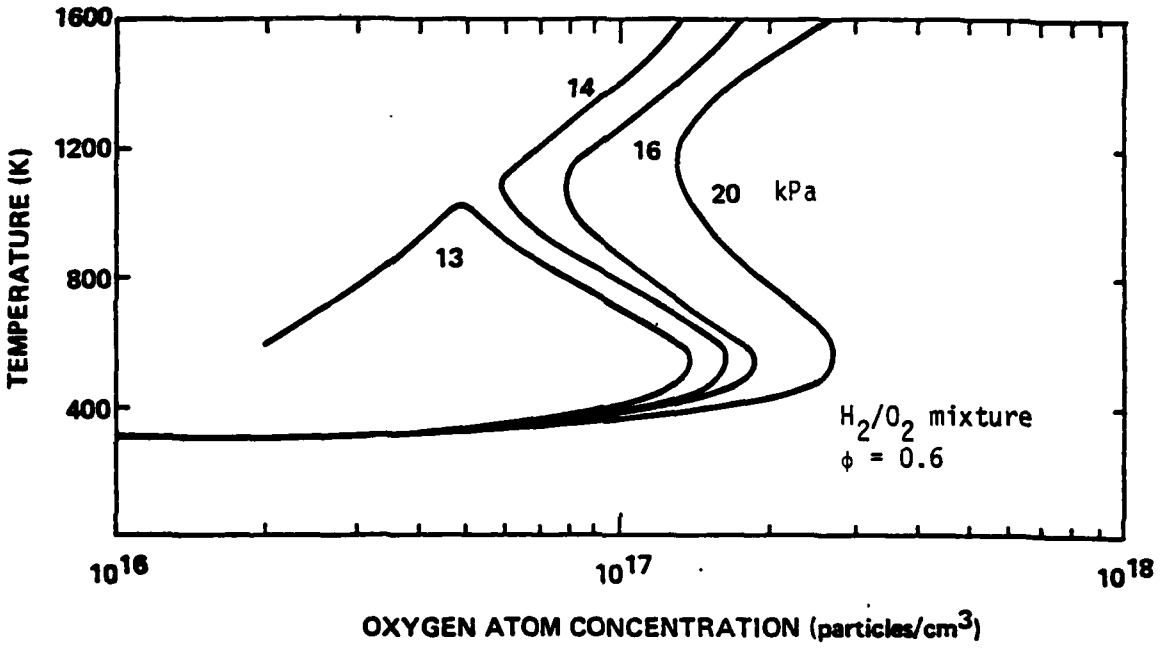

Figure 9. Solution curves for the determination of minimum ignition pressure with fluorine laser.

that for spark ignition in which minimum ignition is found to occur at about equivalence ratio of unity (12). Again, the explanation is that increased molecular oxygen results in higher atomic oxygen concentration. However, when equivalence ratio is further reduced, the rate of chemical heat release is decreased due to the lessened availability of fuel molecules, which necessitates higher minimum pressure for ignition.

Detailed analysis of the combustion enhancement experiments would have required a major modificatin of the code to allow for flame propagation. Therefore a quite different numerical model (14,16), developed at Lawrence Livermore Laboratory, was used to examine the enhancement results obtained in a propane-air flame. This model allows prediction of laminar flame properties. It consists of a one-dimensional, time-dependent treatment of the conservation equations, together with detailed chemical kinetic mechanism including photodissociation reactions. This attempt proved unsuccessful (11).

CATALYTIC AUGMENTED COMBUSTION

The objective of this research was to evaluate the feasibility of using catalytic honeycomb flameholders to expand flame stabilization limits for potential applications such as in aircraft afterburners. This was performed by experimentally evaluating flame stablization using catalytic and noncatalytic flameholders in a research scale continuous flow tube combustor. Experiments were conducted using premixed propane/air to determine the effects of fuel/air ratio, flow velocity, and flameholder type on the flame stability limits. Several other diagnostics were also used to gauge the efficiency of the flame stabilization and combustion process. These diagnostics included gas temperature profiles in the combustor, flameholder temperatures, pressure drop across the flameholders, and CO and CO_2 concentrations in the burned combustion gases.

- Flame Stabilization Experiments

The experiments on catalytic flame stabilization were carried out by AeroChem Research Laboratories. A report covering their research is provided in Appendix I. The combustor used for these experiments is shown in Figure 11. The test section, which contained the flameholder, had 5.3 cm internal diameter.

Three types of cylindrical flameholders were used: solid brass, noncatalytic ceramic honeycomb and catalytic ceramic honeycomb. The ceramic flameholders were fabricated from Cordierite monolithic cylindrical shaped honeycomb plugs. The catalytic flameholders were custom prepared by impregnating the Cordierite with palladium catalyst. Several different diameter and cell densities were screened. The catalytic flameholder for the majority of the experimental runs had a 2.0 cm outside diameter and a honeycomb density of 31 cells/cm^2.

It was expected that a larger pressure difference would exist across a solid body flameholder than across a more porous body, such as ceramic honeycomb. Also higher gas flow velocities were expected to increase the pressure difference across the bodies. Both of these effects were confirmed in room temperature flow. Experimental data for a solid bluff body, a fully open honeycomb, and a partially blocked honeycomb are shown in Figure 11. While the magnitude of the pressure drops were small due to the scale being tested, a substantial difference existed between the flameholders (e.g. the pressure drop for a solid body was approximately 65% greater than for an open honeycomb at 12 m/sec velocity).

Fuel lean blowoff limits were measured to assess the effect of the porous catalytic flameholders upon the flame stability limits. Reactant flow velocities were varied from 9 to 13 m/s with equivalence ratios varying from 0.6 to 0.9 on the fuel lean side of stoichiometric. The experimental results illustrated in Figure 12 compare the lean blowoff limits for the three types of flameholders tested. Blowoff limits are significantly wider for the catalytic honeycomb than for the noncatalytic. In addition the limiting equivalence ratio for the catalytic flameholder decreases (i.e. more lean conditions) at higher flow velocities. This was an unexpected result since normally solid body limits shift toward stoichiometric with increasing velocity. For these experiments the catalytic body showed a wider limit than the solid body above a velocity of about 11 m/sec.

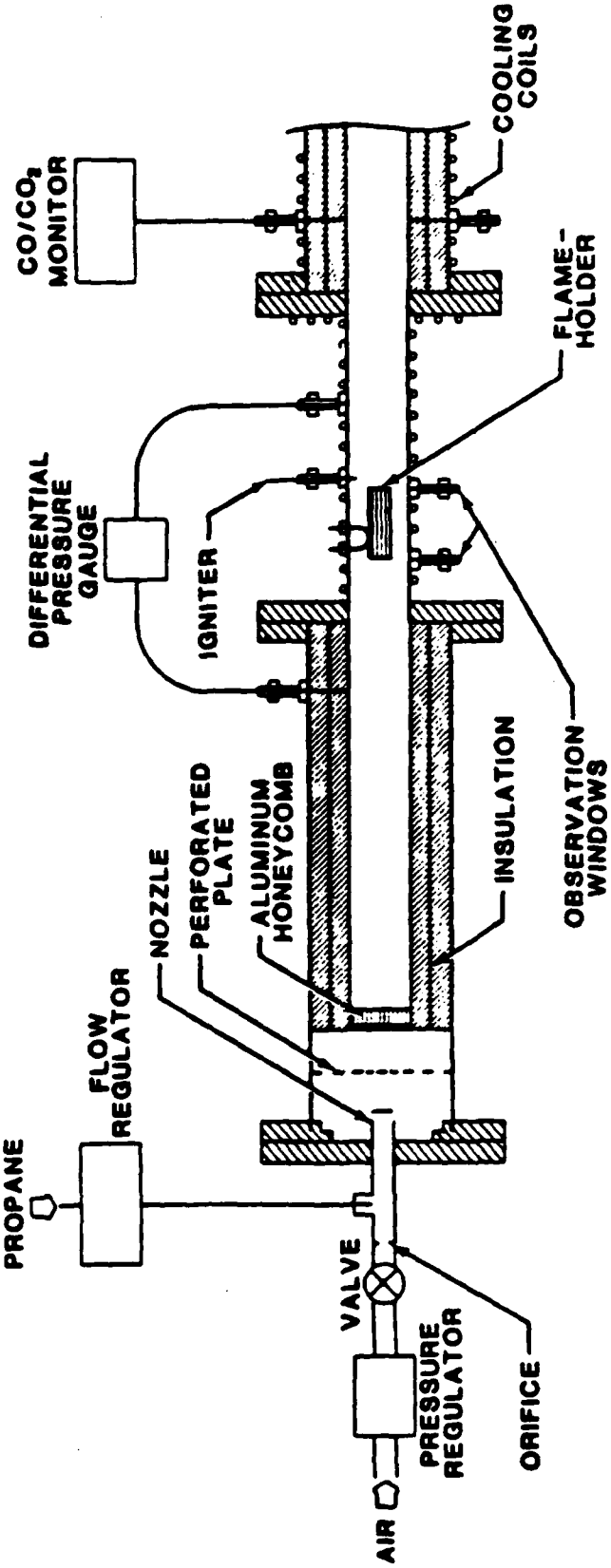

FIGURE 10. FLOW TUBE COMBUSTOR

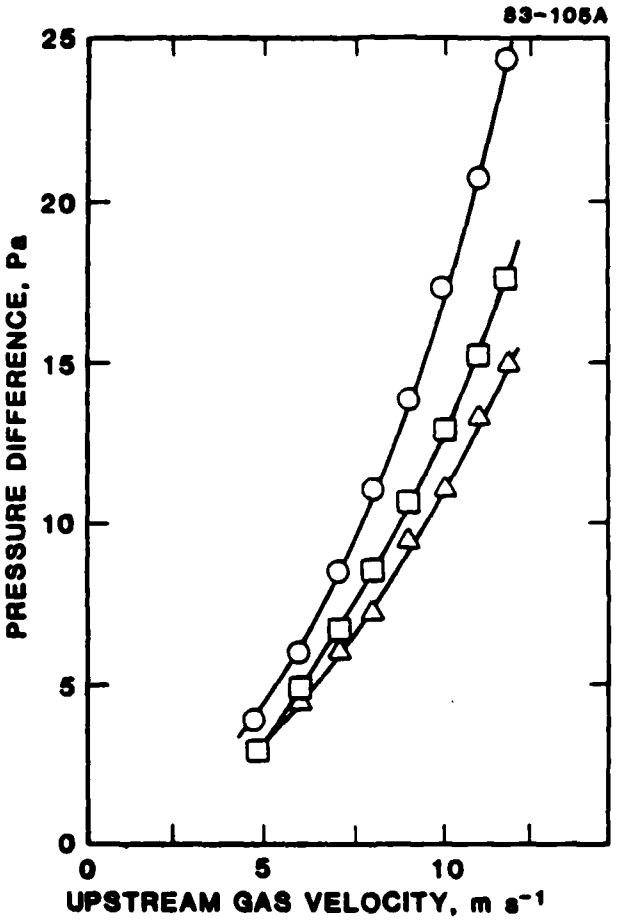

O = solid bluff body; □ = partially blocked ceramic honeycomb (31 cells cm^{-2}) with 89 cells open; Δ = ceramic honeycomb with 157 cells open. All results for 300 K air flows.

FIGURE 11. PRESSURE DROPS FOR 2.79 cm o.d. FLAMEHOLDERS

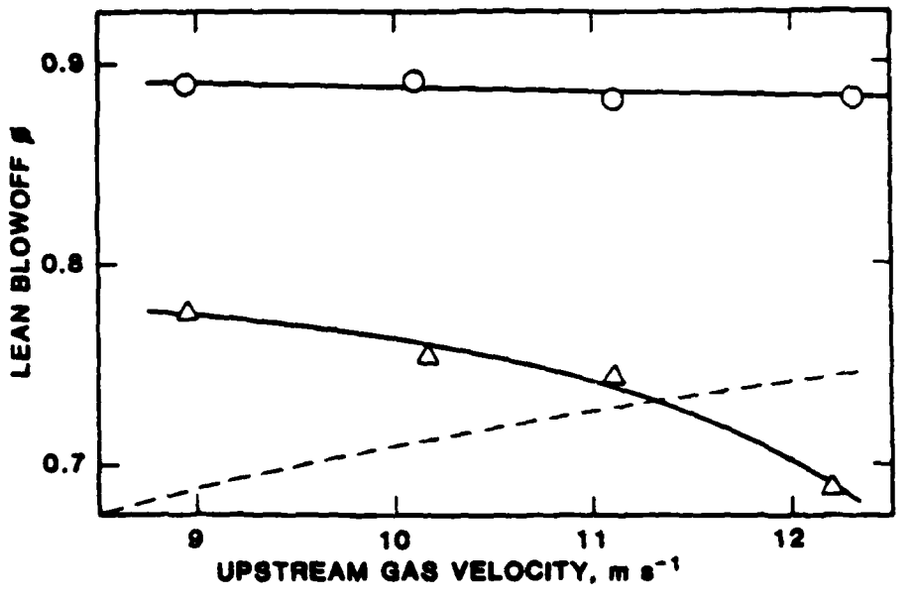

FIGURE 12. COMPARISON OF BLOWOFF LIMITS FOR 2.79 cm diam CERAMIC HONEYCOMB FLAMEHOLDERS AND 2.87 cm diam SOLID BODY FLAMEHOLDER

Δ ≈ catalytic
o ≈ noncatalytic
Dashed line ≈ solid body

The findings of this program show that catalytically coated ceramic (or other material) flameholders may be a promising approach to enhanced stabilization of highly diluted partially combusted gas streams such as those exiting the main burner section of a gas turbine engine. The conditions necessary for efficient combustion while employing catalytic flameholders must, however, be more thoroughly investigated before practical catalytic combustors can be manufactured.

Primary practical disadvantages of the catalytic flameholders used in this feasibility study appear to be associated with the ceramic substrates, which in the case of Cordierite, restrict operation to rather low temperatures. In the case of some other ceramics suitable for higher temperatures, the substrates are susceptible to fracture due to thermal shock and are less porous. The palladium catalyst investigated in this program is also probably not practical in view of its significant vapor pressure at temperatures above 1500 K.

In view of the progress achieved on this program and the potential advantages of catalytic enhanced flame stabilizations, the following recommendations are made:

1. A similar program should be performed to compare catalytic and noncatalytic honeycomb flameholders in a larger diameter combustor and at higher velocities. The larger combustor would reduce wall interactions and a wider range of velocities would better define the variation of blowoff limits with velocity.
2. Further studies of the CO, CO_2, and hydrocarbon emissions should be performed along with (1) above.
3. Catalytic flameholder substrates other than the Cordierite used in this work should be tested. These substrates would include other coated ceramics, coated metals, and ceramics incorporating the catalysts into their lattice.
4. Catalytically active coatings other than palladium should be tested.
5. Tests should be performed under conditions of pressure, velocity, inlet temperature, and fuel air ratio which more closely simulate the practical combustors of interest, and jet fuels should be used for the tests.

The above recommendations define the direction of future work but are not meant to be comprehensive. Whether this technique can eventually be practical is not clear at this time but an evaluation can probably be made after some of the recommended additional experiments have been performed.

- Analytical Modelling

Mathematical modeling of catalytic, porous flameholders was divided into two parts. In the first part, conditions within the porous flameholder were modeled. Here catalytic reactions are dominant. The second part considers the slow split around and through the flameholder as well as the critical wake/recirculation region where the actual flame stabilization occurs.

Description of the internal catalytic combustion processes is the most advanced and tested part. Flexibility and utility is provided by the simultaneous consideration of the relevant chemical and physical processes using a one-dimensional, steady state, plug flow model with global reaction rates. Heterogeneous (catalytic) and homogeneous (gas-phase) reactions, velocity variation, and axial heat conduction in the catalytic substrate are included as are diffusion and temperature-dependent surface kinetics for the heterogeneous reactions. Combustion initiation (light-off) and extinction limits are particularly dependent on the processes included in the model. Appendices II and III provide a more detailed description of this part of the model. In particular, Appendix III demonstrates the excellent agreement between the catalytic model and experimental results.

The second part of the modeling effort considers the aerothermochemistry occurring external to the catalytic flameholder as depicted conceptually in Fig. 13. This model is based on the usual wake recirculation formulation, as influenced by the work of Zukoski and Marble (17,18) on critical ignition times. The split of flow through and around the catalytic monolith is determined by pressure drop considerations. The flow into the recirculation zone is thus the sum of the flow through the monolith and that resulting from turbulent inclusion. Even in the absence of catalytic effects, the need to account for flow through the flameholder represents a departure from the usual solid body flameholder description. The distance needed for a flame to develop is predicted as a product of mean convective velocity and reaction time obtained from the analysis of Kunder et al. (8) and compared to a recirculation zone length calculated on the basis of flow parameters. Comparison of these lengths allows the determination of blowout or flameholding.

In this way, this model allows:

1. Description of the influence of overall geometry, blockage ratio, and substrate configuration on aerodynamic and thermodynamic variables, especially pressure drop.
2. Determination of the degree of approach flow penetration through the catalytic section, recirculation zone size and shape, and shear layer characteristics.
3. Description of the concept's ability to widen stability and ignition limits and to widen the cross-sectional area occupied by the stabilization devices.

Additional details on this flameholder model development is provided in Appendix IV.

If further research on the porous catalytic flameholder's concept is undertaken, a full model combining the two models (part 1 and 2) should be developed. Together with experimental results, this complete model would form the basis for performance optimization and extension of the work to practical combustor systems.

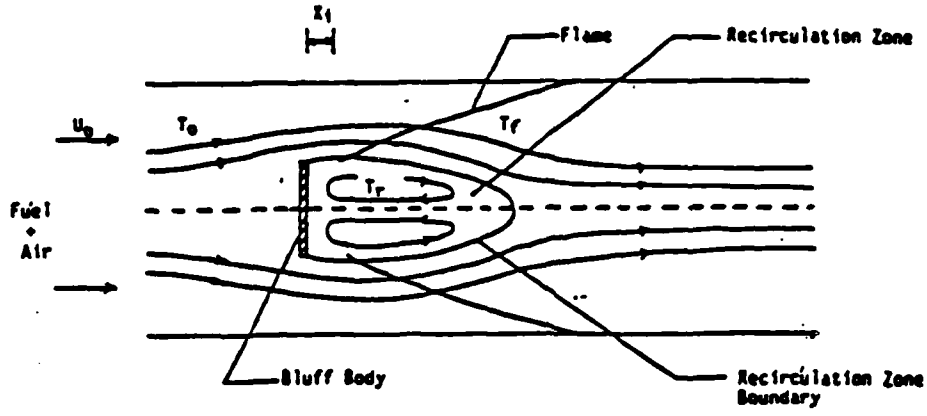

a. FLAME STABILIZATION BEHIND A BLUFF BODY

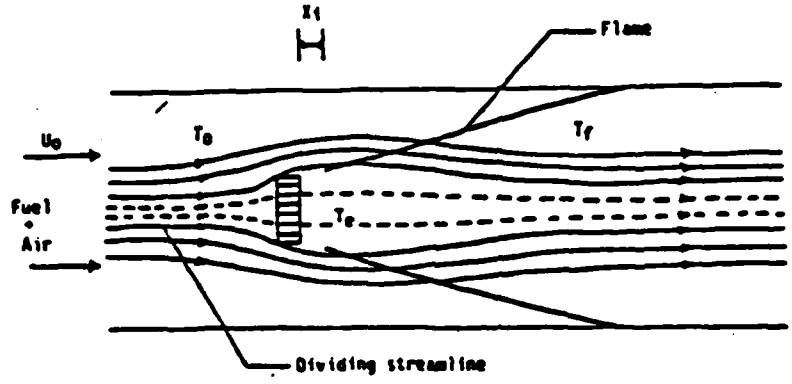

b. FLAME STABILIZATION BEHIND OPEN CATALYTIC MONOLITH
(NO RECIRCULATION ZONE)

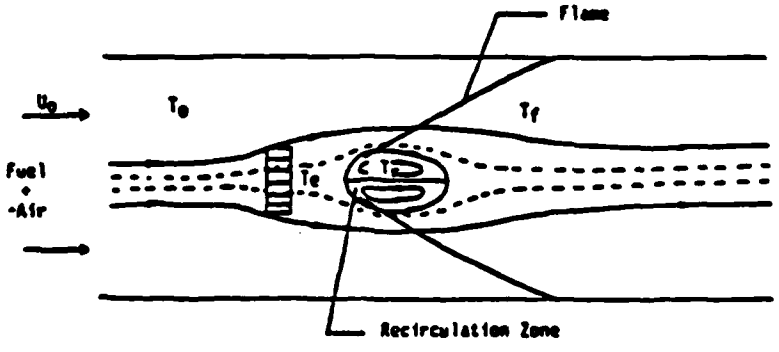

c. FLAME STABILIZATION BEHIND LOW POROSITY CATALYTIC MONOLITH
(RECIRCULATION ZONE FORMED)

FIGURE 13. BLUFF-BODY AND CATALYTIC FLAMEHOLDERS

CONCLUSIONS AND FUTURE WORK

Both the radiative and catalytic techniques have demonstrated the capability to enhance combustion processes and to broaden normally encountered stability limits.

The work on radiative ignition and combustion enhancement is providing fundamental information on two novel combustion processes. Concepts which represent a new departure and extension of conventional combustion practice can evolve from the experimental data being obtained. Aspects of the radiative ignition and enhancement concept have been demonstrated under static (no flow) conditions. Successful pulsed light source ignition experiments confirm the radiative augmented concept and demonstrate the technical feasibility of designing an advanced optical-radiative igniter. Successful ignition with a continuous light source implies the possibility of using the light as an optical radiative flame stabilizer (with zero pressure drop) instead of the conventional flameholders. The ability to use laser radiative sources further broadens the future potential of the photoaugmentation technique. Rather than point ignition or local enhancement, line ignition or area ignition (by using optical scanning) may be possible with lasers. The results of combustion enhancement in terms of higher flame propagation velocities and extended extinction times and distances demonstrate a potential opportunity to extend the combustor operating limits by utilizing the radiative technique. It is construed that the enhanced flame propagation can be translated into higher combustion rate and extended flammability limits.

From the experimental results reported here we gain confidence that radiative augmented combustion is a potentially viable technique to extend current aircraft operating limits. Eventual application to gas turbine engine systems is envisioned both for improved combustor operation and flameholding. Some future areas of potential application are: high altitude combustor reignition following flame-out, drag-free flame stabilization in supersonic combustors, and added flexibility for conventional combustors to use future alternate fuels. To this end, radiative ignition and combustion enhancement experiments under flow conditions are required as well as continued VUV light source development in the direction of improved beam optics.

The catalytic flame stabilization concept is particularly important to aeropropulsion combustion: turbopropulsion mainburners, afterburners, duct burners, and ramjet dump combustors. Potential benefits include improved ignitability, stability as well as efficiency, and combustion design flexibility for alternate fuel usage. In the afterburner application, the conventional bluff-body flameholder can be replaced by a porous catalytic device resulting in less pressure drop than a solid flameholder of equal cross-sectional area. It can broaden afterburner stability range by allowing for operation at inlet velocities, temperatures, and fuel mixtures where conventional flameholders begin to fail. In addition, it has the advantage of being a passive autoignition device. Additional catalytic flameholding experiments should be performed at higher reactant flow rates where the maximum benefit of the catalytic flameholders can be realized. Further development of high temperature substrate material is also required.

In both the photochemical and catalytic areas, continued development and use of the mathematical models will provide maximum flexibility in experimental design and analysis, and for transfer of the concepts to practical combustor systems.

REFERENCES

1. Cerkanowicz, A. E., "Photochemical Enhancement of Combustion and Mixing in Supersonic Flows", Final Report, AFOSR-TR-74-0153, November, 1973.

2. Cerkanowicz, A. E., Levy, M. E., and McAlery III, R. F., "Photochemical Ignition of Gaseous Fuel-Oxidizer Mixtures at Subatmospheric Pressures", Final AFOSR Scientific Report No. 70-1664, April 1970.

3. Cerkanowicz, A. E., "Photochemical Initiation of Sustained Combustion in Unsensitized Gaseous Fuel-Oxygen Mixtures", Ph.D. Dissertation, Stevens Institute of Technology, June 1970.

4. Cerkanowicz, A. E., Bartok, W., Radiation Augmented Combustion", Interim Report AFESR-TR-78-1508, July 1978.

5. Cerkanowicz, A. E., "Radiation Augmented Combustion", Interim Report AFOSR-TR-79-1096, July 1979.

6. Gray, B. F. and Yang, C. H.: J. Phys. Chem., 69, 2747 (1965).

7. Kocharts, G.: Planetary Space Science, 24, 589 (1976).

8. Kundu, K. M., Banerjee, D., and Bhaduri, D., Combustion Science and Technology, Vol. 17, p. 153, 1977.

9. Lavid, M., "Radiation/Catalytic Augmented Combustion", Interim Report AFOSR-TR-80-0287, September, 1980.

10. Lavid, M., "Radiation/Catalytic Augmented Combustion", Final Technical Report AFOSR-TR-82-0132, July 1981.

11.. Lavid, M., "Radiation/Catalytic Augmented Combustion", Interim Report AFOSR-TR-82, May 1982.

12. Lewis, B. and Von Elbe, G.: Combustion, Flames and Explosion of Gases, 2nd ed., p. 334, Academic Press, 1967.

13. Lovachev, L. A. and Lovachev, L. N., Combustion Science and Technology, 23, 181, 1980.

14. Lund, C., HCT - A general computer program for calculating time dependent phenomena involving one-dimensional hydrodynamics, transport, and detailed kinetics, Report UCRL-52504, Univ. California, Lawrence Livermore Lab., Aug. 1978.

15. Sutherland, C. D. and Zinn, J., Chemistry Computations for Irradiated Hot Air, Los Alamos Laboratory Report No. LA-6055-MS, Los Alamos, New Mexico, September, 1975.

16. Westbrook, C. K. and Dryer, F. L., "Prediction of Laminar Flame Properties of Methanol - Air Mixtures", Combustion & Flame, 37, pp. 171-190, 1980.

17. Zukoski, E. E., and Marble, F. E., "The Role of Wake Transition in the Process of Flame Stabilization on Bluff Bodies", Combustion Researches and Reviews, pp. 167-180, Butterworths, 1955.

18. Zukoski, E. E., and Marble, F. E., "Experiments Concerning the Mechanism of Flame Blowoff from Bluff Bodies", Proc. Gas Dynamics Symposium, pp. 205-210, Northwestern University, 1956.

STATEMENT OF WORK

The work statement covering the contract period April 1981 through March 1983 is presented below. The contractor shall furnish scientific effort, together with all related services, facilities, supplies and materials needed to conduct the research.

(1) Radiative Augmentation

A. Static Experiments

1. Continue radiative static combustion experiments. Use pulsed ILC and continuous EIMAC light sources to determine and measure photochemical ignition and combustion enhancement.

2. Select and employ appropriate vacuum ultraviolet lasers to conduct radiative static experiments. Investigate the dependence of radiative ignition and enhancement on light wavelength. Identify the most effective wavelength widths(s) for augmentation and applications.

B. Flow Experiments

1. Provide a combustion test facility to conduct radiative and catalytic experiments under flow conditions. Use advanced diagnostics where necessary to obtain high quality experimental data.

2. Design and conduct radiative experiments under flow conditions. Investigate radiative effects on ignition and combustion enhancement in premixed flowing reactive mixtures subjected to pulsed or continuous vacuum ultraviolet light. The objective is to attempt to demonstrate radiative augmentation under flow conditions.

C. Analytical Modeling

1. Incorporate the emission characteristics of the light sources used into the current combustion initiation model. Compare the experimental data with the model result. Use the model to elucidate the photoabsorption-kinetics interaction and to assist in system optimization. Include heat loss mechanism, species diffusion and wall recombination in the model. Undertake additional model revisions and refinements as deemed necessary.

D. Evaluation

1. Analyze and assess the experimental and analytical results, particularly as they apply to application in practical combustion hardware.

2. Develop a test plan for larger scale combustion tests of the most promising radiative augmentation technique(s).

(2) Catalytic Augmentation

A. Design and Acquistion

1. Design, fabricate, and/or acquire catalytic flameholders. Evaluate and screen chemical and physical characteristics of flameholders to determine best candidates for flow experiments.

B. Flow Experiments

1. Perform experimental flame stabilization tests on a standard V-gutter, and non-catalytic and catalytic monoliths under both non-reacting and reacting flow conditions.

2. Perform experimental flame stabilization test on best flameholder candidates determined in Work Statement (2)A.1.

C. Analytical Modeling

1. Review and revise existing catalytic flameholding model to obtain a sufficiently detailed, balanced engineering model. Compare model predictions to experimental data to ascertain agreement and resolve any discrepancies in regimes of interest. Use the model to explore the interaction of aerodynamic effects and catalytic and homogeneous combustion. Utilize the model, as an adjuct to the experimental effort in initially analyzing the data and ultimately in performance optimization.

D. Evaluation

1. Analyze and assess the experimental and analytical results, particularly as they apply to application in practical combustion hardware.

2. Develop a test plan for larger scale combustion tests of the most promising catalytic augmentation technique(s).

APPENDIX

I. CATALYTIC FLAME STABILIZATION (AeroChem)

II. CASE STUDIES IN THE SIMULATION OF NOVEL COMBUSTION TECHNIQUES

III. CATALYTIC COMBUSTION MODELLING: COMPARISONS WITH EXPERIMENTAL DATA

IV. CATALYTIC FLAME HOLDING MODEL (NSF Supported)

APPENDIX I

Catalytic Flame Stabilization

R. J. Gill and D. B. Olson
AeroChem Research Laboratories, Inc.
P.O. Box 12
Princeton, New Jersey 08540

Prepared for Exxon Research and Engineering Co.
Subcontract ESC-57

Under Contract F49620-81-C-0028

FOREWORD AND ACKNOWLEDGMENTS

This is the final report on a subcontract from Exxon Research and Engineering Co., covering the period 13 October 1982 to 31 March 1983. The authors would like to acknowledge contributions to this program by J.C. Pickens and Drs. H.F. Calcote and C.H. Berman.

TABLE OF CONTENTS

LIST OF FIGURES

LIST OF FIGURES (CONTINUED)

I. INTRODUCTION

The objective of this subcontract was to evaluate the feasibility of using catalytic honeycomb flameholders to expand flame stabilization limits for potential applications such as in aircraft afterburners. This was performed by experimentally evaluating flame stabilization using catalytic and noncatalytic flameholders in a research scale flow tube combustor. Experiments were conducted using premixed propane/air to determine the effects of fuel/air ratio, flow velocity, and flameholder type on the flame stability limits. Several other diagnostics were also used to gauge the efficiency of the flame stabilization and combustion process. These diagnostics included gas temperature profiles in the combustor, flameholder temperatures, pressure drop across the flameholders, and CO and CO_2 concentrations in the burned combustion gases.

High output combustors, such as in turbojet engines, require flame stabilization in a high velocity flow of fuel air mixture within a duct. Since the overall flow velocity is usually much greater than the burning velocity of the mixture, recirculation regions behind solid bodies placed in the flow are often used to create stable pilot flames which serve as continuous ignition sources for the total flow. The theory of flame stabilization due to recirculation zones set up behind bluff bodies has been very thoroughly treated in the literature. Both experimental[1-5] and theoretical[6-8] discussions of this process are available. At sufficiently high velocities the flame will no longer be stable and flame blowoff occurs. The conditions at which this happens are dependent on the flameholder shape, size, pressure, temperature, and fuel air ratio. Maximum stabilization, i.e., highest blowoff velocities, occur at fuel air equivalence ratios near stoichiometric.

In the case of catalytic combustion, the efficiency, product gas composition, and temperature profiles can be modeled and compared with experimental results.[9-16] However, there exist no theoretical or experimental results which detail the effect of porous catalytic flameholders on the flammability limits of gas turbine or research combustors. It was the purpose of this feasibility study to determine whether catalytically active flameholders have wider flame stability limits than do noncatalytic flameholders, and to gather sufficient diagnostic information to permit a preliminary analysis of the results.

II. EXPERIMENTAL FACILITIES

In this section the three major components of the combustor facility are discussed. These components are the flow tube combustor, the flameholders, and the combustion diagnostics.

A. FLOW TUBE COMBUSTOR

The atmospheric pressure flow tube combustor is shown in Fig. 1. The three section brass flow tube is 1.88 m long. The first section (0.39 m length) serves as a mixing chamber for the metered fuel/air mixture. The fuel is commercial grade propane and is metered through a 0.13 cm diam calibrated critical orifice. The air is delivered from dried compressed "house" air (rated capacity of compressor: 550 kPa at 2.35 $m^3(STP)min^{-1}$) and metered through a calibrated orifice (0.68 cm diam).

The fuel/air mixture is radially injected into a 7 cm long, 10.2 cm i.d. section of the flow tube to enhance mixing of the fuel and air. Slightly downstream, a perforated disc (0.32 cm diam holes with 0.48 cm spacing) performs additional mixing. The remainder of this first section (0.32 m) was insulated with alumina cylinders (Zircar Products Inc., Type ALC) which reduced the cross section diameter to 5.1 cm. At the entrance to the insulated portion, a 3 cm long flow straightener fabricated from aluminum honeycomb (roughly circular 0.32 cm diam cells) was situated. Near the end of this first section, a pressure port was installed for connection to the reference side of a differential pressure transducer. Unless otherwise specified, all feedthrough connections to the combustor were made using brass 1/4 in. Swagelok fittings.

The second or middle section of the combustor housed the flameholder. This 0.26 m long, water cooled section (Fig. 2) was fabricated from 5.3 cm i.d. brass tubing with no internal alumina insulation. This water cooled section was used to reduce the operational temperature of the flameholders and to prevent flame stabilization on the hot alumina insulation. Several feedthroughs were provided. Two 1/8 in. Swagelok feedthroughs (1.7 cm apart) provided support and cooling water to the flameholder support. Two Swageloks (a 1/4 in. and a 3/8 in. fitting) were equipped with cemented glass windows for observing the flameholder and the flame front. These two ports were water cooled externally to prevent the epoxy cement from degrading. The (1/4 in.) Swagelok port alternatively served as a thermocouple wire feedthrough when flameholder temperatures

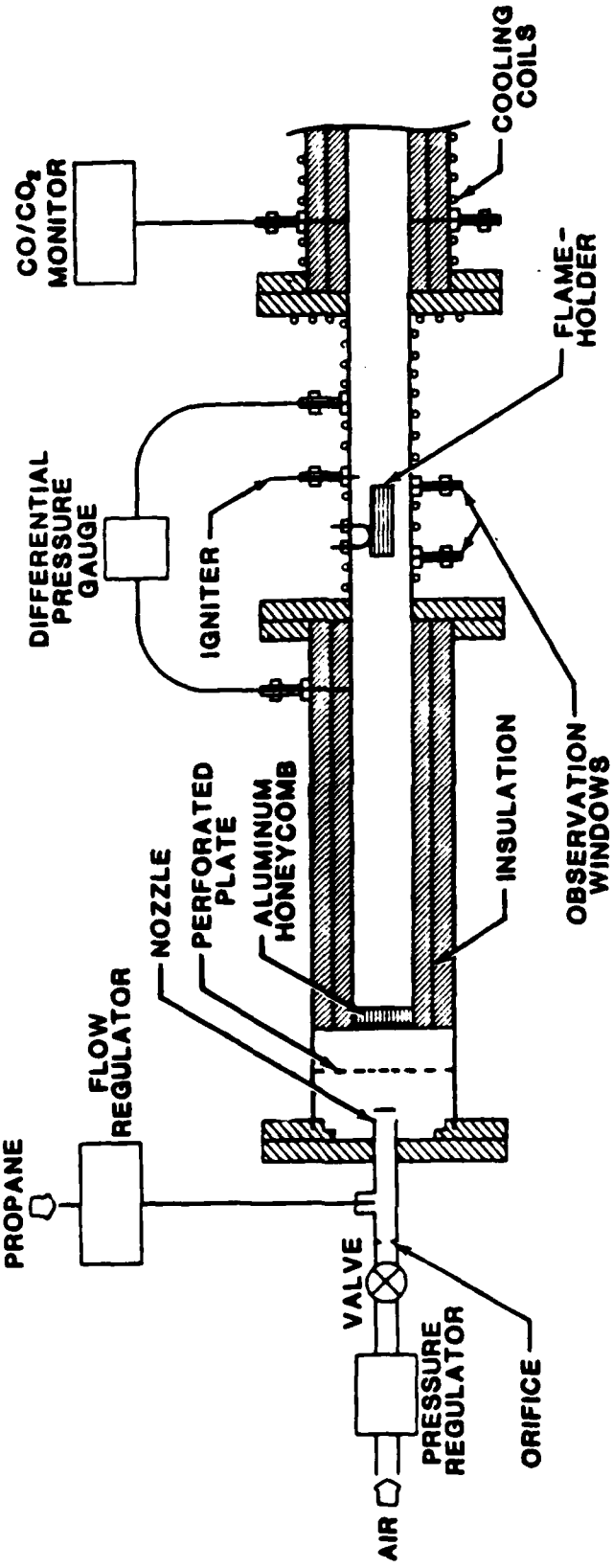

FIGURE 1 FLOW TUBE COMBUSTOR

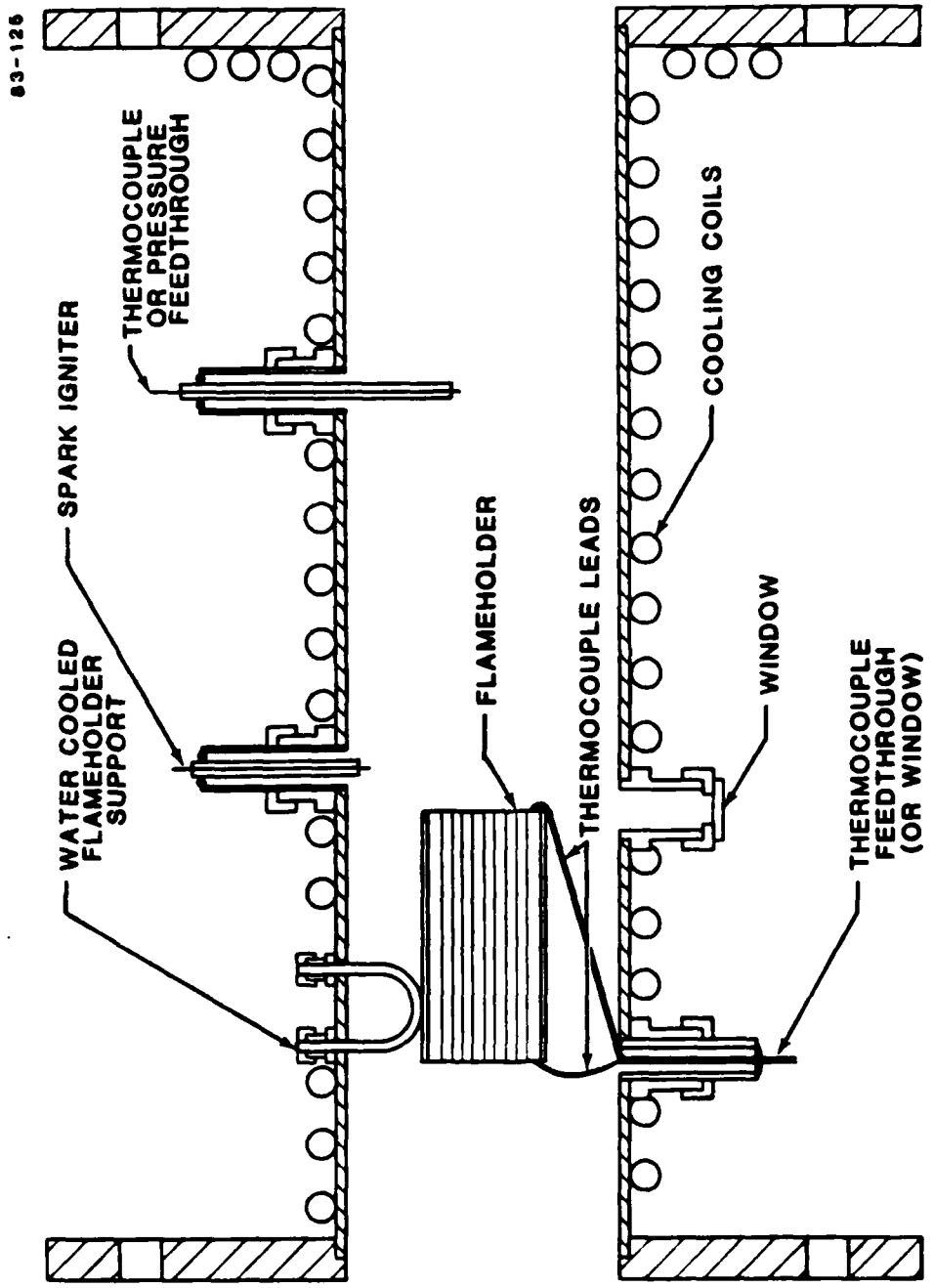

FIGURE 2 MIDDLE COMBUSTOR SECTION

Length = 26 cm.

were measured. Just downstream of the flameholder another feedthrough was equipped with a ceramic tube insulated spark ignition wire which could be inserted and withdrawn from the combustion gas stream. A feedthrough, located 8.4 cm downstream from the flameholder, provided a port for a thermocouple probe or pressure measurements.

The final combustor section, 1.23 m in length, was lined with 5.1 cm diam alumina insulation for its entire length. Several (1/4 in.) Swagelok feedthroughs were provided at 15 cm spacings for various diagnostic probes, such as thermocouples and combustion gas sampling. The exterior tube wall was water cooled.

B. FLAMEHOLDERS

Three types of flameholders were used in this work. These cylindrical flameholders, either catalytic or noncatalytic ceramic honeycomb, or solid brass were held within a (2.8 cm o.d., 2.5 cm i.d., 5.1 cm long) tubular stainless steel housing supported by a loop of 0.32 cm diam stainless steel tubing as shown in Fig. 3. The "U-tube" support was silver soldered to the flameholder housing and was water cooled. Swagelok feedthroughs supported the whole flameholder.

The ceramic flameholders, both catalytic and noncatalytic, were fabricated from Cordierite monolithic cylindrical shaped honeycomb plugs (2.5 cm o.d. and 5.1 cm length; Corning No. 9475) having 31 square cells per cm^2 cross section and cell walls 0.03 cm thick. Cordierite[17] is a magnesia, alumina, silica composite which has a maximum operating temperature of $\sim$ 1570 K, a porosity of about 30%, and a mean pure size of 3.5 μm. Its thermal conductivity is about twice as high in a parallel direction to the cells as it is in a perpendicular direction. Also, it has a low (1×10^{-6} per °C) thermal expansion coefficient. The catalytic ceramic flameholders were custom prepared by a vendor[18] by repeated inpregnation of Cordierite with an organic palladium solution and drying. The palladium mass loading was 2.0 g per bulk liter of monolith (total volume of honeycomb).

In the experiments reported here, some of the honeycomb flameholder cells, catalytic and noncatalytic, were sealed at each end using Ceramabond 503 adhesive as shown in Fig. 3. A total of 89 cells remained open to the fuel/air gas stream with 68 cells blocked. This configuration was used to hold the

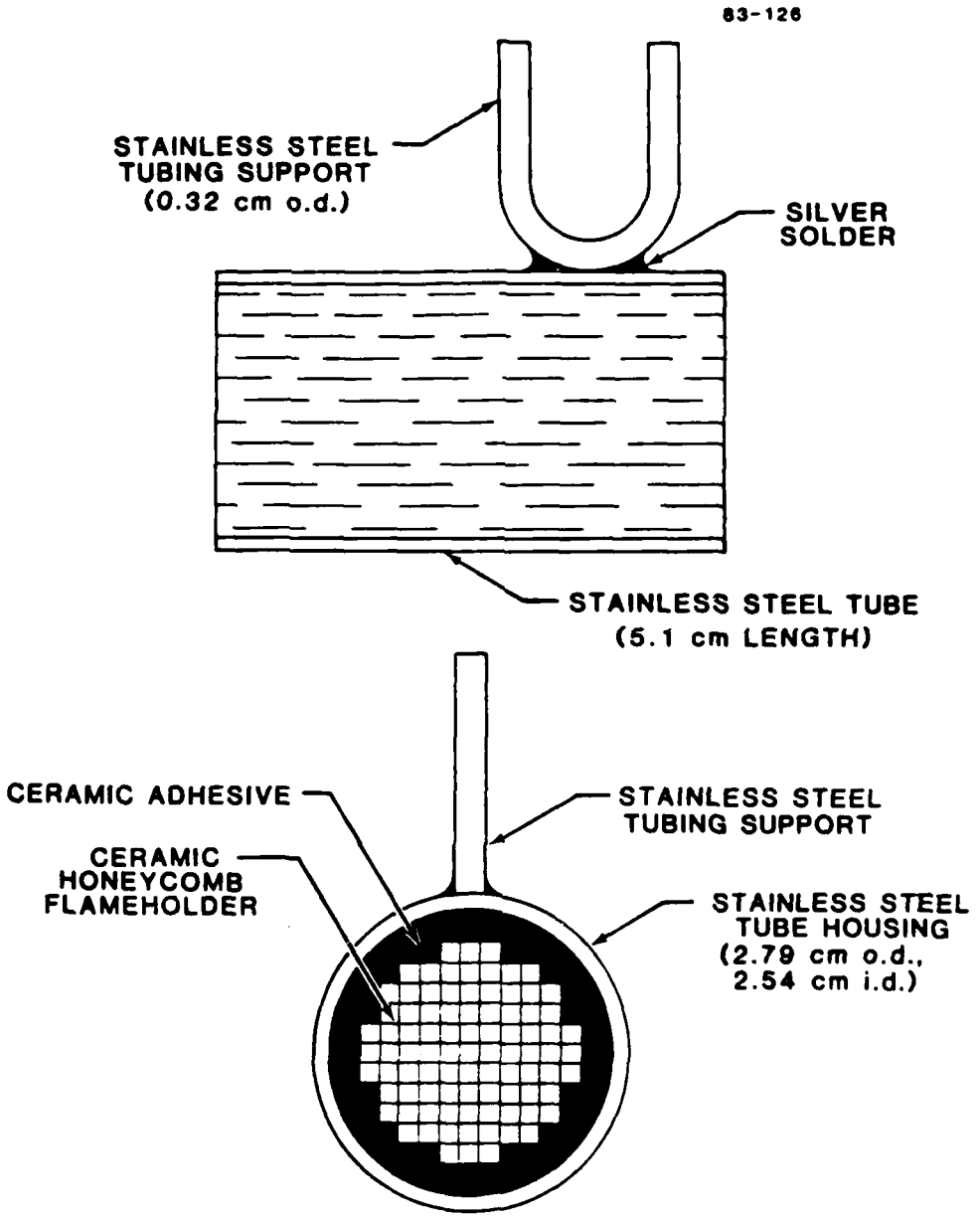

FIGURE 3 FLAMEHOLDER WITH HONEYCOMB INSERT

honeycomb in the steel cylinder and to prevent melting of the Cordierite under combustion conditions (vide infra).

C. COMBUSTOR DIAGNOSTIC INSTRUMENTATION

The apparatus was equipped with three combustion diagnostics. Temperature measurements were made using 0.025 cm diam Pt/Pt-10% Rh (S-type) thermocouples and a calibrated Omega Model 199 digital temperature readout. Dual bore alumina tubing was used to insulate the thermocouple leads. The thermocouple junctions were protected with a thin (less than 1 μm thick) beryllia-yttria coating, and were in direct contact with the combustion gases. Flameholder temperatures were measured using similar thermocouples buried in the ceramic adhesive at either end of the honeycomb.

The pressure drop across the flameholders was measured using a differential pressure transducer (Validyne Engineering Corp. Model DP15-22). The reference side of the transducer was connected upstream of the flameholder (see Fig. 1) while the other side of the transducer was connected to a port 8.4 cm downstream of the flameholder. The connections were made with copper tubing. The differential pressure range for this transducer was 1.3 kPa (10 Torr) with a linearity of ± 0.5% of full scale sensitivity.

At a position 0.25 m downstream of the flameholder, a gas sampling port was attached to the flow combustor. The undiluted, continuously sampled combustion products were analyzed for CO and CO_2 content using a nondispersive infrared (NDIR) analyzer manufactured by Horiba Instruments Inc. (Model MEXA-300B). This instrument measures CO in the range of 0-7% (volume percent) and CO_2 in the range of 0-15%. Reproducibility is quoted as ± 2% of maximum CO or CO_2 concentration. This analyzer was also tested for sensitivity to hydrocarbons. The CO_2 analysis was found to be weakly sensitive to a gas stream of pure methane (100% CH_4 gave an apparent CO_2 concentration of ca. 1%). Both CO and CO_2 detectors were found to give no significant response to pure acetylene, pure propane, or water saturated air streams.

These CO and CO_2 measurements (especially the CO concentrations) were expected to be sensitive to details of the flame stabilization process near blowoff. Preliminary chemiluminescence NO_x measurements were made but were discontinued because of strong water interferences.

III. RESULTS AN DISCUSSION

The basic experimental objective of this work was to establish the effect of catalytic flameholders upon the flame stability limits in a research scale, flow tube combustor. Several different flameholder diameters and honeycomb cell sizes were originally scheduled for detailed testing. However, it was determined experimentally that most of the ceramic flameholders (only Cordierite honeycomb was available for tests) melted before combustion diagnostics could be performed. Monoliths of 5.1 cm length, 2.79 cm and 1.44 cm overall diameters, and cell densities of 31, 62, and 93 cells per cm^2 were tested. All combinations gave only short combustion service lifetimes. Only the 2.79 cm diam honeycombs having 31 cells per cm^2 and modified by sealing off some of the outer cells (Fig. 3) gave reasonable lifetimes. Therefore, all the results presented below are for this type of flameholder.

A. PRESSURE DIFFERENCE MEASUREMENTS

One method of determining if a specific flameholder or a bluff body causes a significant mechanical power loss ("insertion loss") is to measure the pressure drop across the body. It is reasonable to expect a larger pressure difference across a solid body than across a more porous body, such as the ceramic honeycombs. Higher gas flow velocities are expected to increase the pressure differences across the bodies. Both of these effects are fully manifest in the room temperature flow experimental data obtained for a solid bluff body, a fully open honeycomb, and a partially blocked honeycomb as shown in Fig. 4. It should be noted that the magnitudes of the pressure drops are rather small. Even for the highest air flow velocity (ca. 12 m s^{-1}), the drop is only 25 Pa (ca. 3×10^{-4} atm). Also note that the velocities given are for 300 K gas and for flow through the total combustor cross section. In the annular region around the flameholder the velocities are larger due to partial blocking of the combustor cross section. The solid bluff body blocked 28% of the total combustor cross section.

It is of interest to compare the experimental results for the solid bluff body with a theoretical result. Using simple arguments from fluid mechanics[19] one obtains the following expression based on conservation of flow field momentum:

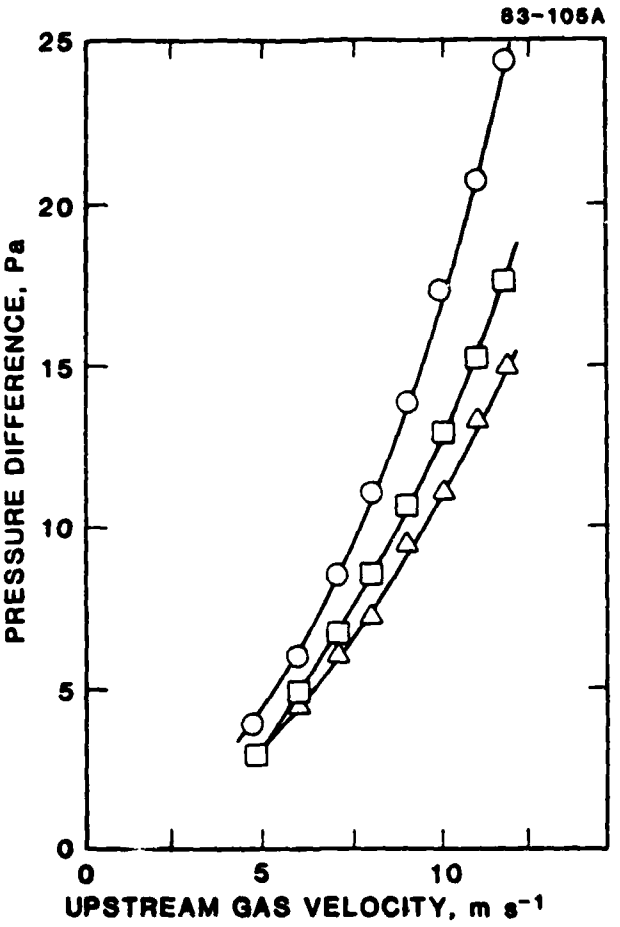

FIGURE 4 PRESSURE DROPS FOR 2.79 cm o.d. FLAMEHOLDERS
O = solid bluff body; □ = partially blocked ceramic honeycomb (31 cells cm^{-2}) with 89 cells open; Δ = ceramic honeycomb with 157 cells open. All results for 300 K air flows.

$$A_1 \Delta P = C_D A_2 \left(\frac{1}{2} \rho \bar{V}^2 \right)$$

where:
- A_1 = flow tube area upstream of flameholder (22.1 cm^2)
- A_2 = cross section area of flameholder (6.1 cm^2)
- C_D = empirical drag coefficient ($\approx$ 0.8 for Reynolds numbers of $\approx 10^4$, Ref. 19)
- ΔP = pressure drop (Pascals)
- ρ = mass density of air (1.2×10^{-3} g cm^{-3})
- $\bar{V}$ = average upstream air velocity (cm s^{-1})

Using this expression, we estimate for the solid bluff body ΔP = 11, 14, 17, and 20 Pa for 8.9, 10.2, 11.2, and 12.4 m s^{-1} average upstream air velocities. At 10.2 m s^{-1} the experimental result is 18.1 Pa or a 23% difference. Thus for solid bluff bodies, the pressure drop, ΔP, can be approximated using the above expression. Probably a much better comparison could be obtained using an experimental C_D. Porous bodies will, of course, offer a smaller resistance to the flow and will result in smaller pressure drops. However, since drag coefficients for honeycomb structures are not available, a similar calculation of pressure drop cannot be made.

B. BLOWOFF LIMITS

In this program, the effect of catalytic honeycomb flameholders as compared to noncatalytic honeycomb and solid body flameholders were of interest. Fuel-rich blowoff limits were found to be nonreproducible. Also the flames oscillated between flameholder attachment and lift-off over a relatively wide range of fuel/air ratios causing difficulties in determining the blowoff limit. Therefore, our efforts were directed towards measurement of fuel lean blowoff limits which were more reproducible, and are of more practical interest.

Before discussing the honeycomb flameholder results, the lean blowoff limits* for three solid flameholders will be presented (Fig. 5). The flow

*In this report, the equivalence ratio, ϕ, is defined as

$$\phi = \frac{(\text{fuel/air})_{\text{actual}}}{(\text{fuel/air})_{\text{stoichiometric}}}$$

The stoichiometric fuel/air ratio is calculated based on complete combustion of fuel to CO_2 and H_2O.

velocity refers to the unburned gas velocity upstream of the flameholder. These data indicate that the lean blowoff limits are dependent on the diameter of the cylindrical flameholder (as would be expected) but in the inverse order to that expected. One anticipates wider blowoff limits (i.e., smaller fuel lean blowoff equivalence ratios) for the larger solid body flameholder. The experimental results are in the opposite order--the smallest diameter flameholder shows the lowest lean blowoff limits. However, if the lean limits are replotted as a function of the (unburned) gas velocity in the annulus between flameholder and combustor inner wall, the results become independent of flameholder diameter as shown in Fig. 6.

This result can be qualitatively understood in terms of two competing processes. The flames should be more stable for larger flameholder diameters[20] (blowoff velocity $\propto d^{0.45}$) but the annular flow velocity increases for larger flameholders, decreasing the flame stability. Plotting the data as a function of annular velocity should show the true variation of blowoff velocity with flameholder diameter, but Fig. 6 shows no significant systematic variation. For a $d^{0.45}$ dependence, we estimate relative blowoff velocities of 1.00, 0.91, and 0.66 for 3.56, 2.87 and 1.44 cm o.d. flameholders (normalized to d = 3.56 cm). The 10% difference between the 3.56 and 2.87 cm diam flameholders would not be visible considering the scatter in these data. For the d = 1.44 cm flameholder only two points were measured and the accuracy of the blowoff limit is estimated to be significantly poorer, so even the absence of an observed trend in these data is not surprising. Also in this work the flameholders were of significant size relative to the combustor diameter. In this case it would not be unexpected to see that flame interactions with the combustor wall affect the blowoff limits.

To measure the effect of a catalytic flameholder upon the blowoff limits, two types of partially blocked Cordierite honeycombs were tested. One type was palladium coated whereas the other was uncoated. They were otherwise identical. When tested in the flow tube combustor, the results shown in Fig. 7 were obtained. Not only does the palladium coated flameholder show a consistently leaner blowoff limit (smaller ϕ), but, in addition, the limiting equivalence ratios decrease at higher flow velocities. This is an unexpected result since normally solid body limits shift toward stoichiometric with increasing velocity. At the relatively small velocities utilized here, this shift is expected to be slight, so the fact that the noncatalytic blowoff limits show no

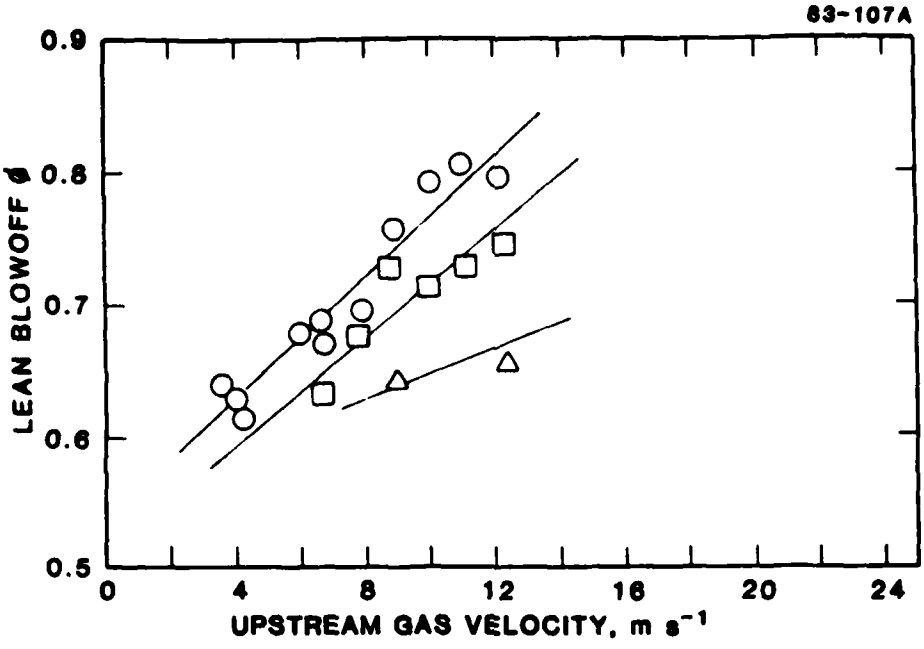

FIGURE 5 BLOWOFF LIMITS FOR SOLID BODY FLAMEHOLDERS

○ = 3.56 cm diam; □ = 2.87 cm diam; △ = 1.44 cm diam.

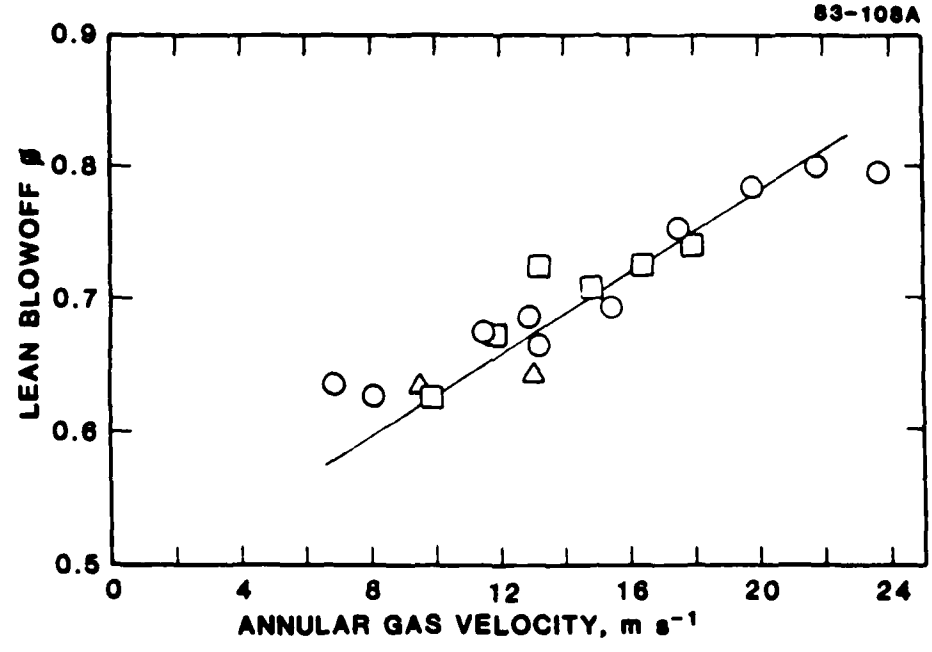

FIGURE 6 BLOWOFF LIMITS FOR SOLID BODY FLAMEHOLDERS

○ = 3.56 cm diam; □ = 2.87 cm diam; △ = 1.44 cm diam.
Gas velocity for annular region between flameholder and combustor wall.

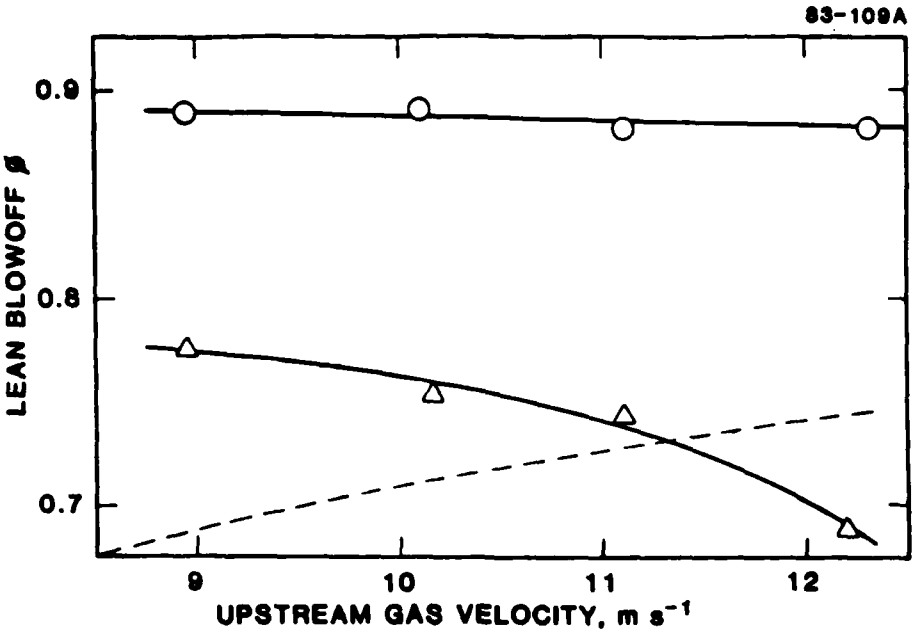

FIGURE 7 COMPARISON OF BLOWOFF LIMITS FOR 2.79 cm diam CERAMIC HONEYCOMB FLAMEHOLDERS AND 2.87 cm diam SOLID BODY FLAMEHOLDER

Δ = catalytic; O = noncatalytic.
Dashed line = solid body. Data as in Fig. 5.

slope is not surprising. Both of these observations strongly suggest that a catalytic flameholder should be more resistant to "flame-out" caused by fuel lean blowoff as compared with a similar noncatalytic flameholder.

The comparison of blowoff limits from a solid body flameholder and honeycomb flameholders of nearly the same diameter is not strictly valid since the honeycomb exhibits a lower pressure drop for a given gas velocity. If the limits were identical, the honeycomb flameholder would be more efficient (smaller pressure drop). Data at higher velocities would be useful in clarifying this comparison, but the available apparatus had a limited velocity span.

C. COMBUSTOR TEMPERATURE PROFILES

Having established the fuel lean blowoff limits for the catalytic and noncatalytic flameholders, several parameters were measured under this range of conditions. The first parameter measured was the axial temperature profile along the flow tube combustor downstream of the flameholder. Because the coated and uncoated flameholder blowoff limits are different, the coated flameholder was operated at both its blowoff limit and at the blowoff limit of the uncoated flameholder in order to make comparisons. Note that it is not possible to operate the noncatalytic flameholder at both sets of conditions. Thus there are three sets of data to compare: (1) the coated flameholder at its blowoff limit conditions; (2) the coated flameholder at the uncoated blowoff limit conditions; and (3) the uncoated flameholder at its blowoff limit conditions.

Actually in each case the equivalence rat was 0.02 unit fuel richer than the reported limit. This results in extremely stable combustor operation.

In Figs. 8 through 11, the temperature profiles for four (unburned) flow velocities tested are shown The origin of the x axis is placed at the upstream face of the flameholder so the first two points are upstream and downstream flameholder temperatures. These flameholder temperatures were measured by embedding thermocouples in the ceramic adhesive at each end of the honeycomb, near the edge. At 8.4 cm, 25 cm, and 40 cm downstream of the origin, gas temperatures were measured. No corrections were made for radiation/convection cooling of the thermocouple data for either gas or flameholder temperatures. Since the insulated combustor walls were hot, radiative losses were much lower than in, for example, an unenclosed flame where the surroundings are cool. Thus the reported gas temperatures are probably slightly lower than actual by approximately 50 K.

With the catalytic and noncatalytic honeycomb flameholders operated under identical conditions (ϕ = 0.89), the temperature profiles at low velocities (8.9 and 10.2 m s^{-1}, Figs. 8 and 9) are essentially identical, both in the gas phase and in the ceramic flameholders. Both flameholders ran quite hot, T > 1000 K, and were hotter at the downstream end than at the upstream end. At the two higher velocities, Figs. 10 and 11, the gas phase temperatures remain nearly identical but the flameholder temperatures are observed to be different under these conditions. The noncatalytic honeycomb is much cooler, with an upstream temperature of about 700 K compared to a catalytic flameholder temperature which is above 1000 K.

The temperature rise observed between the upstream and downstream end of the ceramic flameholders is shown in Fig. 12. These data show that at ϕ = 0.89 both the catalytic and noncatalytic flameholders exhibit similar behavior with a temperature rise of about 300 K at velocities greater than 10 m s^{-1} and a temperature rise of only about 100 K at the lowest velocity. So we see that at the higher flow velocities, the catalytic flameholder runs much hotter but with approximately the same difference in temperature as the noncatalytic flameholder.

When the catalytic flameholder was operated at conditions near its fuel lean blowoff, ϕ = 0.7 to 0.8, significantly different results were obtained. Figures 8 through 11 show that the final gas phase flame temperature is ca. 200 K lower than for the other conditions. Calculated adiabatic flame temperatures with the two sets of conditions, ϕ = 0.75 and ϕ = 0.89 are 1960 K and 2180 K[21] compared with the experimental data taken at 25 cm and 10.2 m s^{-1}

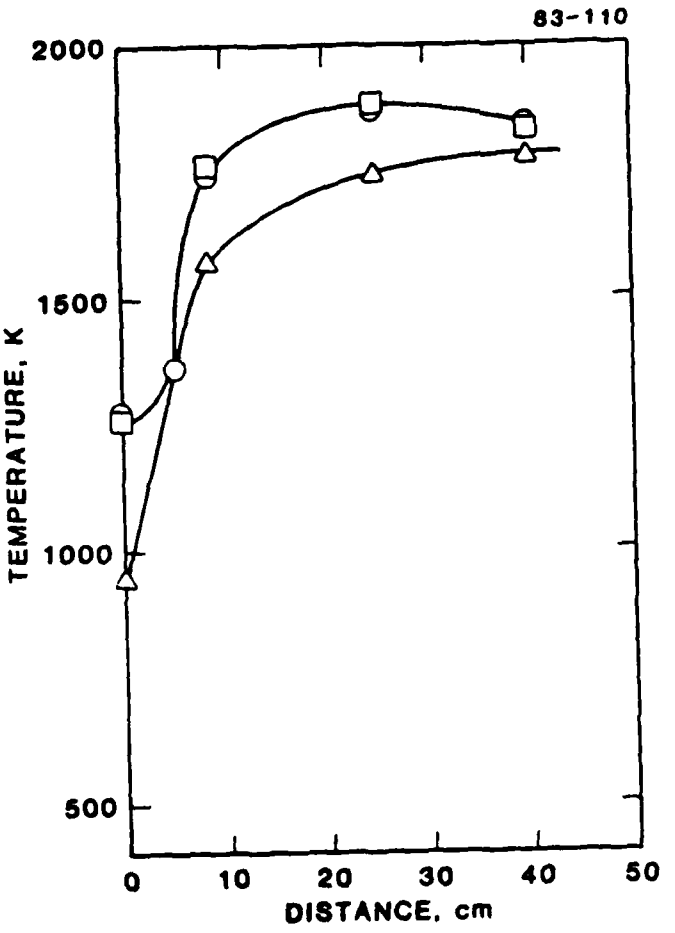

FIGURE 8 COMBUSTOR TEMPERATURE PROFILES USING HONEYCOMB FLAMEHOLDERS

Upstream gas velocity = 8.9 m s^{-1}. O = noncatalytic flameholder, ϕ = 0.89; □ = catalytic flameholder, ϕ = 0.89; Δ = catalytic flameholder, ϕ = 0.78. The distance origin is at the upstream end of the 5.1 cm long flameholder so the first points on each curve are honeycomb temperatures.

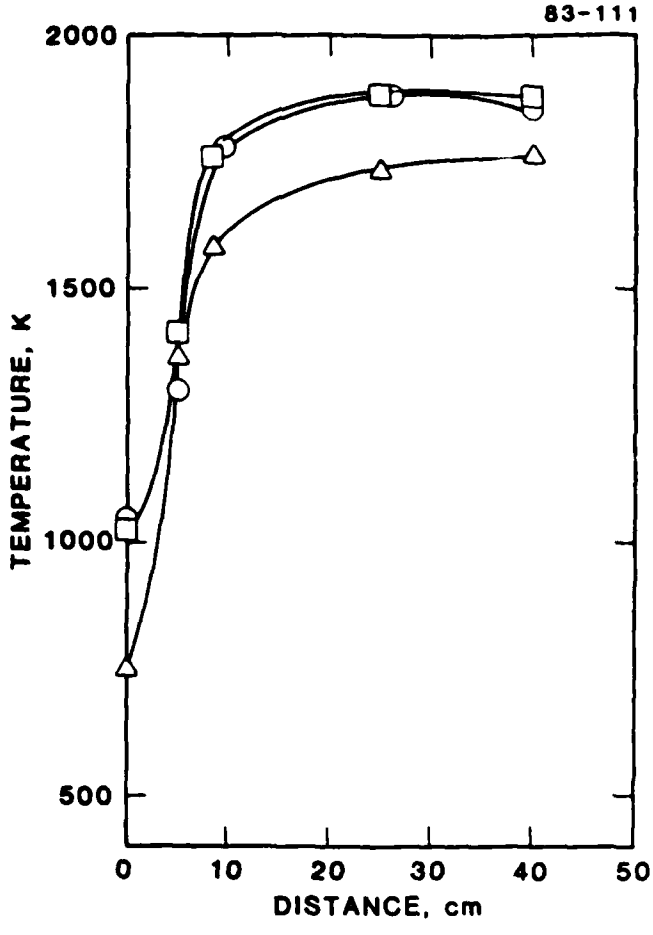

FIGURE 9 COMBUSTOR TEMPERATURE PROFILES USING HONEYCOMB FLAMEHOLDERS

Upstream gas velocity = 10.2 m s^{-1}. O = noncatalytic flameholder, ϕ = 0.89; □ = catalytic flameholder, ϕ = 0.89; △ = catalytic flameholder, ϕ = 0.76. The distance origin is at the upstream end of the 5.1 cm long flameholder so the first points on each curve are honeycomb temperatures.

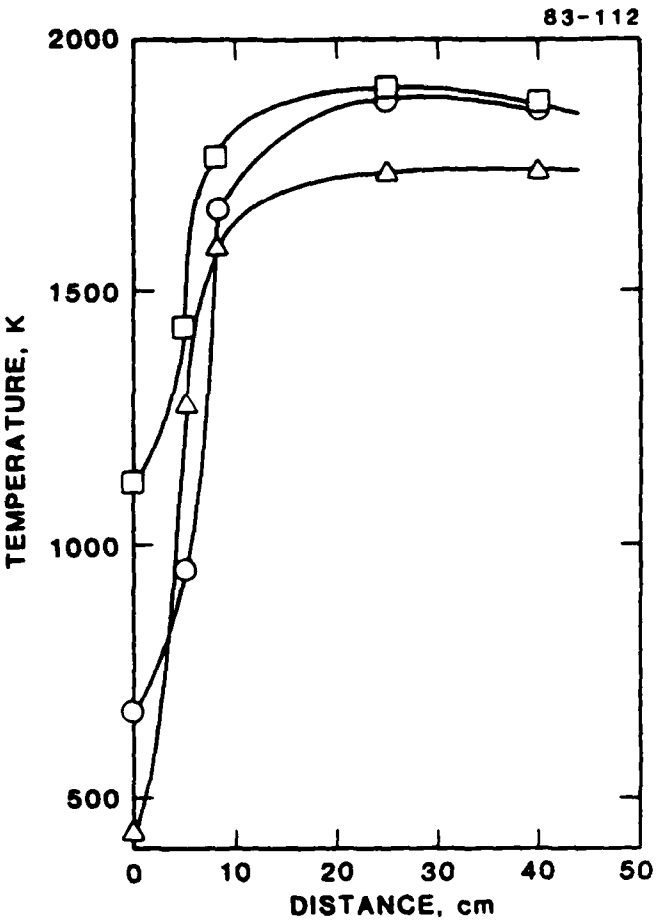

FIGURE 10 COMBUSTOR TEMPERATURE PROFILES USING HONEYCOMB FLAMEHOLDERS

Upstream gas velocity = 11.2 m s^{-1}. O = noncatalytic flameholder, ϕ = 0.88; □ = catalytic flameholder, ϕ = 0.88; Δ = catalytic flameholder, ϕ = 0.75. The distance origin is at the upstream end of the 5.1 cm long flameholder so the first two points on each curve are honeycomb temperatures.

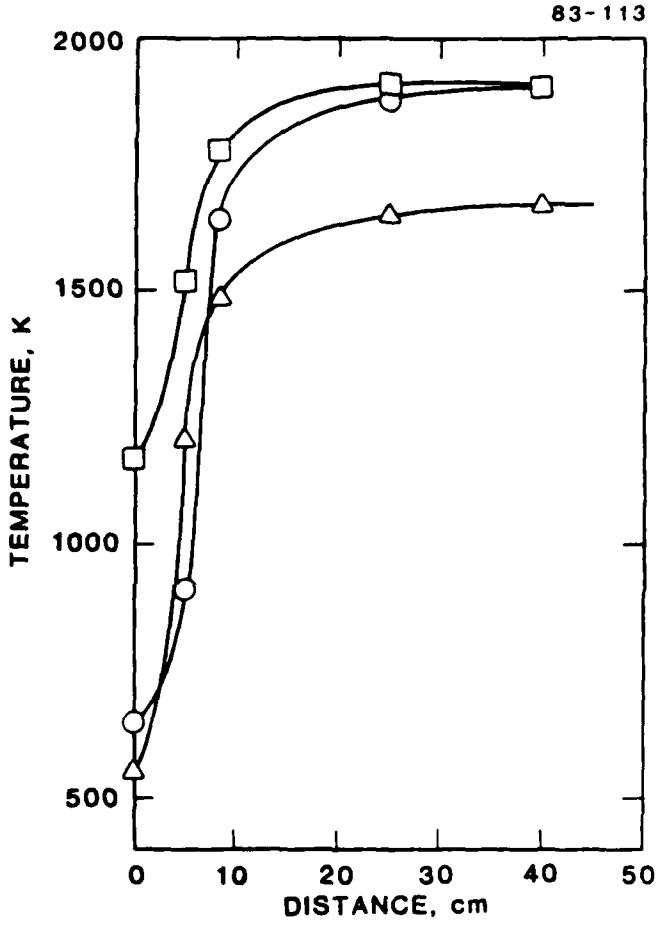

FIGURE 11 COMBUSTOR TEMPERATURE PROFILES USING HONEYCOMB FLAMEHOLDERS

Upstream gas velocity = 12.4 m s^{-1}. O = noncatalytic flameholder, ϕ = 0.88; □ = catalytic flameholder, ϕ = 0.88; Δ = catalytic flameholder, ϕ = 0.71. The distance origin is at the upstream end of the 5.1 cm long flameholder so the first two points on each curve are honeycomb temperatures.

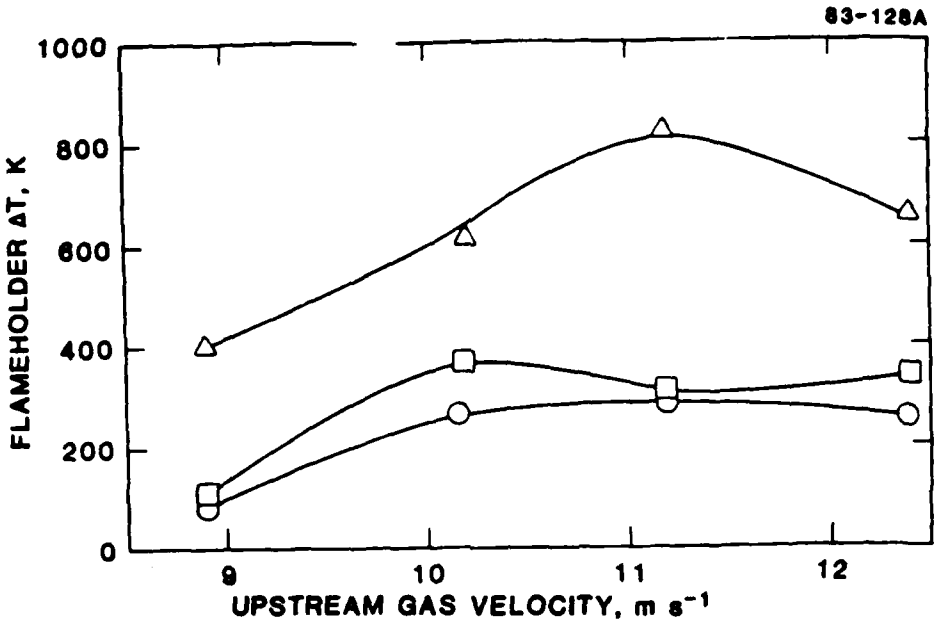

FIGURE 12 TEMPERATURE RISE ACROSS FLAMEHOLDERS.

○ = noncatalytic flameholder; □ = catalytic flameholder, ϕ = 0.88-0.89; △ = catalytic flameholder, ϕ = 0.71-0.78.

which show the experimental temperatures to be about 250 K below adiabatic for both sets of conditions. Thus the difference in the gas phase temperature measurements in Figs. 8 through 11 for the two sets of conditions is simply due to the difference in fuel/air equivalence ratios. Figure 12, however, shows that the temperature rise in the flameholder is much larger under the more fuel/lean conditions even though the upstream temperature is lower in every case. This is interpreted to mean that a larger amount of catalytic reaction is occurring at ϕ = 0.7 to 0.8 than at ϕ = 0.89.

D. CO/CO_2 GAS ANALYSIS

Combustion of fuel lean propane/air premixed flames at atmospheric pressure is expected, thermodynamically, to almost quantitatively convert the fuel to carbon dioxide and water. Using the data from Ref. 21, the equilibrium concentrations of CO_2 and CO are plotted in Fig. 13. The CO_2 concentration varies from 6-10%, essentially due to dilution by excess air, while the CO concentration only exceeds 0.1% at equivalence ratios greater than 0.8. The experimental results in this work are given in Figs. 14 and 15. One difficulty with these concentration measurements is the large quantity of water vapor in the exhaust

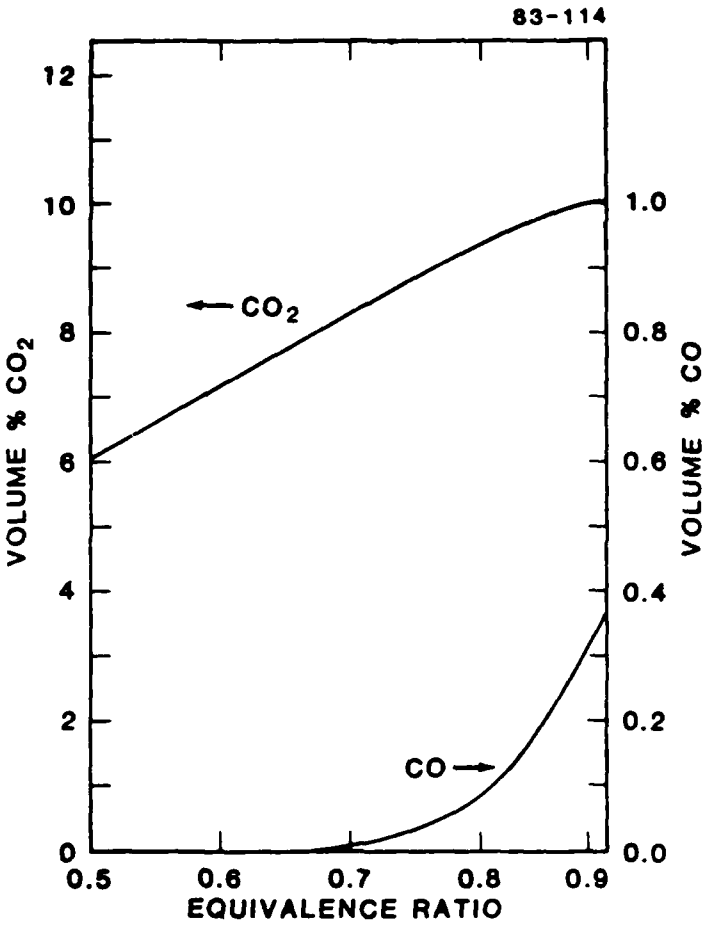

FIGURE 13 CALCULATED EQUILIBRIUM CONCENTRATIONS OF CARBON MONOXIDE AND CARBON DIOXIDE FOR PROPANE AND AIR COMBUSTION

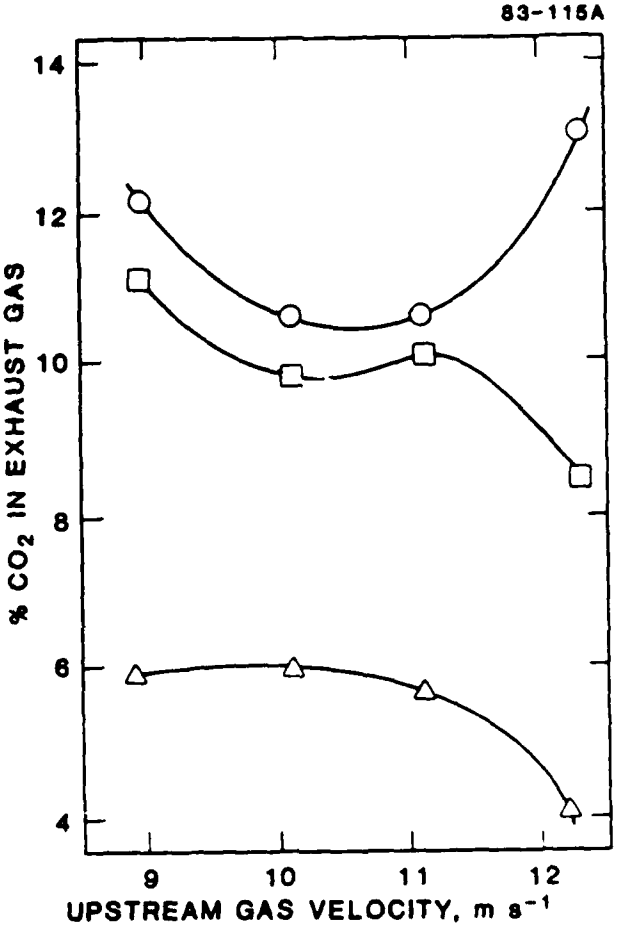

FIGURE 14 CARBON DIOXIDE CONCENTRATIONS FOR HONEYCOMB FLAMEHOLDERS

The noncatalytic (○) and catalytic (□) flameholder data for noncatalytic flameholder blowoff limits ($\phi \approx 0.9$); the catalytic (△) flameholder data at catalytic flameholder blowoff limits ($\phi \approx 0.7$ to 0.8).

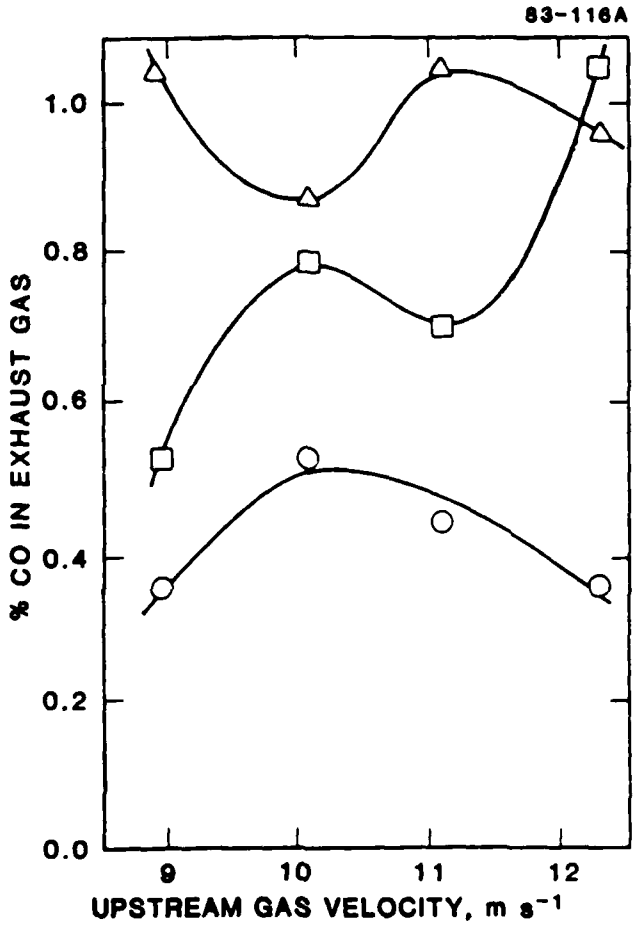

FIGURE 15 CARBON MONOXIDE CONCENTRATIONS FOR HONEYCOMB FLAMEHOLDERS

The noncatalytic (○) and catalytic (□) flameholder data for noncatalytic flameholder blowoff limits ($\phi \approx 0.9$); the catalytic (△) flameholder data at catalytic flameholder blowoff limits ($\phi \approx 0.7$ to 0.8).

gases, about 15%, which was assumed to have condensed in the metal lines and filter before the CO/CO_2 concentrations were measured in the NDIR instrument. This introduces additional uncertainty in the absolute value of these concentrations. A better technique would have been to keep the lines, filter, and instrument above the dew point, but this was not done. The noncatalytic honeycomb flameholder results show the highest CO_2 concentration and the lowest CO concentration. The reason for the higher efficiency, i.e., higher CO to CO_2 conversion is not known. The catalytic flameholder under the same conditions, $\phi = 0.89$, shows roughly similar results with only slightly higher CO concentrations at velocities up to 11 m s^{-1}, but with drastically different results at the highest flow velocity where the CO_2 concentration decreases sharply with a corresponding increase in CO concentration. Unfortunately, when the sum of the CO and CO_2 concentrations under these conditions, $\phi = 0.89$, is compared with the equilibrium concentration, Fig. 13, a larger yield is observed than theory predicts. For example, at 10.2 m s^{-1}, the CO + CO_2 concentration is observed to be about 11%, slightly larger than the calculated 10.2%. This is considered indicative of the uncertainties in the overall calibration of the NDIR instrument and in the correction for the change of gas volume due to water condensation. No reasonable amount of small hydrocarbon would have a significant effect. Under the leaner conditions corresponding to blowoff limits for the catalytic flameholder, CO_2 concentrations are observed to be considerably smaller and the CO concentrations somewhat larger, approximately 1%. These data were obtained between $\phi = 0.71$ and 0.78 where the calculated CO concentration is negligible. The sum of the CO and CO_2 experimental measurements at $\phi = 0.74$ and a velocity of 10.2 m s^{-1} gives an approximate value of 7% (compared to the calculated value of 9%). No experimental reason for this difference was found and it may indicate the presence of unburned hydrocarbons under these conditions.

In order to interpret the experimental results, we have attempted to remove the discrepancy between the experimental and theoretical predictions by normalizing the experimental CO concentrations. Figure 16 shows the relative fraction of CO, normalized to the sum of CO and CO_2, vs. the flow velocity. These data again show that the catalytic and noncatalytic flameholders at $\phi = 0.89$ are similar except at the highest velocities, where the catalytic flameholder near its blowoff limits yields much more CO. This can be qualitatively understood if we assume that the catalytic honeycomb produces a larger quantity of CO in its

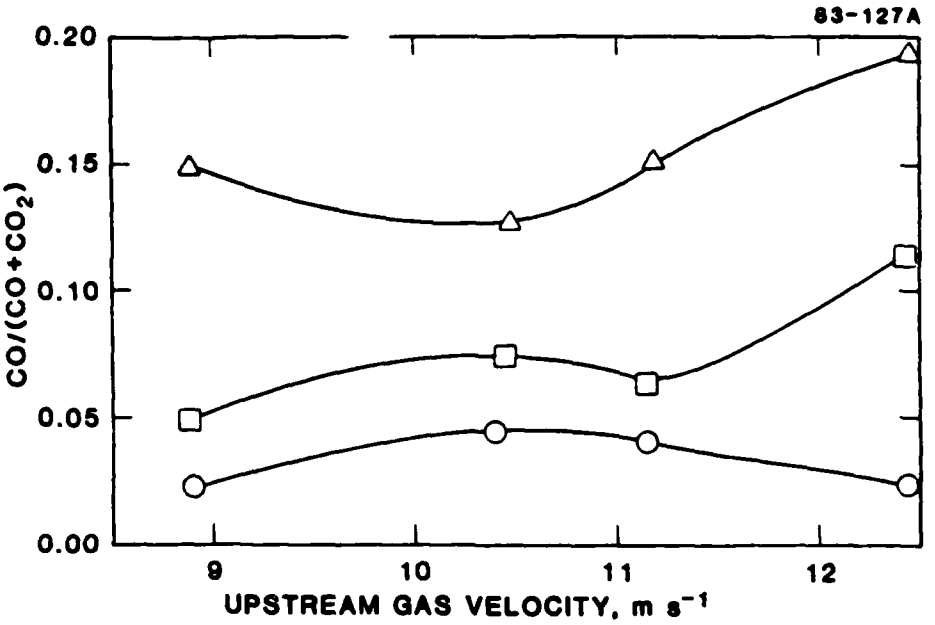

FIGURE 16 RELATIVE CARBON MONOXIDE FRACTION FOR HONEYCOMB FLAMEHOLDERS

The noncatalytic (O) and catalytic (□) flameholder data for noncatalytic flameholder blowoff limits ($\phi \gtrsim 0.9$); the catalytic (Δ) flameholder data at catalytic flameholder blowoff limits ($\phi \gtrsim 0.7$ to 0.8).

exhaust gases at $\phi = 0.75$ compared to $\phi = 0.89$. This carbon monoxide would mix with the unburned propane and air to yield a $CO/C_3H_8/O_2$ mixture which might be less efficient towards conversion (i.e., combustion) to CO_2 than a simple C_3H_8/O_2 mixture. The temperature rise data in Fig. 12 support the assumption that much more catalytic activity, i.e., CO production occurs under the leaner conditions. Also supporting this thesis is the fact that CO/air mixtures support a stable flame only for CO concentrations greater than 12.5%[22] compared to propane/air mixtures which are stable for propane concentrations down to 2.2%. Therefore, it seems reasonable to assert that large quantities of CO are produced earlier in the combustor by the catalytic flameholder and that it would take longer, or different operating conditions, for complete conversion of CO to CO_2.

IV. SUMMARY AND RECOMMENDATIONS

The objective of this program was to investigate the feasibility of combustion enhancement in the form of increased flame stability by the use of catalytically active flameholders. The results of this work were obtained in an atmospheric pressure, 5.1 cm diam, research combustor and were not intended to simulate actual operating conditions of any particular device. The results show conclusively that the fuel lean blowoff limits are wider with a catalytic flameholder than with noncatalytic but otherwise identical flameholders. The combustion efficiencies, i.e., conversion of CO_2, for both catalytic and noncatalytic flameholders when operated under identical conditions are similar except at the highest velocities. For the catalytic flameholder at the extended (leaner) conditions, however, the combustion efficiency appears to be lower than for either flameholder at higher equivalence ratios, i.e., the ratio $CO/(CO_2 + CO)$ is higher. A larger amount of heat release is observed in the catalytic flameholder under the leaner conditions and the resulting gas phase mixture probably requires a longer residence time for complete combustion than for noncatalytic flameholders.

The amount of catalyst required to achieve significant widening of the blowoff limits is small; therefore larger catalyst loading or more efficient catalysts may widen the blowoff limits even further although this hypothesis was not investigated in the program.

Primary practical disadvantages of the catalytic flameholders used in this feasibility study appear to be associated with the ceramic substrates, which in the case of Cordierite, restrict operation to rather low temperatures. In the case of some other ceramics suitable for higher temperatures, the substrates are susceptible to fracture due to thermal shock and are less porous. The palladium catalyst investigated in this program is also probably not practical in view of its significant vapor pressure at temperatures above 1500 K.

The findings of this program show that catalytically coated ceramic (or other material) flameholders may be a promising approach to enhanced stabilization of highly diluted partially combusted gas streams such as those exiting the main burner section of a gas turbine engine. The conditions necessary for efficient combustion employing catalytic flameholders must, however, be more thoroughly investigated before practical catalytic combustors can be manufactured.

In view of the progress achieved on this program and the potential advantages of catalytic enhanced flame stabilizations, the following recommendations are made:

1. A similar program should be performed to compare catalytic and non-catalytic honeycomb flameholders in a larger diameter combustor and at higher velocities. The larger combustor would reduce wall interactions and a wider range of velocities would better define the variation of blowoff limits with velocity.
2. Further studies of the CO, CO_2, and hydrocarbon emissions should be performed along with (1) above. If the catalyst produces enough CO to significantly reduce the burning velocity of the mixture, the advantages of the catalytic flameholder may be reduced.
3. Catalytic flameholder substrates other than the Cordierite used in this work should be tested. These substrates would include other coated ceramics, coated metals, and ceramics incorporating the catalysts into their lattice.
4. Catalytically active coatings other than palladium should be tested.
5. Tests should be performed under conditions of pressure, velocity, inlet temperature, and fuel air ratio which more closely simulate the practical combustors of interest, and jet fuels should be used for the tests.

The above recommendations define the direction of future work but are not meant to be comprehensive. Whether this technique can eventually be practical is not clear at this time but an evaluation can probably be made after some of the recommended additional experiments have been performed.

V. REFERENCES

1. Longwell, J.P., Chenevy, J.E., Clark, W.W., and Frost, E.E., "Flame Stabilization by Baffles in a High Velocity Gas Stream," Third Symposium on Combustion, Flame and Explosion Phenomena (The Williams & Wilkins Co., Baltimore, 1949) pp. 40-44.
2. Grumer, J., Harris, M.E., and Schultz, H., "Flame Stabilization on Burners with Short Ports or Noncircular Ports," Fourth Symposium (International) on Combustion (The Williams & Wilkins Co., Baltimore, 1953) pp. 695-701.
3. Wohl, K., Kapp, N.M., and Gazley, C., "The Stability of Open Flames," Third Symposium on Combustion, Flame and Explosion Phenomena (The Williams & Wilkins Co., Baltimore, 1949) pp. 3-21.
4. Williams, G.C., Woo, P.T., and Shipman, C.W., "Boundary Layer Effects on Stability Characteristics of Bluff Body Flameholders," Sixth Symposium (International) on Combustion (Reinhold Publishing Corp., New York, 1957) pp. 427-438.
5. Hottel, H.C., Williams, G.C., Jensen, W.P., Tobey, A.C., and Burrage, P.M.R., "Modeling Studies of Baffle-Type Combustors," Ninth Symposium (International) on Combustion (Academic Press, New York, 1963) pp. 923-935.
6. Cheng, S.I. and Kovitz, A.A., "Theory of Flame Stabilization by a Bluff Body," Seventh Symposium (International) on Combustion (Butterworths Sci. Publ., London, 1953) pp. 681-691.
7. Löblich, K.-R., "Semitheoretical Consideration on Scaling Laws in Flame Stabilization," Ninth Symposium (International) on Combustion (Academic Press, New York, 1963) pp. 949-957.
8. Wohl, K., "Quenching, Flash-Back, Blow-Off--Theory and Experiment," Fourth Symposium (International) on Combustion (The Williams & Wilkins Co., Baltimore, 1953) pp. 68-89.
9. Harrison, B.K. and Ernst, W.R., "Catalytic Combustion in Cylindrical Channels: A Homogeneous-Heterogeneous Model," Combust. Sci. Techn. 19, 31-38 (1978).
10. Ablow, C.M. and Wise, H., "Theoretical Analysis of Catalytic Combustion in a Monolith Reactor," Combust. Sci. Techn. 21, 35-42 (1979).
11. T'ien, J.S., "Transient Catalytic Combustor Model," Combust. Sci. Techn. 26, 65-75 (1981).
12. Prasad, R., Tsai, H.L., Kennedy, L.A., and Ruckenstein, E., "Effect of Inlet Parameters and Bed Length on the Operating Characteristics of a Catalytic Combustor," Combust. Sci. Techn. 25, 71-84 (1981).

13. Prasad, R., Kennedy, L.A., and Ruckenstein, E., "Kinetics of Catalytic Combustion of Propane on Transition Metal Oxides," Combust. Sci. Techn. 27, 171-181 (1982).

14. Wampler, F.B., Clark, D.W., and Gaines, F.A., "Catalytic Combustion of C_3H_8 on Pt Coated Monolith," Combust. Sci. Techn. 14, 25-31 (1976).

15. Bracco, F.V., Royce, B.S.H., and Santavicca, D.A., "High Temperature Catalytically Assisted Combustion," AFOSR-81-0248; presented at 1982 AFOSR Contractors Meeting held at U.S.C. on "Air Breathing Combustion Dynamics Research," pp. 152-155.

16. Bruno, C., Walsh, P.M., Santavicca, D.A., Sinha, N., Yaw, Y., and Bracco, F.V., "Catalytic Combustion of Propane/Air Mixtures on Platinum," Combust. Sci. Techn. 31, 43-74 (1983).

17. Cordierite is described in the product literature from Corning Glass Works, Corning, NY, 14831 in a bulletin on Celcor ceramics.

18. William B. Retallick, Consulting Chemical Engineer, 1432 Johnny's Way, West Chester, PA 19380.

19. Schlicting, H., Boundary Layer Theory (McGraw-Hill, New York, 1955) Chap. 1-2.

20. Williams, G.C., Hottel, H.C., and Scurlock, A.C., "Flame Stabilization and Propagation in High Velocity Gas Streams," Third Symposium on Combustion, Flame and Explosion Phenomena (The Williams & Wilkins Co., Baltimore, 1949) pp. 21-40.

21. Steffensen, R.J., Agnew, J.T., and Olsen, R.A., Combustion of Hydrocarbons--Property Tables, Engineering Extension Series No. 122 (Purdue University, Lafayette, IN, 1966).

22. Lewis, B. and von Elbe, G., Combustion, Flames and Explosions of Gases, 2nd ed. (Academic Press, New York, 1961) p. 706.

APPENDIX II

Case Studies in the Simulation of Novel Combustion Techniques

A. E. Cerkanowicz and J. G. Stevens

This paper, along with the one provided in Appendix III presents details on the modeling of catalytic combustion processes within porous honeycomb catalysts through which a reactant mixture is passed. Since the paper in Appendix III had a very limited outside distribution, both papers have been included to provide a complete set of references on this modeling.

CASE STUDIES IN THE SIMULATION OF NOVEL COMBUSTION TECHNIQUES*

A. E. Cerkanowicz
Government Research Laboratories
Exxon Research and Engineering Company, Linden, New Jersey 07036

John G. Stevens
Department of Mathematics and Computer Science
Montclair State College, Upper Montclair, New Jersey 07043

ABSTRACT

Digital simulation is an area of considerable activity and growing importance in combustion research. This paper presents considerations involved in the simulation of two novel combustion augmentation techniques -- catalytic and radiative (photochemical) enhanced combustion. Both simulations are documented as to the interrelationships between the physical and chemical bases and assumptions used in deriving the model equations, the program objectives, and the influence of these objectives on the approaches utilized and the results obtained. The goals of the simulations differed from their inception and the implications of these differences are explored. In our approach, catalytic combustor operation is described by a two-point boundary value problem for a non-linear system, which is solved using an adaptive, variable-order, finite difference scheme. The numerical stubbornness encountered and the occurrence and numerical treatment of bifurcation are presented. The radiative augmented combustion initiation model is constituted as an initial value problem for a large non-linear system of differential equations and is solved numerically using a software package implementing the popular backward differentiation formulas. The results of these simulations are compared with the experimental data available and show generally excellent agreement. Specific applications of these simulations are reported.

INTRODUCTION AND OBJECTIVES

Combustion systems are limited by combustion-associated phenomena such as flammability, flame propagation, ignition, and stable combustion and by the formation of combustion-related pollutants. The mechanisms and processes associated with promising techniques for combustion initiation and enhancement and for reduction of pollutant formation are not sufficiently well understood. We shall discuss and contrast from a simulation viewpoint two advanced combustion augmentation techniques evaluated in the Government Research Laboratories of Exxon Research and Engineering Company.

One approach involves combustion assistance via the use of an oxidizing catalyst. In such systems, the fuel-air mixture is passed over a catalytic surface which heterogeneously promotes combustion. A number of potential applications have been identified. Conventional gas turbine combustors produce unacceptable levels of the oxides of nitrogen (NO_x), due to the high temperatures developed in the primary combustion zone before the injection of secondary air. This high temperature zone is necessary to insure stable combustion. Catalytic combustors can achieve stable combustion without these high peak temperatures, resulting in a substantial reduction in NO_x emissions (1). Fuel-air mixtures which cannot be combusted stably by ordinary homogeneous means can be burned catalytically and thereby the energy content of many types of low heating value streams can be utilized (2). Automotive catalytic converters are a much studied application of catalytic combustion, one which differs from the applications in which we are interested by the absence of significant gas temperature rise in the catalytic reactor (3, 4).

The operation of a catalytic combustor involves several chemical and physical processes. The modeling of such systems was undertaken to study the interaction of these processes, to provide a more detailed understanding of experimental data, to predict trends in and levels of combustor performance as a function of operating characteristics, and to assess new areas of application.

A second novel combustion technique, radiative (photochemical) augmented combustion, is being investigated as part of an Air Force sponsored program. In this approach, combustion of an unsensitized fuel-air mixture is initiated or enhanced by irradiation with ultraviolet light which results in the photodissociation of oxygen molecules and combustion intermediate species (5). The overall program encompasses both experimental and analytical approaches. The goal of the modeling effort is the elucidation of the fundamental interaction of photon absorption, subsequent dissociation, and the chemical kinetics of the reactant mixture. After comparison of model results with experimental data, the model is to be used to provide guidance for the experimental effort and as a basis for the interpretation and comparison of experimental results. The model is currently limited to photochemical initiation of combustion in hydrogen-oxygen mixtures. Component modules of this model are being used in a succession of more complex models which will allow the examination of enhancement effects, the results of which will be reported elsewhere (6).

THE MODELS

This section provides a brief description of the models used in the simulation of catalytic combustion and radiative augmented combustion. The derivation of the governing equations for catalytic combustion is included in (7), with references to earlier work. Only the underlying assumptions are summarized, with emphasis on their relation to our objectives.

Catalytic Combustion

In catalytic combustion a fuel-air mixture is passed through a honeycomb monolithic substrate coated with an oxidation catalyst, typically, finely dispersed platinum. Combustion results from heterogeneous reaction at the catalytic surface and from homogeneous oxidation within the gas phase. Figure 1 exhibits the relationship of some of the physical and chemical phenomena underlying catalytic combustion. In addition to the oxidation reactions, these include heat and mass transport between the surface and the gas, momentum transport within the gas stream, and axial heat conduction in the substrate.

As previously stated, our aim is to relate catalytic combustor performance, which is measured by overall fuel conversion efficiency (and to a lesser extent by conversion and temperature profiles), to operating characteristics. The variables specifying the operating conditions are listed in Table 1. In order to accomplish this objective, it is necessary to model each of the relevant processes at an appropriate and balanced level of detail. Our approach

*Research supported in part by the Air Force Office of Scientific Research, U.S. Air Force, under Contract No. F49620-77-C-0085. The United States Government is authorized to reproduce and distribute reprints for governmental purposes notwithstanding any copyright notation hereon.

is that of a system study in which each of the components (i.e., the physical phenomena) of the system is modeled as simply as possible in order to arrive at a system model which is tractable and yet does not neglect important physical and chemical events.

The type of model employed is a plug-flow, steady-state, one-dimensional model, frequently used in the simulation of chemical reactors. This choice is appropriate in that we do not propose to study the transient behavior of the system nor the details of the fluid dynamics or transport phenomena. Rather, a one-dimensional model incorporating heat and mass transport coefficients is in line with the level of detail desired. This choice is also indicated by the desire to simulate conditions leading to both laminar and developing turbulent flow.

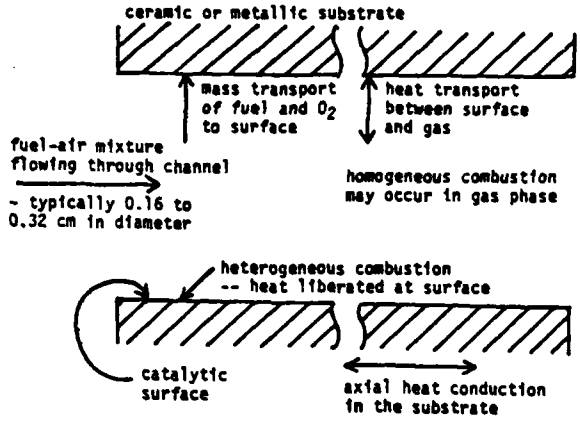

Figure 1

Chemical and Physical Processes Modeled in Catalytic Combustion

Table 1

Variables Specifying Operating Conditions

Fuel Composition	Catalytic Pre-exponential Factor and Activation Energy
Equivalence Ratio	Homogeneous Pre-exponential Factor and Activation Energy
Heat of Combustion	Substrate Conductivity
Diffusivity of Fuel	Channel Diameter
Inlet Gas Temperature	Length of Bed
Inlet Pressure	Porosity
Inlet Velocity	

The assumptions underlying the model are summarized in Table 2, together with comments relating them to our objectives. The dimensional form of the governing equations, boundary conditions, and nomenclature are presented in Table 3. Simplification of the equations leads to a two-point boundary value problem for a non-linear system in fuel flux, substrate temperature, gas temperature and velocity. The equations were set in dimensionless form before solution. The dimensionless groupings (e.g., the ratio of characteristic residence time to characteristic catalytic reaction time) were studied to increase our understanding of the interaction of the physical processes involved (7).

Table 2

Assumptions of the Catalytic Combustion Model

Assumption	Comment
1. Gas-phase properties, substrate temperature and fuel concentration at the catalyst surface are uniform throughout a reactor cross-section. Axial dispersion is neglected.	The assumption of plug-flow is discussed in the text. In the presence of large gradients, axial dispersion can affect the shape of the profiles.
2. Fuel oxidation can occur at the catalyst surface and in the gas phase. Global (one-step) Arrhenius rate expressions are employed for complete oxidation reactions in each phase. The heterogeneous reaction is taken to be first order in fuel and zero order in oxygen.	The use of global kinetics has proved useful in modeling combustion systems (8) and is consistent with the overall level of detail and the state of knowledge of catalytic mechanisms for complex fuels. The assumption concerning reaction order is reasonable for fuel-lean conditions of interest.
3. Heat and mass transport are modeled using transfer coefficients where the driving forces are the temperature and concentration differences between the bulk gas phase and the catalytic surface.	This assumption allows the use of a one-dimensional model and permits treatment of both laminar and turbulent flow by the choice of appropriate correlations for the transport coefficients.
4. Transport of the fuel is considered to occur by diffusion through the boundary layer and to be balanced by the catalytic reaction rate at the surface.	This assumption permits the study of regimes in which the catalytic conversion can be transport or kinetically limited.
5. The velocity is allowed to vary axially, subject to a momentum balance which includes the use of a Fanning friction factor.	Earlier work often assumed constant velocity. The temperature rise within the reactor increases the gas velocity, thus decreasing the residence time and thereby significantly affecting the conversion predicted (9).
6. Axial heat conduction in the substrate is included in the model.	This is important as a feedback mechanism and for correct comparison of ceramic and metallic substrates.
7. All the heat released in the reactor is assumed to emit the combustor in the gas stream.	For some system configurations, loss of adiabatic operation by radiant heat loss from the combustor can play an important role (10).

Table 3

Equations and Nomenclature for the Catalytic Combustion Model

(1) Fuel-species balance (gas-phase)

$$S\frac{d(vC_f)}{dz} + SA_h \exp\left(-\frac{E_{ah}}{RT}\right)(C_f)^{n_f}(C_{O_2})^{n_O} + \sigma k\,(C_f - C_{fs}) = 0$$

(2) Fuel-species balance (surface)

$$k(C_f - C_{fs}) = A_c \exp\left(-\frac{E_{ac}}{RT_s}\right) C_{fs}$$

(3) Gas-phase energy balance

$$-S\rho v C_p \frac{dT}{dz} + \sigma h(T_s - T) + S(-\Delta H)A_h \exp\left(-\frac{E_{ah}}{RT}\right)(C_f)^{n_f}(C_{O_2})^{n_O} = 0$$

(4) Solid-phase energy balance

$$S_s\lambda_s \frac{d^2T_s}{dz^2} - \sigma h(T_s - T) + \sigma(-\Delta H)A_c \exp\left(-\frac{E_{ac}}{RT_s}\right) C_{fs} = 0$$

(5) Momentum equation

$$-(\rho v)\frac{dv}{dz} - \frac{dp}{dz} - \frac{\sigma f}{2S}(\rho v)\,v = 0$$

(6) Continuity equation

$$\frac{d}{dz}(\rho v) = 0$$

(7) Equation of state

$$\rho = \frac{p}{M}RT = \frac{p_o v_o R}{M}\frac{T}{v}$$

(8) Stoichiometry

$$\frac{vC_{O_2}}{(vC_{O_2})_o} = 1 - \phi\left(1 - \frac{vC_f}{(vC_f)_o}\right)$$

(9) Boundary conditions

$$\text{at } z = 0:\quad C_f = (C_f)_o,\ C_{O_2} = (C_{O_2})_o,\ v = v_o,\ T = T_o,\ \frac{dT_s}{dz} = 0$$

$$\text{at } z = L:\quad \frac{dT_s}{dz} = 0$$

Table 3 (continued)

Nomenclature

A = pre-exponential factor; A_c, m/s; A_h, $(mol/m^3)^{1-n}/s$, where n is total homogeneous reaction order

C = concentration (associated with catalyst layer if subscripted by s; otherwise, gas-phase), mol/m^3

C_p = specific heat capacity of gas at constant pressure, J/(kg·K)

E_a = activation energy, J/mol

f = fanning friction factor

h = heat transfer coefficient, $J/(m^2 \cdot s \cdot K)$

$(-\Delta H)$ = heat of reaction, J/mol

k = mass transfer coefficient, m/s

M = molecular weight, kg/mol

n = reaction order

p = pressure, Pa

R = gas constant, J/(mol·K)

S = void cross section, m^2

S_s = solid cross section, m^2

T = temperature, K

u = velocity, m/s

z = axial dimension, m

λ = thermal conductivity, J/(m·s·K)

ρ = density, kg/m^3

σ = wetted perimeter, m

ϕ = equivalence ratio

Subscripts

0 = inlet

c = catalytic

f = fuel

h = homogeneous

O_2 or O = oxygen

s = surface (solid)

Radiative Initiation

Based on qualitative and quantitative analysis of and subsequent agreement with experimental results, a mechanism for the photochemical initiation of sustained combustion in unsensitized fuel-air systems has been developed (5). The initiation mechanism follows a path in which the critical intermediate species, atomic oxygen, is generated by photodissociation of oxygen molecules via radiant energy absorption at wavelengths below 245 nm

$$O_2 + h\nu \rightarrow O + O.$$

The most efficient production of oxygen atoms occurs at wavelengths below 180 nm where one of the atoms produced is in the excited electronic state, O('D).

When a critical concentration of oxygen atoms is exceeded, combustion initiation occurs. Subsequent reaction of the atomic oxygen with the fuel, as well as other intermediates and products, leads to ignition and sustained combustion. Conceptually illustrated in the phase-plane diagram of temperature versus the logarithm of oxygen atom concentration, Figure 2, the photochemical initiation process follows path NP (5). Ideally, the photochemical path need not involve a temperature rise. In reality, some thermalization does occur as will be evident from results subsequently presented. The normal thermal (spark) path is shown along NT and can be expected to show different ignition characteristics from the photochemical path. It should be noted that other combustion intermediates do play a role and that a multidimensional phase analysis is necessary for a complete description of the processes involved. Nevertheless, oxygen atom concentration provides a satisfactory surrogate representation of the general behavior of the intermediate species involved and the two-dimensional analysis gives a useful framework for understanding photochemical initiation.

The initiation model includes the reactant mixture kinetics, photodissociation of light absorbing species, and temperature rise due to reaction heat release. The species considered for hydrogen-oxygen systems are listed in Table 4. It is important to observe the inclusion of several excited state species, the effect and necessity of which will be described. Some ninety chemical reactions that occur between these species are included in the model. An extensive literature review was undertaken and best values for rate constants in the form $AT^{-B}\exp(-C/T)$ were chosen for temperature, T, in the initiation and early ignition range (300-1200K).

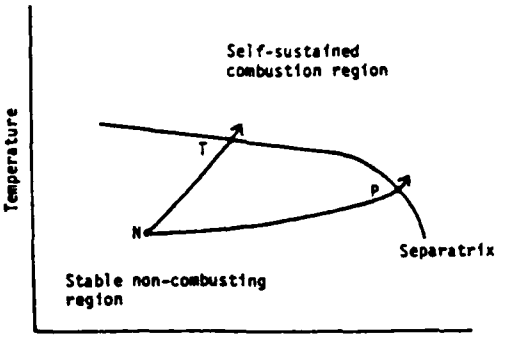

Figure 2

Conceptual Phase Plane Diagram Showing Thermal Initiation Path (NT) and Photochemical Initiation Path (NP)

Table 4

Hydrogen-Oxygen Photochemical System

REACTANT SPECIES

$O(^1D)$	O_2	OH
O	O_3	H_2O
$O_2(^1\Sigma_g^+)$	H	HO_2
$O_2(^1\Delta_g)$	H_2	H_2O_2

PHOTODISSOCIATION REACTIONS

O_2	+ $h\nu$ (λ < 245)	→ O	+ O
O_2	+ $h\nu$ (λ < 175)	→ O	+ $O(^1D)$
O_3	+ $h\nu$ (λ < 1140)	→ O_2	+ O
O_3	+ $h\nu$ (λ < 310)	→ $O_2(^1\Delta_g)$	+ $O(^1D)$
O_3	+ $h\nu$ (λ < 260)	→ $O_2(^1\Sigma_g^+)$	+ $O(^1D)$
H_2O	+ $h\nu$ (λ < 242)	→ OH	+ H
HO_2	+ $h\nu$ (λ < 456)	→ OH	+ O
H_2O_2	+ $h\nu$ (λ < 365)	→ OH	+ OH

Radiant absorption by reactant and combustion intermediate species is considered to follow a Beer-Lambert Law. The dissociation products formed, which may include excited states, are dependent on the energy of the photon absorbed. The photodissociation reactions which can occur are listed in Table 4.

Photochemical dissociation is handled as a unimolecular reaction in which the rate of production of dissociation products is given by the product of the concentration of the given absorbing species and a pseudo first-order rate constant, which depends on time, the distance from the light source window, and the concentration of all absorbing species to that point. The expression for the rate constant is

$$k(x,t) = \int_0 I(x,t,\lambda)T(\lambda)\phi(\lambda)[\lambda/hc]\sigma(\lambda)\exp\left[-\sum_{i=1}^{N}\sigma_i(\lambda)\int_0^x n_i(z,t)dz\right]d\lambda$$

where: t = time
x = distance from light source window
λ = wavelength
n_i = concentration of light absorbing species
σ_i = absorption cross-section of light absorbing species
ϕ = quantum yield of dissociation
T = window transmission
I = source irradiance

Quite general light source characteristics can be considered in the specification of the source irradiance. Intensity is considered to be dependent on wavelength, time, input energy, and optical arrangement (i.e., parallel beam, focused beam, point source). As well, the transmission characteristics of window material such as quartz or sapphire can be incorporated by specification of window transmission. Absorption coefficients for all light absorbing species are tabulated, and the treatment of molecular oxygen absorption in the Schumann-Runge bands follows that given by G. Kockarts (11). In the current implementation of the model, all absorbing species are reckoned to dissociate with the rate constant calculated from the cited equation, but the attenuation of light intensity by the mixture is taken to be due solely to O_2. This assumption is reasonable, even in wavelength regions in which O_2 does not absorb strongly, due to the low column density of the other absorbers during the irradiation period.

For each of the species there is thus a resulting equation for the rate of change in its concentration

$$\frac{dY_i}{dt} = \Sigma \pm (k_{chem,j}) \begin{pmatrix}\text{reactant}\\ \text{concentrations}\end{pmatrix} + \Sigma (k_{photo,j}) \begin{pmatrix}\text{absorber}\\ \text{concentration}\end{pmatrix}$$

chemical reactions involving i^{th} species; photochemical reactions of i^{th} species

where Y_i = concentration of i^{th} species, particles/cm^3; the + sign is used if the i^{th} species is a product; -, if a reactant.

To these equations is added a simple energy balance of the form

$$\frac{dT}{dt} = \Sigma \frac{(-\Delta H)}{A_v \rho C_p} (k_{chem}) \begin{pmatrix}\text{reactant}\\ \text{concentrations}\end{pmatrix}$$

all chemical reactions

where ΔH = heat of reaction, J/mol
ρ = mixture density, kg/cm^3
A_v = Avagadro's number, particles/mol
C_p = specific heat capacity at constant pressure, J/kg-K

The model is finally constituted as an initial value problem for a large nonlinear system of differential equations. Diffusion and convective effects, as well as heat loss to the surroundings, have been neglected. We shall subsequently discuss the use of this approach for the study of initiation and the early stages of ignition, i.e., to describe in this time period the photon-reactant mixture interaction in the neighborhood of the light source window prior to the breakdown of the assumptions made.

SOLUTION TECHNIQUES

The equations of the catalytic combustion and photochemical initiation models were solved numerically using general purpose software. Our experiences with the methods used are detailed in the following sections.

Catalytic Combustion

For the catalytic combustion model, the boundary value problem was solved using an adaptive, variable-order, finite-difference scheme developed by Lentini and Pereyra and implemented in subroutine SYSSOL (12). Variable order is provided through deferred corrections. An asymptotic error estimator is used to keep track of the rate of convergence upon successive use of deferred corrections. When this rate is not sufficiently fast according to built-in criteria, the basic mesh for the finite-difference discretization is automatically refined (the adaptive feature), the last iterate interpolated to the new mesh, and the process repeated. The solution of the non-linear system of equations required for the deferred corrections is accomplished using Newton's method and thus requires the Jacobian of the system.

In solving the catalytic combustion model equations using this method, the choice of initial iterates is critical. For a given solution and a given mesh, there exists a tube about the solution in which the initial iterate must lie in order to assure convergence of the Newtonian iteration. The size of this tube, that is, how close the initial iterate must lie to the solution, is an indication of the numerical stubbornness of the system for a given set of operating conditions.

There are two sources of numerical difficulty present in this system; the first is the stiffness often encountered in the modeling of chemically reacting systems. A good general discussion of solving stiff equations is given in (13); specific attention is given to chemical systems in (14). One source of stiffness is the disparity between heterogeneous and homogeneous reaction rates (dependent, in fact, on substrate and gas temperatures). To a lesser extent, even in cases of dominant catalytic activity, the difference in rates of change for the substrate temperature and the other system variables is also a source of stiffness. In the course of solving the equations, we have performed several parametric studies which illustrate these points vividly, which we shall not present here.

The system also has stiffness associated with very small values for the substrate conductivity, λ_s. (More properly, it occurs for large values of the Peclet number for heat transfer, $Pe_s = L_o v_g C_p S/\lambda_s S_s$.) After simplification equation 4 of Table 3 becomes

$$S_s \lambda_s \left(\frac{dT_s}{dz} - \frac{dT_s}{dz}\bigg|_{z=0} \right) = S_o v C_p (T - T_o) + (-\Delta H)(v C_f - v_o (C_f)_o).$$

Recall that the boundary conditions for substrate temperature are

$$\frac{dT_s}{dz}\bigg|_{z=0} = \frac{dT_s}{dz}\bigg|_{z=L} = 0.$$

For λ_s very small, the solution is essentially that given by setting the right hand side equal to zero. However, the boundary conditions are not now in general satisfied. Thus the substrate temperature as given by the solution of the full equations has a component which changes rapidly toward the entrance and the exit of the combustor. This development thus gives rise to a "boundary layer" phenomenon (a mathematical term, here not to be confused with a flow boundary layer) and the accompanying stiffness (15).

One approach to overcoming these difficulties is to choose an initial iterate which lies quite close to the solution. This initial iterate can be obtained by approximating the solution analytically. However, a further complication is that there are regimes in which the system has multiple solutions. The source of this bifurcation is important in understanding the operation of a catalytic combustor, as will be shown in the discussion of the results. The numerical investigation of multiple solutions was accomplished by examining the solutions obtained from three different types of initial iterates. These were: an "unignited" initial iterate which represents no fuel conversion, a "lower-ignited" one obtained from the assumption of mass-transport limited catalytic conversion, and an "upper ignited" one reflecting significant homogeneous conversion. Generally, for a given set of parameters, use of these initial iterates sufficed either to give considerable assurance that there was a unique solution (i.e., different initial iterates would converge to the same solution); or, when there were multiple solutions, to determine easily the upper and lower solutions.

On occasion, for choices of parameters for which the numerical stubbornness mentioned above was present, it was necessary to use parametric continuation to obtain convergence to within the absolute error tolerance specified, usually 10^{-3} (12, 16). Thus a sequence of solutions was obtained, starting with a value for the particular "offending" parameter, for which convergence could be obtained. This solution was then used as the initial iterate in solving the equations for a value of the parameter closer to that desired. This process was repeated until the solution was obtained for the desired parameter value. SYSSOL contains an option to perform continuation "automatically", though we found the authors' choice of only one Newton step for each of the continuation steps was not sufficient to conquer the most challenging situations.

Parametric continuation was carried out for large values of the Peclet number and successful integration was obtained for values of Pe_s up to 10^4. However, as was observed earlier, for the bulk of the reactor length the substrate temperature profile and even more so the other profiles agree with those obtained for much lower Pe_s values. Thus high values were routinely replaced by a value known to give good agreement and which resulted in more easily achieved successful integration. We chose this approach rather than solve the locally adiabatic (infinite Pe_s) case by initial value methods because we were often interested in investigating the use of metallic substrates which can give Pe_s values below 20 and did not wish to implement two different solution techniques.

Finally, we had only limited success using the adaptive feature for stubborn problems. That is, we observed cases which we could successfully integrate using an analytical initial iterate with an initial choice of 101 or 201 mesh points, yet the same initial iterate on 26 or 51 mesh points would fail to converge even after the mesh had been refined to 201 points. The reason for this behavior is that the iterate on the smaller number of mesh points was not in the tube of convergence of the Newton iteration. The result of deferred correction when interpolated to the refined mesh was thus not a sufficiently good initial iterate to permit convergence on the new mesh. This is not a serious problem and can, of course, easily be overcome by using the finer mesh to begin with. On problems not involving these numerical difficulties, the adaptive feature permits efficient solution both at high and "engineering" precisions. Indeed, SYSSOL has proved to be remarkably versatile and capable of economically integrating the equations, even when the problem lies in the truly "horror" range.

Radiative Augmented Combustion

The equations of the photochemical initiation model were solved using the stiff option incorporating the backward differentiation formulas implemented in one of the Gear family of codes, STIFF, by Kahaner and Sutherland (17, 18). Because of the excellent state of the art in codes for the solution of initial value problems for stiff ordinary differential equations, such problems can be solved today quite routinely. The stiffness of the system seemed readily apparent to us at the outset. For example, the oxygen singlet O('D) participates in very fast reactions, is produced only be photodissociation, and virtually tracks the shape of the vacuum ultraviolet radiant pulse. Other species change on a much different timescale. Nevertheless, we did experiment using the Adams-Moulton method in STIFF, only to find that indeed for one sample problem the use of the chord method with an analytic Jacobian (a rather unusual combination) more than quadrupled the execution time compared to the stiff option with the same solution technique, while use of functional iteration was not successful within the prescribed criteria.

To aid in the formidable task of coding the photochemical initiation model equations, an equation-writer program from Los Alamos Scientific Laboratory was used, after modification to include the heat balance (19). The program accepts species and reaction cards as input and produces subroutines coded in FORTRAN for both the species rate expressions and the Jacobian of the system. Although there exist several chemical kinetics packages, this approach lends itself well to the photochemical application and by producing the intermediate source code provides the flexibility to use the modules already completed in a succession of more complex models, treating, for example, diffusion and wall recombination effects. The complete program package includes subroutines to compute the chemical and photodissociation rate constants.

RESULTS: CATALYTIC COMBUSTION

The model was used to simulate experimental results obtained by Pfefferle, et al. (20). Solutions to the model equations were obtained using input values corresponding to the experimental operating conditions. It is important to observe that the model solutions depend on input values not only for quantities which can be specified precisely (e.g., reactor length), but also for quantities for which it is more difficult to assign values. These include the catalytic and homogeneous reaction rate parameters. Since many studies have dealt with the determination of these quantities, it would, however, clearly be inappropriate to choose values contrary to the bulk of the experimental results. The same considerations apply to the choice of the correlations for the heat and mass transport coefficients. Initially we used correlations recommended by Hawthorne (4). Subsequently, Votruba, et al. (21) have pointed out that the correlations given by Hawthorne tend to give somewhat low values for the transport coefficients. Preliminary comparison of model results with the experimental data of Pfefferle, et al. was given in (7). We present here new results based on the correlations given by Votruba, et al. and a previously unreported feature of the model solutions.

Figure 3 shows the effect of varying inlet gas temperature on conversion for combustor operating conditions given in the legend. Further experimental details can be found in (20). The experimental data points are indicated by solid circles, while the solid curve was obtained from computer solutions of the model including both homogeneous and heterogeneous contributions. Agreement between the experimental and modeling results is striking.

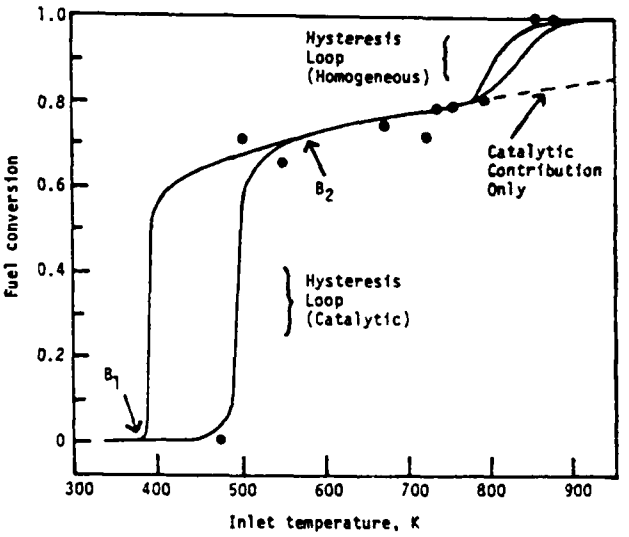

Figure 3

Experimental Data (●) and Model-Generated Curves Showing the Effect of Inlet Temperature On Conversion

For a given inlet temperature below 390K (point B_1), there is a unique solution which predicts that substrate and gas temperature throughout the bed equal the inlet temperature and that there is no appreciable conversion. In the range 390-500K, there are at least two solutions for

each inlet temperature. The upper and lower solutions are shown and undoubtedly represent stable operating states. The branch labelled I would be followed upon increasing the inlet gas temperature. At a "light-off" temperature of approximately 490K, catalytic ignition has occurred and there is a substantial increase in conversion. The extinction branch, labelled E, would be followed upon decreasing inlet temperature after having obtained catalytic ignition and having passed point B_2 on the curve. At approximately 390K, a sharp extinction is predicted. This phenomenon was observed by Pfefferle, et al. (20, p. 6) and observed and discussed by Hlavacek and Votruba (22).

The values used for the catalytic pre-exponential factor and activation energy directly affect the temperatures predicted for light-off and extinction. Values of 914 m/s for A_c and 48 kJ/mol for E_{ac} were used, which conform quite well to those cited in the literature, especially Hawthorne (4).

For temperatures in the range 390-750K, the conversion predicted is due almost completely to the catalytic reaction with no significant contribution from the homogeneous reaction. At the higher temperatures in this range, the catalytic reaction rate is limited by the rate of mass transport to the surface. At lower temperatures, some kinetic limitation is present as well.

A second hysteresis loop, which is associated with the homogeneous oxidation reaction, is encountered in the range 750-850K. Similar considerations apply to its branches as to those of the catalytic hysteresis loop. In our first comparison with these data, this feature was not reported. Our model prediction of this hysteresis was subsequently confirmed by unreported experimental results (23).

The curve in Figure 3 labelled "catalytic only" is obtained by setting the homogeneous reaction rate to zero and is thus due to the catalytic contribution only. For inlet temperatures in this range, no homogeneous combustion would occur in the absence of the catalytic reaction. For this case, in the absence of homogeneous reaction incomplete conversion would occur. Thus the homogeneous combustion, which completes fuel conversion, is supported or "bootstrapped" by the catalytic reaction. These results depend on the values for the homogeneous pre-exponential factor and activation energy. Consistent with (8), A_h was taken to be 2.87×10^9 $m^3/mol \cdot s$ and E_{ah} to be 167 kJ/mol.

The use of the model has revealed other phenomena that were unexpected for which the physical basis has subsequently been provided (e.g., the occurrence of gas temperatures exceeding the adiabatic flame temperature even for a Lewis number of unity (7)). The model has been employed in many applications which cannot be described in detail here. We have used it to examine the potential for the catalytic combustion of several low heating value streams, to predict successfully combustor geometry needed for catalytic light-off for a U.S. Air Force afterburner study, and to provide information needed for the economic component of an environmental assessment of advanced gas turbine systems (24). In all, the model has proved to be a useful tool in the interpretation of experimental data and for simulations used to screen diverse potential applications of this promising technology.

RESULTS: RADIATIVE AUGMENTED COMBUSTION

The equations of the photochemical initiation model were solved for experimental conditions of interest. Model solutions for the irradiation of a 298K, 40 kPa stoichiometric hydrogen-oxygen mixture are shown in Figure 3. Each curve represents a photochemical path for a given radiant intensity in the temperature versus oxygen atom concentration phase plane, with time implicit. The radiant pulse was assumed to be a critically damped discharge with time to peak intensity of 20 μs (see inset curve of Figure 3). The radiant energy was assumed to be uniformly distributed over the wavelengths 140 to 360 nm. The numbers labelling each curve indicate the source intensity, I, (more properly, irradiance per unit wavelength) relative to the value I_1 = 0.0587 $J/cm^2 \cdot s \cdot nm$ (e.g., 85 = 85·I_1).

For curves with relative intensity 80 and below, the radiant pulse generates oxygen atoms and some temperature increase. Oxygen atoms are then consumed by reaction with O_2, H_2, and other intermediates. The temperature profile flattens out and no rapid temperature rise characteristic of ignition is obtained. For I = 80, the integration was carried out to one hundred milliseconds without further appreciable temperature rise. At radiant intensities of 85 and above, the pulse generates somewhat higher oxygen atom concentrations than at the lower intensities. The oxygen atoms are again consumed and the mixture temperature increases in the process. However, along this path the mixture has entered an unstable region eventually leading to oxygen atom generation, more rapid temperature rise, and finally rapid burning.

In interpreting these results, it is important to remember that no heat loss mechanism is included in the model. In a physical system, heat transport and heat loss to the surroundings do occur. An indication of whether the mixture would, in a real system, obtain ignition is provided by the time required to obtain the rapid temperature rise characteristic of ignition. Thus if the model predicts rapid temperature rise within a time period for which heat loss would not be sufficient to overcome the rate of heat generation, then ignition in the physical system is indicated. (For our experimental conditions, a characteristic heat loss period of 300 μs is reasonable.) Equivalently, for the phase plane analysis of Figure 2 which includes heat loss, the mixture has crossed the separatrix and entered the region of self-sustained combustion.

The curves shown in Figure 4 are instructive for the further study of the phase plane. Curve A exhibits the effect of the complete pulse with relative intensity 100. Curves B and C show the result of shutting the light source off at 70 and 65 μs, respectively. Both curves show the eventual onset of rapid temperature rise. However, the time to 1200K is 135 μs for B and 14 000 μs for C. Comparison of these times reveals that in a system with heat loss, if the light were shut off at B_1, ignition would almost surely still be obtained; but by doing so at C_1, it would not. Hence, curve A must cross the separatrix at a point between B_1 and C_1. In this fashion, the initiation model can be used to determine details of the phase plane for a given set of experimental conditions.

The general phase plane analysis of Figure 2 suggests that the trajectory for a mixture which just manages to cross the separatrix would then follow a path of decreasing oxygen atom concentration and increasing temperature to slightly above the thermal ignition temperature. The trajectory would then turn around and proceed to ignition. The curves in Figure 3 are in excellent agreement with this qualitative analysis, as is clear from the comparison of the behavior of curves 80 and 85 and the known thermal ignition temperature (point T on the temperature scale). These results are consistent with the existence of a critical intensity below which ignition is not achieved, in agreement with earlier experimental results (5).

In order to assess the importance of including excited state species, we obtained solutions with O('D) and its reactions included and then with the assumption that the photodissociation of O_2 produced only ground state oxygen atoms. The results differed greatly -- the pulse energy required for ignition and the time to ignition without consideration of O('D) was twice that for the full kinetic set. Hence it is clear that the metastable species O('D) (and possibly other excited state species) and its reactions must be included in the modeling of photochemical initiation.

Final comparison of modeling and experimental results cannot be made yet. The radiant energy required to obtain ignition for the 40 kPa stoichiometric hydrogen-oxygen mixture as indicated by the modeling results thus far is greater than earlier experimental results would have led us to expect. However, many factors remain to be investigated. For example, if ten percent of the radiant energy is peaked in the 144 to 148 nm spectral region, then a pulse of the same total radiant energy as that of the 80 curve in Figure 3 reaches 1200K four times faster

than does the 85 curve which is based on a flat spectral distribution. A detailed investigation of the characteristics of the light sources being used is in progress. For the same conditions, another important modeling result is that for critically damped discharges at constant total pulse energy there exists a pronounced optimal time to peak intensity, as measured by the time required to reach 1200K. The existence and determination of this optimal point is of evident importance for light source design. In order to develop a consistent, detailed description of photochemical initiation and enhancement of combustion, the investigation is continuing with the complementary experimental and modeling efforts.

SUMMARY/CONCLUSIONS

Both modeling projects have enhanced our understanding of the interactions of the physical and chemical processes involved in the combustion augmentation techniques under consideration. For catalytic combustion, some of the phenomena which result from these interactions and have been further elucidated in the course of the modeling are the effect of velocity increase in the reactor on fuel conversion, the "bootstrapping" of homogeneous combustion by the catalytic reaction, and the catalytic and homogeneous light-off/extinction hystereses. In addition, the model has proved valuable as a tool to predict combustor performance for given operating conditions and has been used in this capacity to guide experimental efforts and examine promising areas of application.

The results of the photochemical initiation modeling have already identified important considerations for the experimental effort. The importance of careful spectral characterization of the light source has been confirmed. The prediction of the approximate radiant energy needed to produce ignition for a given system is possible with the present model, allowing comparison with experimental results. Further, for pulses of constant total energy, a pronounced effect of pulse width on the production of ignition has been predicted. This effect, apparently due to partial thermalization allowing more efficient use of the oxygen atoms subsequently produced by photodissociation, can be of considerable importance for light source design. As well, the model has been used to study features of the fundamental phase plane. Work is continuing on the application of the model in support of the experimental effort.

Both projects have benefited from the use of general purpose software for the integration of the model equations. We anticipate that the laudable trend in the development and availability of high quality software for these purposes, which is easy and economical to use, widely applicable, and reliable, will continue and even accelerate. Of course, such programs still require informed use, as is likely to be the case for some time. In the meantime, we find generally applicable the advice of Shampine and Gear (13) that a conservative choice of tolerance, careful use of the error criterion, experimentation, and a thoughtful examination of the numerical results are indispensible.

Finally, we observe that the two models differ in the level and placement of detail in the consideration of the underlying chemical and physical phenomena. The objective of the catalytic combustion modeling project is the description of steady-state system performance. Because the details of the combustion mechanisms or the formation of trace species were not in the scope of the study, simplified chemical kinetics were employed. The model equations are, however, quite inclusive in the balanced treatment of the processes involved. The photochemical initiation model, on the other hand, incorporates detailed consideration of photon absorption and chemical kinetics, but uses a simplified heat balance. This approach is consistent with the objective of using the model to study photon/reactant mixture interaction in combustion initiation. In these examples, the project objectives have guided the model formulations. Thus in the light of modeling objectives, a balance must be sought. Unneeded detail results in costly consumption of computer time and can hinder the discovery of significant solution features. Lack of appropriate detail can make modeling results useless or even misleading.

ACKNOWLEDGMENTS

The authors wish to acknowledge the help and encouragement received from Messrs. W. Bartok, R. B. Cole, H. Shaw, A. Skopp, and E. N. Ziegler. The generosity of C. D. Sutherland in sharing the STIFF and equation-writer codes with us is greatly appreciated. Portions of the catalytic combustion modeling were supported by the U.S. Environmental Protection Agency under Contract No. 68-02-2146 and the NSF Summer Faculty Research Participation Program. The investigation of Radiative Augmented Combustion is sponsored by the Air Force Office of Scientific Research, United States Air Force. The second author gratefully acknowledges the support of Montclair State College for portions of the modeling effort through the provision of released time. Finally, we would like to express our appreciation to Ms. Corinne Barron for her patience and assistance in preparing this manuscript.

REFERENCES

1. Blazowski, W. S., and Walsh, D. E., "Catalytic Combustion: An Important Consideration for Future Applications," Combustion Science and Technology, Vol. 10, pp. 233-244, 1975.

2. Pfefferle, W. C., "The Catalytic Combustor: An Approach to Cleaner Combustion," Journal of Energy, Vol. 2, No. 3, pp. 142-146, 1978.

3. Young, L. C., and Finlayson, B. A., "Mathematical Models of the Monolith Catalytic Converter: Part II. Application to Automobile Exhaust," AIChE Journal, Vol. 22, No. 2, pp. 343-353, Mar., 1976.

4. Hawthorne, R. D., "Afterburner Catalysts - Effects of Heat and Mass Transfer Between Gas and Catalyst Surface," AIChE Symposium Series No. 137, Vol. 70, pp. 428-438, 1974.

5. Cerkanowicz, A. E., "Photochemical Enhancement of Combustion and Mixing in Supersonic Flows," Final AFOSR Scientific Report No. TR-74-0153, November, 1973.

6. Cerkanowicz, A. E., and Stevens, J. G., "Modeling of Radiative Augmented Combustion: Comparisons with Experimental Data" (in preparation).

7. Cerkanowicz, A. E., Cole, R. B., and Stevens, J. G., "Catalytic Combustion Modeling; Comparisons with Experimental Data," Journal of Engineering for Power, Vol. 99, Series A, No. 4, pp. 593-600, October, 1977.

8. Longwell, J. P., and Weiss, M. A., "High Temperature Reaction Rates in Hydrocarbon Combustion," Industrial Engineering Chemistry, Vol. 47, No. 8, pp. 1634-1643, Aug., 1955.

9. Stevens, J. G., and Ziegler, E. N., "Effect of Momentum Transport on Conversion in Adiabatic Tubular Reactors," Chemical Engineering Science, Vol. 32, pp. 385-391, 1977.

10. Lee, S., and Aris, R., "On the Effects of Radiative Heat Transfer in Monoliths," Chemical Engineering Science, Vol. 32, pp. 827-837, 1977.

11. Kocharts, G., "Absorption and Photodissociation in the Schumann-Runge Bonds of Molecular Oxygen in the Terrestrial Atmosphere," Planetary Space Science, Vol. 24, pp. 589-604, 1976.

12. Lentini, M., and Pereyra, V., "A Variable Order Finite Difference Method for Nonlinear Multipoint Boundary Value Problems," Mathematics of Computation, Vol. 28, No. 128, pp. 981-1003, Oct., 1974.

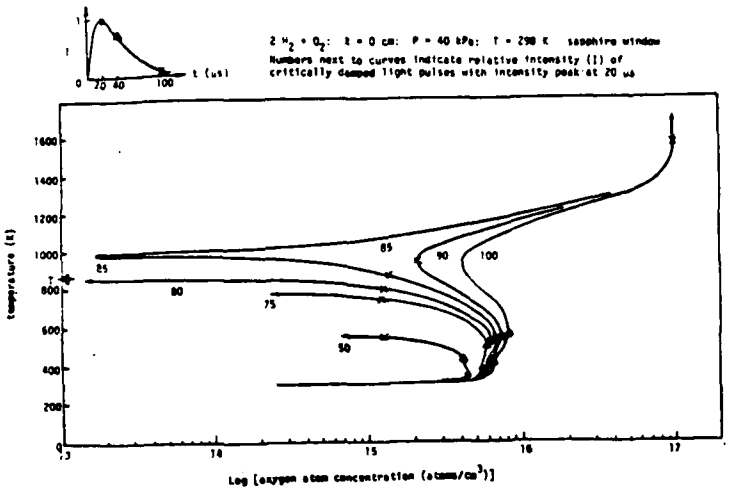

Figure 4

Reactant Mixture Phase Plane Paths Resulting from Pulsed Vacuum Ultraviolet Irradiation

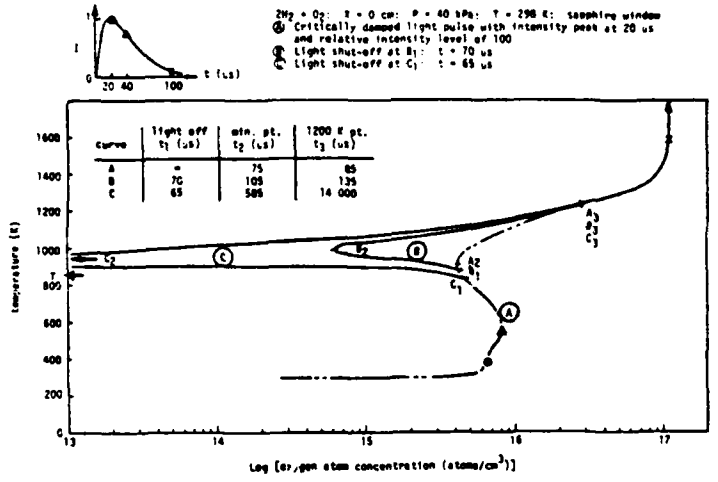

Figure 5

Influence on Irradiation Time on Reactant Mixture Phase Plane Paths Resulting from Pulsed Vacuum Ultraviolet Irradiation

REFERENCES (continued)

13. Shampine, L. F., and Gear, C. W., "A User's View of Solving Stiff Ordinary Differential Equations," SIAM Review, Vol. 21, No. 1, pp. 1-17, Jan., 1979.

14. Lapidus, L., Aiken, R. C., and Liu, Y. A., "The Occurrence and Numerical Solution of Physical and Chemical Systems Having Widely Varying Time Constants," in Stiff Differential Systems (R. A. Willoughby, ed.), Plenum Press, New York, 1974, pp. 187-200.

15. Gear, C. W., Numerical Initial Value Problems in Ordinary Differential Equations, Prentice-Hall, Inc., Englewood Cliffs, New Jersey, 1971, pp. 223, 224.

16. Keller, H. B., Numerical Methods For Two-Point Boundary Value Problems, Blaisdell Publishing Co., Waltham, Mass., 1968, pp. 162-168.

17. Gear, C. W., "The Automatic Integration of Stiff Ordinary Differential Equations," Information Processing, 1969, pp. 187-193.

18. Kahaner, D., and Sutherland, C. D., Code D207 of the program library at Los Alamos Scientific Laboratory, Los Alamos, New Mexico.

19. Sutherland, C. D., and Zinn, J., "Chemistry Computations for Irradiated Hot Air," Los Alamos Scientific Laboratory, LA-6055-MS, Sept., 1975.

20. Pfefferle, W. C., et al., "Catathermal Combustion: A New Process for Low-Emissions Fuel Conversion," ASME Paper No. 75-WA/Fu-1.

21. Votruba, J., et al., "Heat and Mass Transport in Honeycomb Catalysts-II," Chemical Engineering Science, Vol. 30, pp. 201-206, 1975.

22. Hlavacek, V., and Votruba, J., "Experimental Study of Multiple Steady States in Adiabatic Catalytic Systems," Chemical Reaction Engineering II, American Chemical Society, Washington, 1974, pp. 545-558.

23. Carrubba, R. V., private communication.

24. Cerkanowicz, A. E., Shaw, H., and Stevens, J. G., "Environmental Assessment of Advanced Open Cycle Gas Turbine Power Plants," ASME Paper No. 79-GT-187.

APPENDIX III

Catalytic Combustion Modeling; Comparisons with Experimental Data

A. E. Cerkanowicz, R. B. Cole and J. G. Stevens

A. E. Cerkanowicz
Government Research Laboratories,
Exxon Research and Engineering Co.,
Linden, N. J.
Assoc. Mem. ASME

R. B. Cole
Department of Mechanical Engineering,
Stevens Institute of Technology,
Hoboken, N. J.
Assoc. Mem. ASME

J. G. Stevens
Department of Mathematics,
Montclair State College,
Upper Montclair, N. J.

Catalytic Combustion Modeling; Comparisons With Experimental Data[1]

A model for catalytic combustor operation is described for a well-mixed plug-flow reactor. Heterogeneous and homogeneous reactions are considered with heat and mass transfer handled using transport coefficients. Gas velocity is allowed to vary axially and heat conduction in the catalyst bed is included. Computer solutions were obtained for axial profiles of conversion, gas and substrate temperature, velocity, and pressure. Model predictions are compared to catalytic combustion data, showing excellent agreement. Catalytic light-off, hysteresis, and homogeneous contribution are discussed. Data from a hybrid combustor developed in this laboratory are analyzed using a simplified model.

Introduction

Conventional gas turbine combustors produce unacceptable levels of NO_x because of the high temperatures developed in the primary combustion zone, especially under high-power conditions. If the high flame temperatures can be significantly reduced without compromising combustion efficiency, then a substantial reduction in NO_x emissions can be achieved. Catalytic combustion is being investigated experimentally and theoretically in this laboratory as a means of achieving this end, as well as improvements in performance and cost such as improved stability and product gas uniformity. This paper describes the theoretical modeling effort.

The objective of this effort was to develop a sufficiently detailed model of the operation of catalytic combustors to enhance the understanding of this new technology. Currently, the model considers steady-state operation of a well mixed plug flow reactor with heat and mass transfer between gas and solid phases. Reaction and heat release are considered to occur both on the catalyst surface and in the gas phase. By employing the appropriate conservation equations for the two phases, combustor operation can be described in terms of a two-point boundary value problem. A powerful solution technique is employed to obtain computer solutions for temperature (gas and substrate), pressure, velocity, and fuel conversion profiles as a function of reactor geometry, catalyst and substrate properties, and inlet conditions. Reactor configurations containing screens, pellets, or monoliths can be handled by selection of appropriate heat and mass transfer correlations.

A discussion of the numerical technique mentioned in the foregoing and of earlier modeling work in which the possibility of parallel gas-phase reaction was not considered was reported previously [1].[2] This initial analysis indicated that velocity variation through the reactor (and hence reactant residence time) cannot be neglected in calculating combustor operating characteristics. Indeed, constant velocity models result in significant overestimation of conversion. Many previous modeling efforts neglect the effect of velocity variation since they were concerned primarily with catalytic clean-up of exhaust or tail gas where insufficient heat release occurs to affect the gas velocity significantly.

The effectiveness and practicality of the model were demonstrated by excellent agreement between model predictions and experimental catalytic combustion data. Data from a hybrid combustor are presented and analyzed using a simplified model. Refinement and extension of our current model are in progress to provide for the inclusion of multiple fuel species, two-step reaction schemes, and internal heat removal from the catalytic section.

Physical Assumptions of the Model

The following assumptions were made in the derivation of governing mass, heat, and momentum balances for the steady-state catalytic combustor model:

[1] Supported in part by the Environmental Protection Agency under Contract No. 68-02-2146 and the National Science Foundation Summer Faculty Research Participation Programs, 1975 and 1976.

Contributed by the Gas Turbine Division and presented at the Gas Turbine Conference, Philadelphia, Pa., March 27-31, 1977, of THE AMERICAN SOCIETY OF MECHANICAL ENGINEERS. Manuscript received at ASME Headquarters December 22, 1976. Paper No. 77-GT-85.

[2] Numbers in brackets designate References at end of paper

1 Properties for the gas-phase are uniform throughout a reactor cross section (plug flow). Axial dispersion is neglected.

2 The solid temperature and fuel concentration associated with the substrate/catalyst layer are similarly uniform.

3 Reaction of the fuel to products can occur at the catalyst surface and in the gas phase. Global (one-step) Arrhenius rate expressions are employed for complete oxidation reactions in each phase. Assignable orders in fuel and oxygen are incorporated in the homogeneous expression, while the heterogeneous reaction is provisionally taken to be first order in the fuel and zero order in oxygen. The latter assumption is considered adequate for the fuel-lean conditions of interest (2).

4 Transport of the fuel species is considered to occur by diffusion through the boundary layer and to be balanced by the catalytic reaction rate on the surface.

5 Heat released by the catalytic oxidation reaction is liberated at the surface and subsequently convected into the gas phase. Heat and mass transport are modeled using transfer coefficients where the driving force is provided by temperature and concentration differences between the bulk gas and the catalytic surface.

6 The velocity is allowed to vary axially, subject to a Fanning friction factor. For a given application, the transfer coefficients are evaluated using appropriate correlations at estimated axially mean conditions.

7 Axial heat conduction in the substrate is included in the model, but solid-to-solid radiant effects, gas-phase conduction and radiation are neglected. All the heat released by combustion in the reactor is assumed to be carried out of the combustor by the gas stream.

Conservation Equations

The resulting model equations are given below in a form applicable to a monolithic (constant channel cross section) support. Similar equations have been written for packed-bed or screen geometries but will not be presented.

Fuel-species balance (gas-phase)

$$S\frac{d(vC_f)}{dz} + SA_h \exp\left(-\frac{E_{ah}}{RT}\right)(C_f)^{nf}(C_{O_2})^{no} + \sigma k\,(C_f - C_{fs}) = 0 \tag{1}$$

Fuel-species balance (surface)

$$k(C_f - C_{fs}) = A_c \exp\left(-\frac{E_{ac}}{RT_s}\right) C_{fs} \tag{2}$$

Gas-phase energy balance

$$-S\rho v C_p \frac{dT}{dz} + \sigma h(T_s - T) + S(-\Delta H)A_h \exp\left(-\frac{E_{ah}}{RT}\right)(C_f)^{nf}(C_{O_2})^{no} = 0 \tag{3}$$

Solid-phase energy balance

$$S_s\lambda_s\frac{d^2T_s}{dz^2} - \sigma h(T_s - T) + \sigma(-\Delta H)A_c \exp\left(-\frac{E_{ac}}{RT_s}\right) C_{fs} = 0 \tag{4}$$

Momentum equation

$$-(\rho v)\frac{dv}{dz} - \frac{dp}{dz} - \frac{\sigma f}{2S}(\rho v)\,v = 0 \tag{5}$$

Continuity equation

$$\frac{d}{dz}(\rho v) = 0 \tag{6}$$

Equation of state

$$p = \frac{\rho}{M}RT = \frac{\rho_0 v_0 R}{M}\frac{T}{v} \tag{7}$$

Stoichiometry

$$\frac{vC_{O_2}}{(vC_{O_2})_0} = 1 - \phi\left(1 - \frac{vC_f}{(vC_f)_0}\right) \tag{8}$$

Boundary conditions

$$\text{at } z = 0\text{: } C_f = (C_f)_0,\ C_{O_2} = (C_{O_2})_0,\ v = v_0,\ T = T_0,\ \frac{dT_s}{dz} = 0$$

$$\text{at } z = L\text{: } \frac{dT_s}{dz} = 0$$

Considerable simplification of the above equations is possible. Equation (6) allows ρv to be replaced by $\rho_0 v_0$, while equation (7) and (8) can be used to eliminate pressure and oxygen concentration as explicit variables.

Dimensionless Equations and Groupings. Techniques

Rearrangement and introduction of the dimensionless variables

$$\zeta = \frac{z}{L},\ \theta = \frac{T - T_0}{T_0},\ \theta_s = \frac{T_s - T_0}{T_0},\ \upsilon = \frac{v}{v_0},$$

$$\psi_f = \frac{C_f}{(C_f)_0},\ \psi_{fs} = \frac{C_{fs}}{(C_f)_0},\ \omega = \frac{vC_f}{v_0(C_f)_0} = \upsilon\psi_f$$

provides the following set of catalytic combustor equations:

$$\frac{d\omega}{d\zeta} + \mathrm{D}_{ah}\exp\left(\frac{\gamma_h\theta}{1+\theta}\right)\left(\frac{\omega}{\upsilon}\right)^{nf}\left(\frac{1-\phi(1-\omega)}{\upsilon}\right)^{no} + J_D(\psi_f - \psi_{fs}) = 0 \tag{9}$$

$$J_D(\psi_f - \psi_{fs}) = \mathrm{D}_{ac}\exp\left(\frac{\gamma_c\theta_s}{1+\theta_s}\right)\psi_{fs} \tag{10}$$

$$\frac{d\theta}{d\zeta} = J_H(\theta_s - \theta)$$

Nomenclature

Note: Dimensionless groupings found in Table 1 are not included.

A = pre-exponential factor; A_c, m/s; A_h, $(\mathrm{mol/m^3})^{1-n}$/s, where n is total homogeneous reaction order

C = concentration (associated with catalyst layer if subscripted by s; otherwise, gas-phase), mol/m³

C_p = specific heat capacity of gas at constant pressure, J/(kg·K)

E_a = activation energy, J/mol

f = fanning friction factor

h = heat transfer coefficient, J/(m²·s·K)

$(-\Delta H)$ = heat of reaction, J/mol

k = mass transfer coefficient, m/s

M = molecular weight, kg/mol

n = reaction order

Pr = Prandtl number

p = pressure, Pa

R = gas constant, J/(mol·K)

S = void cross section, m²

S_s = solid cross section, m²

Sc = Schmidt number

T = temperature, K

v = velocity, m/s

z = axial dimension, m

λ = thermal conductivity, J/(m·s·K)

ρ = density, kg/m³

σ = wetted perimeter, m

ϕ = equivalence ratio

ψ = dimensionless concentration (see text for definitions)

ω = dimensionless mass fraction

θ = dimensionless temperature

υ = dimensionless velocity

ζ = dimensionless axial dimension

Subscripts

0 = inlet

c = catalytic

f = fuel

h = homogeneous

O_2 or O = oxygen

s = surface (solid)

Table 1 Dimensionless groupings of conservations equations for monolith

Symbol	Definition	Name	Significance
J_D	$\left(\frac{L}{v_o}\right)\left(\frac{ak}{\varepsilon}\right)$	Mass Transport Number	Ratio of Characteristic Residence Time of Gas in Reactor to Mass Transport Time
J_E	$\frac{p_o}{\rho_o v_o^2}$	Euler Number	Ratio of Pressure Force to Inertia Force
J_F	$\frac{\sigma L f}{2\varepsilon}$	Friction Number	
J_H	$\left(\frac{L}{v_o}\right)\left(\frac{\sigma h}{\varepsilon \rho_o C_p}\right)$	Heat Transport Number	Ratio of Characteristic Residence Time of Gas in Reactor to Heat Transport Time
B	$\frac{(C_f)_o(-\Delta H)}{\rho_o C_p T_o}$	Adiabatic Temperature Rise	Ratio of Heat Release to Thermal Energy of Gas Stream
γ_h	$\frac{E_{ah}}{RT_o}$	Characteristic Homogeneous Activation Energy	-
γ_c	$\frac{E_{ac}}{RT_o}$	Characteristic Catalytic Activation Energy	-
D_{ah}	$\left(\frac{L}{v_o}\right)\left(\frac{A_h (C_f)_o^{n_f} (C_{O_2})_o^{n_o} e^{-\gamma_h}}{(C_f)_o}\right)$	Homogeneous Damkohler Number	Ratio of Characteristic Residence Time of Gas in Reactor to Characteristic Homogeneous Reaction Time
D_{ac}	$\left(\frac{L}{v_o}\right)\left(\frac{\sigma A_c e^{-\gamma_c}}{\varepsilon}\right)$	Catalytic Damkohler Number	Ratio of Characteristic Residence Time of Gas in Reactor to Characteristic Catalytic Reaction Time
Pe_s	$\left(\frac{L\rho_o v_o C_p}{\lambda_s}\right)\left(\frac{\varepsilon}{1-\varepsilon}\right)$	Peclet Number (Heat Transfer)	Ratio of Axial Heat Convection to Axial Heat Conduction in Substrate

$$-BD_{ah}\exp\left(\frac{\gamma_h\theta}{1+\theta}\right)\left(\frac{\omega}{v}\right)^{n_f}\left(\frac{1-\phi(1-\omega)}{v}\right)^{n_o}=0 \quad (11)$$

$$\frac{1}{Pe_s}\frac{d^2\theta_s}{d\zeta^2}-J_H(\theta_s-\theta)+BD_{ac}\exp\left(\frac{\gamma_c\theta_s}{1+\theta_s}\right)\psi_{fs}=0 \quad (12)$$

$$\frac{dv}{d\zeta}=\frac{J_E v\frac{d\theta}{d\zeta}+J_F v^3}{J_E(1+\theta)-v^2} \quad (13)$$

subject to

$$\zeta=0: v=\omega=1, \theta=\frac{d\theta_s}{d\zeta}=0$$

$$\zeta=1: \frac{d\theta_s}{d\zeta}=0$$

Equation (10) and the relation $\omega = v\psi_f$ can now be used to eliminate ψ_f and ψ_{fs}. Moreover, upon substituting for the last two terms in equation (12) from equations (9)–(11) and integrating one obtains:

$$\frac{d\theta_s}{d\zeta}=Pe_s(\theta-B(1-\omega)) \quad (12')$$

subject to $\theta(1) - B(1 - \omega(1)) = 0$.

The definitions of the dimensionless groupings occurring in the above equations for a monolith are given in Table 1, together with an indication of their physical significance.

High-order approximations to the solutions of the governing equations were obtained using an adaptive, variable-order, finite-difference scheme developed by Lentini and Pereyra [3]. Much of the power of this method results from the combination of Newton's method with iterated deferred corrections. As for most finite difference methods employed to solve nonlinear problems, some care must be taken to insure that the initial iterate lies in the neighborhood of convergence about a solution, especially in regions having multiple steady states. Where stiffness and partial instability were encountered it was on occasion found necessary to employ parametric continuation. Further discussion of the use of this method can be found in [1].

Parametric Variations

In order to investigate the behavior of solutions of the model equations, several parametric variations were carried out. Our aim was to study the relation of the homogeneous to the heterogeneous reaction. Accordingly, the homogeneous Damkohler number, D_{ah}, was varied for three values of the adiabatic temperature rise, B, with the other parameters fixed at physically consistent values. This variation can be thought of as increasing the characteristic homogeneous reaction rate relative to a fixed catalytic reaction so as to ascertain the effect on solution profiles. Fig. 1 exhibits conversion $(1 - \omega)$ profiles for a case which is typical of a combustor operated fuel-lean with relatively low inlet temperature (500 K). $B = 1$ was used, indicating moderately high heat release. The curve with $D_{ah} = 0$ gives the conversion profile for the case where only catalytic combustion is taken into consideration. The effect of increasing D_{ah} is to increase conversion due to contribution from the terms accounting for homogeneous combustion. The onset of gas-phase combustion occurs at a fairly distinct point in the bed. At this point the gas phase has attained a reasonably well-defined homogeneous light-off (ignition) temperature. For combustors utilizing hydrocarbon fuels, the values for D_{ah} needed here to show significant homogeneous contribution are unrealistically high (see discussion of kinetic parameters in the following). Nevertheless, the clearly delimited homogeneous combustion zone exhibited in this case should be typical of conditions for which the dimensionless homogeneous activation energy, here taken to be 40, is high. This results in a strong temperature dependence of the homogeneous reaction rate. In fact, in the absence of any catalytic reaction ($D_{ac} = 0$), no conversion is indicated for any of the values of D_{ah} used. Thus, the homogeneous reaction is "bootstrapped" by the heat released due to catalytic combustion. This strong dependence also gives rise to numerical "stubbornness" as can be appreciated by

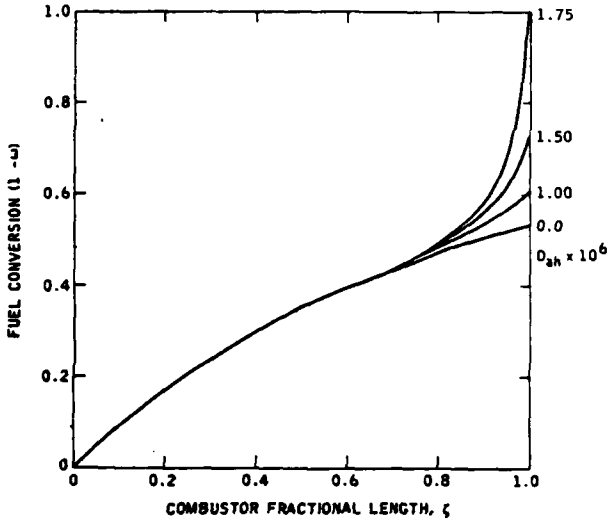

Fig. 1 Effect of variation of homogeneous Damkohler number on conversion profiles for the case with $B = 1$, $\gamma_h = 40$, $\gamma_c = 20$, $D_{ac} = 0.15$, $J_H = J_D = 1$, $J_E = 200$, $J_P = 0$, $Pe_s = 5$

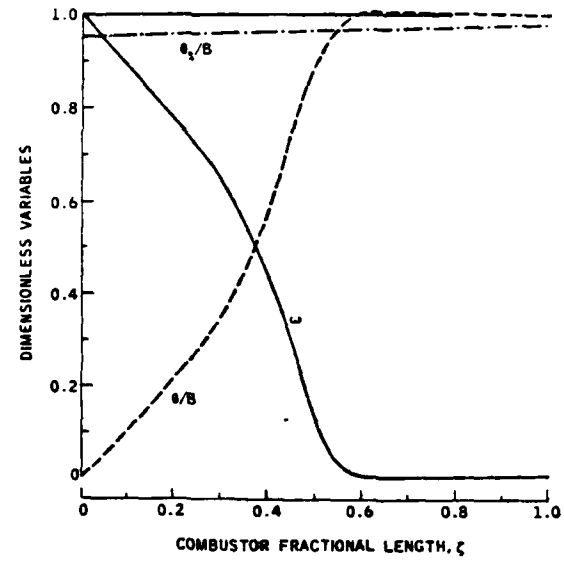

Fig. 3 Unconverted fuel fraction (ω), gas temperature (θ/B), and substrate temperature (θ_s/B) profiles showing gas overtemperature for case with $B = 0.5$, $\gamma_c = 20$, $D_{ac} = 0.15$ $\gamma_h = 20$, $D_{ah} = 0.10$, $J_E = 200$, $J_H = J_D = 1$, $Pe_s = 5$

inspecting Fig. 1. The integration scheme employed together with continuation on D_{ah} successfully overcame this difficulty.

Conversion profiles obtained upon variation of D_{ah} with $B = 0.5$ and $\gamma_h = 20$ are presented in Fig. 2. These values suggest fuel-lean operation but with a much higher gas inlet temperature (1000 K). The solid curves represent a family of solutions showing the effect of varying D_{ah}. With the lower value of 20 for γ_h, the temperature dependence of the homogeneous rate is now much weaker. Consequently, the onset of homogeneous contribution is no longer sharp but gradual. Such a gradual onset could be expected from the presence of a weak but non-negligible homogeneous reaction occurring throughout the reactor length even in the absence of any catalytic reaction. This situation is indicated by the conversion profile with $D_{ah} = 0.10$ and $D_{ac} = 0$ in Fig. 2. Again in this case, the increase in gas

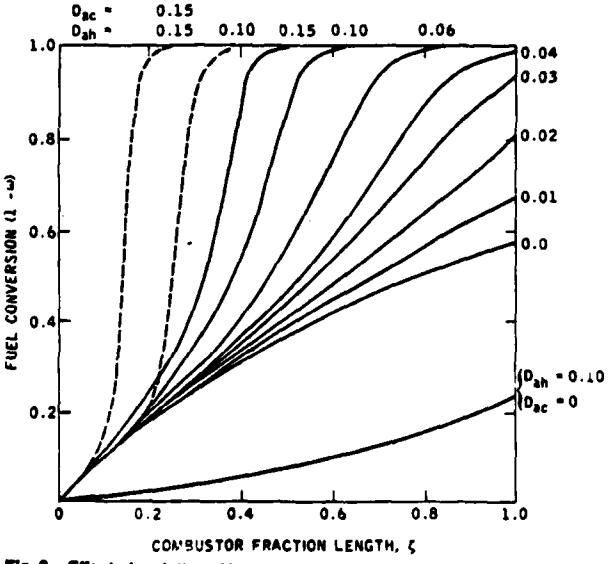

Fig. 2 Effect of variation of homogeneous Damkohler number on conversion profiles for the case with $B = 0.5$, $\gamma_h = 20$, $\gamma_c = 20$, $D_{ac} = 0.15$, $J_H = J_D = 1$, $J_E = 200$, $J_P = 0$, $Pe_s = 5$

temperature due to catalytic combustion greatly enhances the homogeneous reaction rate with the combined effect being significantly increased conversion.

Two more observations about this series of solutions should be made. First, two dashed curves are shown in Fig. 2 which represent additional steady states that show better conversion than those represented by the solid curves (for the same values of D_{ah}). There is strong numerical evidence that the pure catalytic model (i.e., with $D_{ah} = 0$) has a unique solution for these parameter values. Hence, for this case the presence of multiple steady states is apparently attributable to inclusion of the terms related to homogeneous combustion. For other combustor conditions, multiple states have been observed for the pure catalytic model as well. Second, the phenomenon of gas overtemperature can be observed in Fig. 3 showing the profiles of unconverted fuel fraction, gas temperature, and substrate temperatures (both temperatures divided by B) for $D_{ah} = 0.10$. From the boundary condition $\theta(1) = B(1 - \omega(1))$, it is clear that the dimensionless gas temperature at the reactor outlet can not exceed the adiabatic temperature rise. Yet for this case, θ does exceed $B(\theta/B > 1)$ within the reactor. Before reaching the exit, however, heat has been lost by the gas to the substrate thus cooling the gas below the adiabatic flame temperature. In this connection, it should be noted that the value used for the solids Peclet number, $Pe_s = 5$, corresponds to a very conductive substrate (e.g., metallic). For higher values of Pe_s (≥ 100) no such overtemperature is observed. The explanation of this occurrence is thus related to axial heat conduction in the substrate. Indeed if this conduction were not allowed, the condition $\theta = B(1 - \omega)$ would be imposed throughout the bed, i.e., local adiabaticity, with the consequence that θ could never exceed B. This overtemperature phenomenon is different from substrate overtemperature and transient overtemperature which have been previously discussed [4].

The final variation of D_{ah} to be described was carried out with $B = 0.03$ and $\gamma_h = 20$ and is presented in Fig. 4. These values are typical of a combustor being operated extremely fuel-lean at high gas inlet temperature (1000 K). These conditions can arise when a fuel-air mixture is partially oxidized in a preburner before entering the catalytic reactor. Experimental data obtained by Siminski and Shaw [5] from such a hybrid combustor is discussed below. For the chosen values of D_{ah}, a moderate homogeneous reaction occurs in the absence of any catalytic reaction. When both reactions are taken into account,

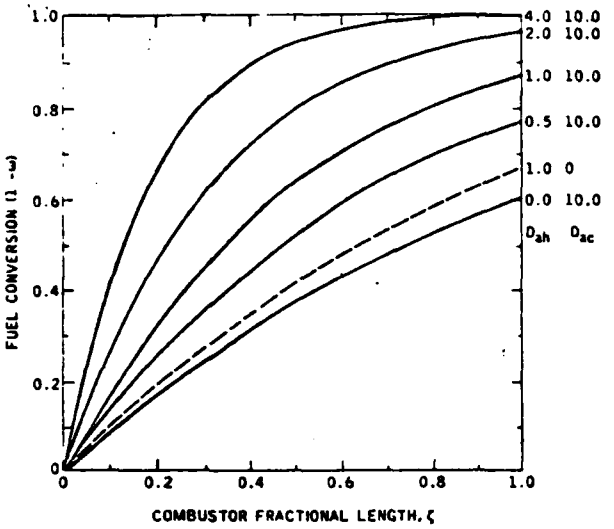

Fig. 4 Effect of variation of homogeneous Damkohler number on conversion profiles: case with $B = 0.03$, $\gamma_e = 5$, $\gamma_h = 20$, $J_H = J_D = 1$, $J_E = 200$, $J_F = 0$, $Pe_e = 200$

the homogeneous reaction contributes significantly throughout the length of the bed. However, in contrast to the "bootstrap" phenomenon observed earlier, the reactions in this case do not appear to enhance each other. Indeed the unconverted fuel fraction is observed to equal closely the product of the fractions that would be obtained for independent catalytic and homogeneous reactions.

Correlations and Kinetics

The analysis of data which will be subsequently discussed was carried out with an option in our computer program which allows for the dimensionless groupings to be calculated from physical input variables. The correlations used to calculate the heat transport coefficient, and thus J_H, were similar to those discussed by Hawthorn [6]. The mass transport number was then computed assuming the constancy of the ratio of $J_H(\mathrm{Pr})^{2/3}$ to $J_D(\mathrm{Sc})^{2/3}$ as in Satterfield [7].

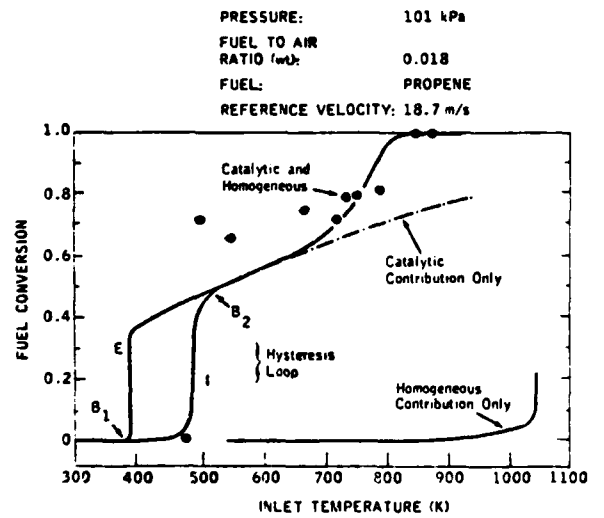

Fig. 5 Experimental data (●) and model-generated curves showing the effect of inlet temperature on conversion

Vortruba, et al. [8] have pointed out difficulties with these theoretically developed expressions and have presented different expressions for laminar flow. Physical properties occurring in the correlations have been taken to be those of air at inlet pressure and provisionally at a temperature equal to the mean of the inlet temperature and the adiabatic flame temperature. The reference binary diffusivity of the specific fuel-air system of interest is provided as an input variable.

The choice of suitable global homogeneous reaction rate expressions is difficult. A major reason is that we are currently treating a complex reaction over a wide range of physical conditions as a one-step reaction. For initial calculations, we have employed a second order expression (first order in fuel and in oxygen) with constant pre-exponential factor. Values for A_h and E_{ah} have been chosen within ranges obtained by suitably interpreting the empirical expressions given by Longwell and Weiss [9].

The choice of an appropriate catalytic rate expression is further complicated by the wide variations in such expressions appearing in the literature and frequently by insufficient information being given to permit their use. References [2, 6, 10] do give rate data for heterogeneous combustion of hydrocarbon fuels. Consonant with the above sources, the catalytic rate expression used for fuel-lean applications was first order in fuel and zero order in oxygen. Care was taken that values for A_c and E_{ac} were within ranges suggested by the literature and that the overall chemical rate thus obtained for relevant temperatures reflected experimental values.

Comparison With Catalytic Combustor Data

A comparison of the model with experimental catalytic reactor data reported by Pfefferle, et al. [11] was made, demonstrating excellent agreement. Computer solutions were obtained using physical input data corresponding to the experimental operating conditions. Thus, actual values for reference velocity, pressure, fuel to air ratio, bed length, channel diameter, and porosity were input parameters. With reference to substrate conductivity, we have successfully solved the equations with values of Pe_s up to 10^4, but experience has shown that such solutions are virtually identical to those obtained for $Pe_s = 200$, which value was adopted for this study. Fuel parameters chosen were those for propene. The choice of kinetic parameters is discussed in the following. Finally, we observe a probable variance between *conversion* as predicted by the model and the *hydrocarbon conversion* reported in [11]. The former, due to the global assumption of the model, means complete oxidation, while the latter appears to be the ratio of exit hydrocarbon (as C_1) concentration to inlet fuel concentration.

Fig. 5 shows the effect of inlet temperature upon conversion with combustor operating conditions given in the legend. Further experimental details can be found in [11]. The experimental data points are indicated by circles, while the solid curve was obtained from our computer solutions for the full model including heterogeneous and homogeneous contributions. We observe the striking agreement in behavior of the theoretical curve with the data.

For a given inlet temperature below 390 K (point B_1), there is a unique solution which predicts that substrate and gas temperatures throughout the bed equal the inlet temperature, the reaction is *kinetically limited*, and there is no appreciable conversion. In the range 390–520 K, there are two solutions for each inlet temperature, labeled as branches I and E between points B_1 and B_2 in Fig. 5. It is reasonable to assume that both branches represent stable solutions. The ignition branch, I, would be followed upon increasing inlet temperature. At a "light-off" temperature of approximately 490 K, catalytic ignition has occurred, the substrate temperature considerably exceeds the gas inlet temperature and there is substantial conversion. The values used for the two catalytic rate parameters, A_c and E_{ac}, directly affect the temperature at which this activation of the catalyst occurs. Values of 914 m/s for A_c and 50.2 kJ/mol for E_{ac} were used for this study. These conform quite well to those cited in the literature, especially by Hawthorne [6].

The extinction branch, labeled E in Fig. 5, would be followed upon decreasing gas inlet temperature after having obtained catalytic

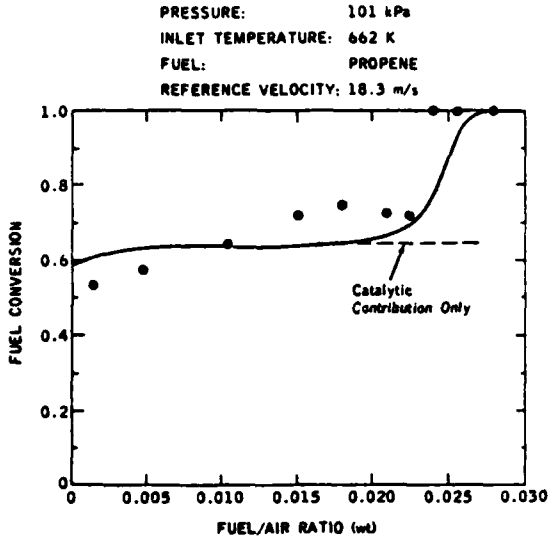

Fig. 6 Experimental data (●) and model-generated curve showing the effect of fuel/air ratio on conversion

ignition and having passed the point B_2 on the curve. At approximately 390 K, a sharp extinction is predicted. The model thus indicates the presence of a hysteresis effect. This phenomenon was observed by Pfefferle, et al. [11, p. 6] and has been observed and discussed by Hlavacek and Vortruba [12].

For temperatures in the range of 390–650 K the conversion predicted can be attributed almost totally to the catalytic reaction with no significant contribution from homogeneous reactions. A good measure of rate domination for catalytic oxidation is provided by the surface fuel concentration to gas fuel concentration ratio (C_{fs}/C_f). When this ratio is close to zero, mass transport limitation exists; when it is close to one, the rate is kinetically limited. For 420 K this ratio averages about 0.14 throughout the bed indicating that the surface reaction rate is still a factor in determining the overall rate. Hence, increased conversion is observed at higher temperatures in this range as a result of enhanced surface reaction rate. Indeed by 644 K the model predicts that the ratio C_{fs}/C_f equals approximately 0.009, indicating that the reaction is approaching mass transport limitation. The computer generated curve clearly predicts the behavior of the data in this interval.

A second pronounced increase in conversion is predicted in the interval 750–850 K. At the lower temperature the conversion is 72 percent, while it exceeds 99 percent for 850 K. The curve in Fig. 5 labelled "catalytic only" is obtained by setting the homogeneous reaction rate to zero and thus considering terms arising only from the catalytic reaction. Comparison of this curve to the solid curve reveals that the rise in conversion in this range (as well as some contribution from 650 K on) results from terms accounting for homogeneous combustion. Thus, the homogeneous reaction is ignited or, perhaps better, supported by the catalytic reaction, as observed by Pfefferle, et al. [11]. This "bootstrapping" phenomenon, observed in the parametric variations discussed previously, is further illuminated upon examining the curve labelled "homogeneous only" obtained when terms for the catalytic reaction are neglected. The temperature needed to achieve homogeneous "light-off" in the absence of any catalytic reaction is 1050 K (Fig. 5). Indeed, axial conversion profiles obtained from the model with catalytic and homogeneous terms begin to diverge from those obtained with only catalytic terms at a reactor location in which the gas temperature is nearing this homogeneous ignition temperature.

The gas temperature range for which the model predicts significant contribution from the homogeneous reaction is dependent upon the values used for A_h and E_{ah}. Consistent with the literature cited previously, A_h was taken to be $2.87 \times 10^9 m^3/(mol \cdot s)$ and E_{ah} to be 167 kJ/mol. Experimental data suggest the onset of significant homogeneous reaction at somewhat higher temperatures than does the model with these values. No attempt was made to vary A_h and E_{ah} to obtain a better fit. Nevertheless, the agreement of model and data throughout the temperature range 300–900 K is striking.

Reactor conversion data and model-generated curve are given in Fig. 6 as a function of fuel-to-air ratio (F/A wt) with other operating conditions fixed as indicated. For F/A values below 0.015, the conversion obtained is indicated by the model to be due to mass transport limited catalytic oxidation. The inlet temperature of 662 K is sufficiently high to allow the catalyst to remain active even to extremely lean conditions. With the kinetic parameters chosen, both data and model exhibit a marked increase in conversion around a F/A of 0.025. This increase is due to the contribution from the terms accounting for homogeneous combustion, as can be seen from comparison with the "catalytic only" curve. The rise suggested by the data is somewhat more rapid than that reflected by the curve, as was also the case for Fig. 5. In that the sharpness of the homogeneous onset is strongly dependent on the value obtained for γ_h and thus upon E_{ah} as was noted in the foregoing, a value for E_{ah} higher than 167 kJ/mol is suggested. Further investigation into kinetic values and sensitivities is being undertaken. However, excellent agreement with the data is again evident.

Comparison With Data From a Hybrid Combustor

The results of a catalytic combustor development program carried out in this laboratory are discussed elsewhere by Siminski and Shaw [5]. In order to achieve stability at low-power (idle) conditions, a hybrid combustor in which the fuel-air mixture is partially oxidized in a preburner prior to entering the catalytic reactor was designed, constructed, and tested. At this time, detailed calculations with the full model for this hybrid system have not been completed. We shall, however, provide a simple analysis of the data, based on the assumption of catalytic rate limitation either by mass transport or by surface kinetics, neglecting homogeneous contribution.

The oxidation of fuel in the preburner results in extremely lean operation for the catalytic reactor and high gas inlet temperature. For these conditions, the assumption that substrate and gas temperatures throughout the bed approximately equal the inlet temperature (and consequently that the velocity remains essentially constant) appears reasonable. On this basis the model equations simplify and can be integrated to obtain:

$$\ln \omega(1) = -D_{ac} \text{ (kinetics limited)} \tag{13}$$

$$\ln \omega(1) = -J_D \text{ (transport limited)} \tag{14}$$

If similarity of heat and mass transport and turbulent flow in the catalytic reactor is assumed, along with constant pressure throughout the preburner section, then, accounting for the various dependencies of D_{ac} and J_D on T_0, we have

$$\ln \omega(1) \sim -\exp(-E_{ac}/RT_0)/T_0 \text{ (kinetics limited)} \tag{15}$$

or

$$\ln \omega(1) \sim -T_0^{0.1} \text{ (transport limited)} \tag{16}$$

The T_0-dependence of the unreacted fuel fraction at the exit $\omega(1)$ is thus much stronger (for reasonable values of E_{ac}) for kinetics-limited than for mass-transport-limited operation.

The subject data for HC (hydrocarbon) and CO oxidation are plotted in such ways as to lead to linear graphs if the data were to represent mass-transport limitation according to equation (16) in Fig. 7 or kinetics limitation according to equation (15) in Fig. 8 and 9. The experimental data for different monolith geometries were corrected, before plotting, according to length and hydraulic diameter dependences implied by the equations.

Fig. 7 shows that, for most catalysts, the T_0-dependence of $-\ln \omega(1)$ is much too high to be consistent with a mass-transport limited op-

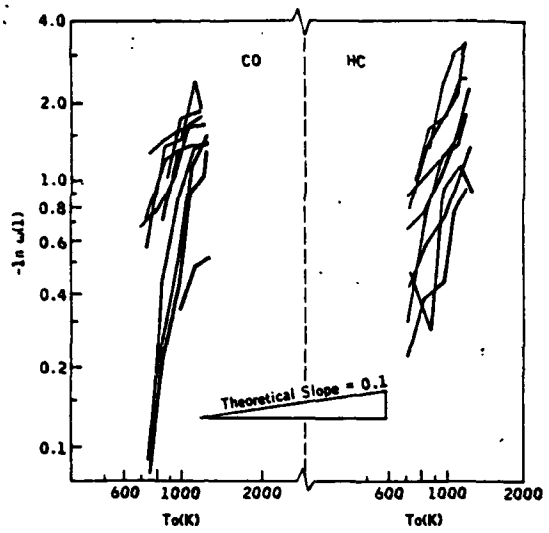

Fig. 7 Test plots for transport limited regime for various monolith catalysts, CO and HC

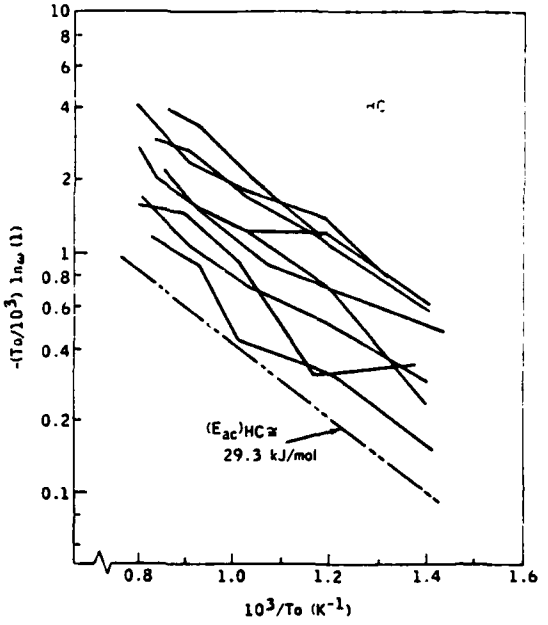

Fig. 9 Test plot for kinetically limited regime for various monolith catalyst, HC

eration. For CO, the values $-\ln \omega(1)$ for these catalysts, however, show a decreasing T_0-dependence at high T_0, suggesting the onset of the mass-transport limited regime, and thus the experimental values of $-\ln \omega(1)$ should nearly equal J_D. The indicated range of J_D values (1.5–1.9) is very close to that calculated for a CO-air mixture at 1200 K and 303 kPa. In contrast, the values of $-\ln \omega(1)$ for the HC conversion data do not, for any catalyst, achieve low enough temperature sensitivity to indicate mass-transport-limited operation.

Examination of the test plot for kinetic limitation of CO oxidation, Fig. 8, shows reasonably consistent linear trends especially for $10^3/T_0$ between 1.0 and 1.4. Interpreting the slope of the visually fitted line, one obtains $(E_{ac})_{CO} \cong 50.2$ kJ/mol. This value is very close to that given by Hawthorn (6) for alumina-based noble metal catalysts. For higher temperatures ($0.8 \leq 10^3/T_0 \leq 1.0$), the graphs appear to be flattening out, i.e., tending toward positive slope as would be expected for the onset of mass-transport domination.

For the HC data presented in Fig. 9, the linear trend is exhibited throughout the entire temperature range. This result is consistent with the previous observation that the HC conversion did not appear to be mass-transport limited. The slope of the line indicated in the figure gives $(E_{ac})_{HC} \cong 29.3$ kJ/mol. This value is well below the range 48–60 kJ/mol suggested by Hawthorn. However, given the range of values reported for $(E_{ac})_{HC}$ in the literature and the intrinsic uncertainties in modeling a hybrid system, e.g., the presence of significant amounts of CO_2 and H_2O and the absence of knowledge of the specific fuel species present in the feed to the catalytic reactor, this variance would not appear significant. The assumption of no contribution from homogeneous combustion was supported by the experimental observation that, even at the highest operating temperatures, no conversion was obtained in the reactor section in the absence of a catalyst. That the hybrid combustor appears kinetically limited for HC oxidation at higher temperatures than would be expected from work with automotive afterburners and "pure" catalytic combustors is most likely due to the considerably higher gas velocities involved. It is somewhat surprising that CO oxidation appears to be tending to mass-transport limitation at temperatures at which the HC oxidation is not showing this trend. Further modeling effort is planned to provide a fuller understanding of hybrid combustor operation.

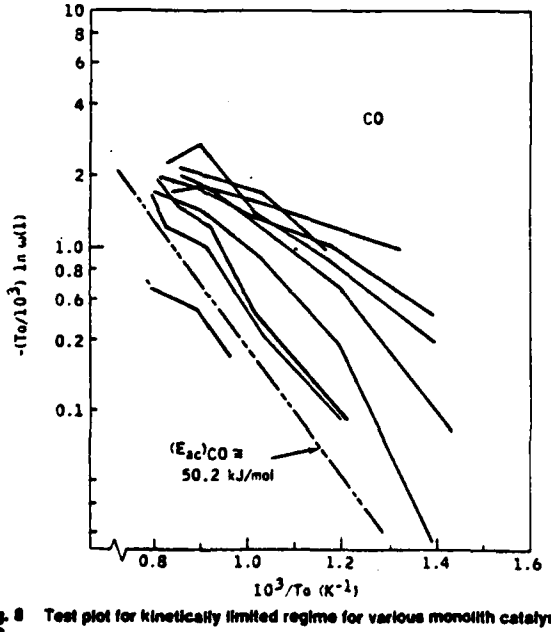

Fig. 8 Test plot for kinetically limited regime for various monolith catalysts, CO

Summary/Conclusions

- A variable-order finite-difference method was employed to solve the two-point boundary value problem which constitutes the model. The approach successfully overcame the nonlinearity, stiffness, and partial instabilities encountered.
- Homogeneous combustion must be considered in any general model which attempts to describe catalytic combustor operation. Under certain conditions, homogeneous combustion is supported or "bootstrapped" by the heat released from catalytic combustion.
- Comparisons of catalytic combustor data and model predictions show excellent agreement. When the model is used to examine conversion as a function of gas inlet temperature for typical lean operating

conditions with a noble-metal catalyst, a sharp catalytic light-off temperature is predicted, as is a light-off/extinction hysteresis. At higher temperatures the onset of gas-phase combustion occurs, resulting in further increased conversion, which rapidly approaches 100 percent.

- Data from a hybrid combustor are reasonably consistent with a simplified analysis of catalytic combustion, neglecting homogeneous contribution. Over the temperature range investigated, CO oxidation tends from surface kinetics limitation with $(E_{ac})_{CO} \cong 50.2$ kJ/mol toward mass transport limitation. Hydrocarbon conversion data, however, exhibit kinetically limited behavior throughout the temperature range with $(E_{ac})_{HC} \cong 29.3$ kJ/mol.

References

1 Stevens, J. G., and Ziegler, E. N., "Effect of Momentum Transport on Conversion in Adiabatic Tubular Reactors," to appear in the *Journal of Chemical Engineering Science*, Vol. 32, No. 4, 1977, pp. 385–391.

2 Margolis, L. Ya., "Catalytic Oxidation of Hydrocarbons," *Advances in Catalysis*, Vol. 14, Academic Press, 1963, pp. 429–501.

3 Lentini, M., and Pereyra, V., "A Variable Order Finite Difference Method for Nonlinear Multipoint Boundary Value Problems," *Mathematics of Computation*, Vol. 28, No. 128, Oct. 1974, pp. 981–1003.

4 Young, L. C., and Finlayson, B. A., "Mathematical Models of the Monolith Catalytic Converter: Part II. Application to Automobile Exhaust," *AIChE Journal*, Vol. 22, No. 2, Mar. 1976, pp. 343–353.

5 Siminski, V., and Shaw, H., "Development of a Hybrid Combustor," ASME Paper No. 77-GT-84.

6 Hawthorn, R. D., "Afterburner Catalysts—Effects of Heat and Mass Transfer Between Gas and Catalyst Surface," *AIChE Symposium Series No. 137*, Vol. 70, 1974, pp. 428–438.

7 Satterfield, C. N., *Mass Transfer in Heterogeneous Catalysis*, MIT Press, Cambridge, Mass., 1970, pp. 79–83.

8 Votruba, J., et al., "Heat and Mass Transfer in Honeycomb Catalysts-II," *Journal of Chemical Engineering Science*, Vol. 30, 1975, pp. 201–206.

9 Longwell, J. P., and Weiss, M. A., "High Temperature Reaction Rates in Hydrocarbon Combustion," *Industrial Engineering Chemistry*, Vol. 47, No. 8, Aug. 1955, pp. 1634–1643.

10 Kuo, J. C. W., Morgan, C. R., and Lassen, H. G., "Mathematical Modeling of CO and HC Catalytic Converter Systems," *SAE Transactions*, Vol. 80, Paper No. 710289, 1971.

11 Pfefferle, W. C., et al., "Catathermal Combustion: A New Process for Low-Emissions Fuel Conversion," ASME Paper No. 75-WA/Fu-1.

12 Hlavacek, V., and Votruba, J., "Experimental Study of Multiple Steady States in Adiabatic Catalytic Systems," *Chemical Reaction Engineering II*, American Chemical Society, Washington, 1974, pp. 545–558.

APPENDIX IV

Catalytic Flame Holding Model

Douglas Cornell
Fairleigh Dickinson University

A first model of the aerothermochemistry associated with catalytic flameholder devices is developed. This work was performed as part of an NSF summer research participation project and is being included here because it was not published in the open literature.

CATALYTIC FLAME HOLDING MODEL

The catalytic flame holder whose properties are modeled in this report consists of a honeycomb support, the surface of which is coated with a catalyst which can promote the oxidation of hydrocarbon fuels. Its properties are investigated with respect to use in a jet engine afterburner. The development of the model is influenced by the finding of Zukowski and Marble[1], that with a conventional flame holding device a critical time for ignition can be determined (L/V_{bo}) where L is the length of a recirculation zone behind the bluff body and V_{bo} is the blow off velocity. A parcel of combustible gas mixture must be ignited in less time than is required to pass by the recirculation region. This ignition time is independent of flame holder size or geometry. The experimental facts concerning the recirculation region are as follows:

1) The length of the wake region is proportional to the diameter of a cone shaped flame holder and is proportional to the square root of diameter of a cylindrical flame holder.[1]
2) The temperature behind the flame holder is uniform and is about 90% of the adiabatic flame temperature.
3) The region is not well stirred.[2]
4) The residence time of the gas in the recirculation zone is much longer than the time required for gas flow past the recirculation zone.[3]

---

[1] Edward E. Zukowski and Frank E. Marble, Proceedings Aerothermochemistry Gas Dynamics Symposium (1955), p. 265.

[2] A. A. Westenberg, W. G. Berl, and J. L. Rice, ibid, p. 211.

[3] T. A. Bovina, Seventh Symposium (International) on Combustion, Butterworths, London, p. 692.

AD-A148 758 RADIATION/CATALYTIC AUGMENTED COMBUSTION(U) EXXON 2/2
RESEARCH AND ENGINEERING CO LINDEN NJ CORPORATE RESEARC
.. A E CERKANOWICZ ET AL. MAY 84 AFOSR-TR-84-1129
UNCLASSIFIED F49620-81-C-0028 F/G 21/5 NL

END
FILMED
DTIC

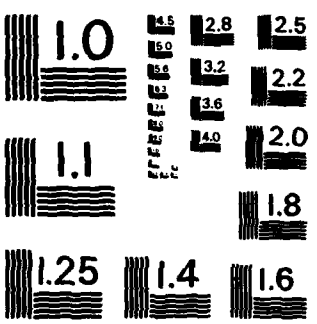

MICROCOPY RESOLUTION TEST CHART
NATIONAL BUREAU OF STANDARDS - 1963 - A

This report proceeds to:

a) determine the flow split of the fuel, air mixture through and around the catalytic monolith.

b) using the results of calculations by A. E. Cerkanowicz[4] for reaction in the catalytic monolith, determine from the predicted flow into the recirculation region whether or not stable ignition and/or flame holding will occur.

c) program these calculations for a digital computer so that the operating characteristics of the flame holder can be readily determined as a function of experimentally adjustable parameters.

Flow Split

The flow split is determined on the basis that pressure drop for the flow around the catalytic monolith is the same as for the flow through the catalytic monolith. In other words, no radial pressure gradients exist in the afterburner. The flow around the flame holder is calculated from Bernoulli's equation for the change in pressure resulting from a change in area of the flow path.

$$(1) \quad P_1 - P_2 = (\rho/2)(Q/A_2)^2[1-(A_2/A_1)^2]$$

where Q is the volume flow rate and A_1 and A_2 are the areas of the duct. The pressure loss due to friction has been evaluated and found to be only about 1% of that due to change in area. The general equation for pressure drop in a duct where chemical reaction and friction losses are occurring is[5]

---

[4] Exxon Report No. 7514 955.

[5] Ascher H. Shapiro, "The Dynamics and Thermodynamics of Compressible Fluid Flow" VI, Ronald Press Co., N.Y. (1953).

(2) $dP/P = [kM^2/(1-M^2)][-(1/C_pT)dh_r-(1+(k-1)M^2)(2f/D)dx + (1/W)dw]$

where k = Cp/Cv, M is the mach number, f the friction coefficient, D the hydrodynamic diameter = 4A/(dAw/dx) and W the molecular weight. The existing Exxon catalytic reactor model uses a simpler form in which $(k-1)M^2$ and dW are considered negligibly small and are not included.

Equations have been developed by Cerkanowicz[4] which allow the evaluation of the pressure drop through the catalyst tubes under conditions where the reaction rate at the catalyst is much larger than the transport rate to the surface and where the Pecklet number is large (>100). The fuel conversion (W) is first evaluated for no pressure loss and is subsequently corrected for pressure drop.

(3) const. $P\ (1+B)\ln w + B(1-w) = -J_D$

(4) $P = (1+A_1)P_o$

(5) $A_1 = -(J_f/J_c)[1+B(1-w)]$

(6) $(1+B)\ln w + B(1-w) = -J_D(1+A_1/2)$

The definitions of the symbols and their values are given in the Appendix. The computer program calculates W from (3) using the Wegstein method, calculated A_1 from (5) and again calculates W from (6). Equations (5) and (6) are solved cyclically until no further change in W and A_1.

The computer program is provided with an initial estimate of the fraction of flow around the catalytic flame holder. It then compares the calculated pressure drops for flow through and around the catalytic monolith and increments the fraction of flow around the flame holder until equal pressure drops are attained by equations (1) and (4).

Flame Holding

Because the velocity of the gas flowing around the catalytic flame holder is greater than that of the exit gas from the flame holder, it is supposed that entrainment will cause a recirculation zone to exist as in the case of the bluff body. This recirculation zone may, however, be longer than in the case of a bluff body (see below). It is assumed that the flame develops at a distance Xi from the catalyst as shown in Figure 1.

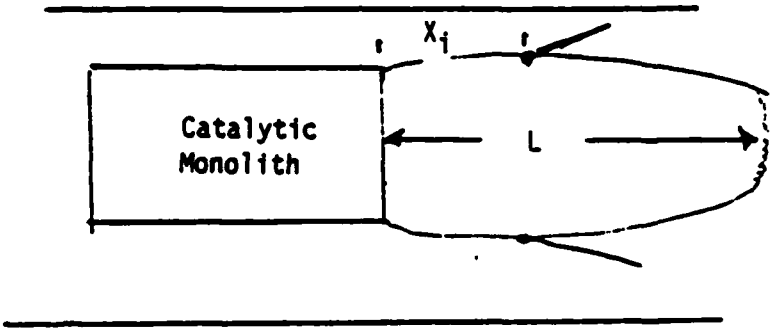

FIGURE 1

Xi is supposed equal to the product of a mean convective velocity and reaction time as in the analysis of Kundu[6], et al.

(7) $X_i = (U_o/2)(\rho_o/W_T)$

The reaction rate which appears in (7) is evaluated at the original concentration and at recirculation zone temperature. Wt is estimated from the relationship between reaction rate and laminar flame propagation velocity.

(8) $S_L = (k_o W_L/Cp_o)^{0.5}/\rho_o$

We therefore obtain

(9) $X_i = (U_o k_o/2\rho_o Cp_o S_L^2)[\exp(E/RT_R)/\exp(E/RT_f)]$

---

[6] Kundu, K. M., Banerjee, D., and Bhaduri, D., Combustion Science and Technology 17, 153 (1977).

The ratio of exponentials occurs because the ignition source for laminar flame propagation is at flame temperature whereas the ignition source for the flame holder is at recirculation temperature. The temperature of the recirculation zone must be obtained from a heat balance equation for the recirculation zone.

The flow rate into the recirculation zone from the catalyst is $\dot{M}$ and from the turbulent transport through the recirculation zone boundary is $\dot{M}_1$ per unit length. It is assumed that the mass of gas entering the recirculation zone at temperature T from the catalyst leaves the recirculation zone at the temperature Tr.

Heat entering = $\dot{M}$ Cp T + $\dot{M}_1$ (CpTf - CpTr)(L - Xi)

Heat leaving = $\dot{M}$ Cp Tr + $\dot{M}_1$ (CpTr - CpTo)(Xi)

(10) $\dot{M}C_pT + \dot{M}_1(C_pT_f - C_pT_R)(L-X_i) = \dot{M}C_pT_R + \dot{M}_1(C_pT_R - C_pT_o)(X_i)$

The value of $\dot{M}_1$ can be evaluated from the measured recirculation zone residence times for bluff bodies.[3]

(11) $tr = KD/U_o$ where $K \approx 104$

(12) $L\dot{M}_1 = \frac{\rho \text{ (volume of recirculation zone)}}{tr} \approx \frac{\rho[\pi(D/2)^2][L]U_o}{104\ D}$

On a per unit length basis we obtain

(13) $\dot{M}_1 = \rho\pi D^2 U_o/132.5$

The recirculation zone length (L) is estimated from the work of Landis and Shapiro[7] and Forstall and Shapiro[8], who investigated the turbulent mixing of concentric jets of gas.

---

[7] F. Landis and A. H. Shapiro, Proc. Heat Transfer and Fluid Mech. Inst., Stanford U. Press (1951).

[8] W. Forstall and A. H. Shapiro, J. of Applied Mechanics (1950), p. 381.

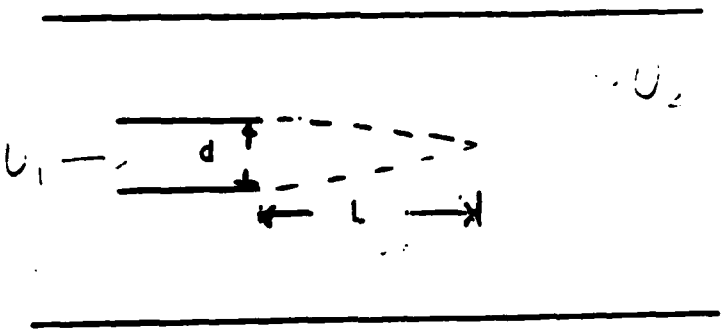

FIGURE 2

L is the length over which the inner jet velocity (U_1) remains unchanged when flowing into a concentric jet at velocity (U_2). They found

(14) $L = 4d(1+3U_2/U_1)$

This is taken to be the recirculation zone length in this model. For the velocities typical of the flame holder, L may be approximately double that for a bluff body.

The computer program solves equations (9) and (10) simultaneously using Tf as the initial estimate for Tr. Xi is first calculated from (9) and then Tr is calculated from (10). The new value of Tr from (10) is then used to recalculate Xi from (9). The cycle repeats until successive calculations of Tr are within a prescribed limit. It is important to approach Tr from the high side as otherwise a converging solution might not be obtained.

Ignition is assumed to take place if Xi calculated from (9) using the catalyst stream exit temperature is less than L. If Xi(T) is greater than L but Xi(Tr) is less than L, a stable flame is possible but may require ignition. If Xi(Tr) is greater than L, blow off occurs.

A listing of the computer program is attached together with the results of some typical calculations. The evaluation of parameters required as input is discussed in the Appendix.

Results of Calculations

Typical jet engine afterburner inlet conditions are T = 950°K

Uo = 130 m/sec

The values given are in mks units.

Table 1. Variation of TD

TL = .25 To = 950° Uo = 130 m/sec D2 = .27 D1 = .40

TD	ΔP/P	G	W	XI	RL
.002	.0712	.995			
.003	.0692	.985	0	.0792	1.259
.004	.0672	.975			
.005	.0633	.960	.00011	.1765	1.57
.007	.0557	.92	.058	.256	2.07
.009	Blow Out				

Table 2. Variation of TL

TD = .007 To = 950° Uo = 130 D2 = .27 D1 = .40

TL	ΔP/P	G	W	XI	RL
.25	.0557	.92	.058	.256	2.07
.20	.0557	.92	.090	.295	2.05
.15	.0484	.88	.23	.637	2.47
.10	Blow Out				

Table 3. Variation of Blockage Ratio

To = 950° Uo = 130 TD = .007 TL = .25 D1 = .40

D2	ΔP/P	G	W	XI	RL
.27	.0557	.92	.058	.256	2.07
.30	.0859	.86	.113	.4533	2.49
.33	.1311	.74	.203	1.11	3.07
.36	Blow Out				

Table 4. Variation of Inlet Temperature

TD = .007 Uo = 130 TL = .25 D2 = .27

T	ΔP/P	G	W	XI	RL
950	.0557	.92	.058	.256	2.07
925	.0572	.92	.063	.331	2.06
900	.0588	.92	.069	.4439	2.06
875	Blow Out				

Table 5. Variation of Velocity

To = 950 TD = .007 TL = .250 D1 = .40 D2 = .27

Uo	ΔP/P	G	W	XI	RL
70	.0178	.95	.00085	.0828	1.70
100	.0352	.94	.01186	.13	1.82
130	.0557	.92	.058	.256	2.07
160	.0816	.91	.109	.426	2.17
190	Blow Off .111	.91	.16	5.96	2.26

Calibration of Model with Experimental Data

The parameter used in this model whose estimated value is in greatest error is probably the laminar flame speed (S_L). Values of S_L have apparently not been measured at the high temperatures (950°) characteristic of afterburner inlets. A convenient calibration can be accomplished using an experimental value for blow off velocity. S_L can be adjusted so as to make XI = RL at the experimental blow off velocity and with Tr = T (of catalyst flow).

Conclusions

The blow off condition is approached rather explosively for the variation of any of the experimental parameters. This is because an increase in XI reduces the temperature of the recirculation region which would in turn require a larger XI for ignition.

The optimum flame holder geometry cannot be reliably determined until calibration of the model with experimental data has been carried out. For preliminary design, TD = .007 m, TL = .25 m appears favorable.

A comparison of flame holder drag with bluff body drag for the same blockage may be made for a typical geometry which provides adequate flame holding. For TD = .007, TL = .25, D1 = .40, D2 = .27 we note that 8% of the flow goes through the catalyst. Using the equation for dP1 with g = .92 shows that a 22% decrease in pressure drop as compared with bluff body (g = 1) results.

Appendix

Program: CATRE

```
C     INLET CONDITIONS (ANY UNITS FOR WHICH F = MA)
      P (PRESSURE), TO (TEMPERATURE), VO (VELOCITY), TD (TUBE DIAMETER),
      TL (TUBE LENGTH), EQ (EQUIVALENCE RATIO), R (GAS CONSTANT),
      WM (MOLECULAR WEIGHT), H (HEAT OF COMBUSTION PER UNIT MASS),
      CPM (MEAN HEAT CAPACITY PER UNIT MASS), CP (HEAT CAPACITY FOR FLAME),
      CPO (HEAT CAPACITY INLET), D1 (DUCT DIAMETER), D2 (MONOLITH DIAMETER),
      Z (FRACTIONAL OPEN AREA OF MONOLITH), TF (FLAME TEMPERATURE),
      G (FRACTIONAL FLOW SPLIT), DG (INCREMENT IN FLOW SPLIT),
      Q (UNITS CONVERSION FACTOR FOR VELOCITY = 1.0 FOR MKS)
```

$J_f = 32(TL)/(TD)(Rey)$

Laminar flow occurs in the catalyst tubes.

$J_D = (17.03)(TL/TD)(1+(.067)(TD/TL)(Rey))^{.45}/Rey$

$B = (FO)H/(1+FO)(CPM)(Tmean)$

CPM is mean heat capacity.

The laminar flame speed for hydrocarbons with more than 3 carbons is independent of the number of carbons. It is not especially sensitive to pressure. S_L for an equivalence ratio of 1.0 was calculated from an empirical equation of Dugger and Simon[9]; $S = 10 + 3.42 \times 10^{-4} To^2$ cm/sec for temperatures up to 615°K. The dependence on ϕ was determined by supposing that $U = Uo + a (\phi - 1.0)^2$.

The value of a was determined by fitting data of Spalding[10] for propane.

Ko - Thermal Conductivity

Ko = (2.5)(viscosity)(Cv) from kinetic theory

[9] Gordon L. Dugger and Dorothy M. Simon, 4th Symposium on Combustion, p. 336.

[10] D. B. Spalding, "Some Fundamentals of Combustion," Butterworths (1955), p. 164.

```
0.111 0.113 0.1637310
0.0486
0.4779
0.7421
0.9945
1.3384
2.0680
5.9688
TO=  950. H= 0.431E+08 CPM= 0.124E+04 CPO= 0.116E+04 Z= 0.750
TF=2976. CV= 0.864E+03 P= 0.233E+05
UO= 190.0 TD=0.007 TL= 0.250 EQ= 1.0000
D1=0.400 D2=0.270 G=.900 DG=.010
BLOW OUT
XI=5.9688 RL=2.2657 TR=  1739.1 G=.900 FRAC P LOSS=.1111

08.35.20 >e catre fortran
EDIT:
>p 200
      READ(5,*) R,S,UM,H,CPM,CP,CPO,Z,CV,E,Q
2      READ(5,*,END=150) P,TO,UO,TD,TL,EQ,D1,D2,G,DG
      A0=3.14*(D1/2.)**2
      A1=3.14*(D2/2.)**2
      A=Z*A1
      A2=A0-A1
      D=P*UM/(R*TO)
      VIS=SQRT(R*TO*UM/3.14)/(6.0E23*S)
      TC=2.5*VIS*CV
      FR=D*UO*A0
      J=0
3     FRA=G*FR
      FRT=(1.-G)*FR
      UTO=FRT/(D*A)
      REY=D*TD*UTO/VIS
      P1=P-(FRA**2/(2.*D*A2**2))*(1.-(A2/(G*A0))**2)
      DP1=(P-P1)/P
      CF=2.*TL*16./(TD*REY)
      CE=P/(D*UTO**2)
      F0=.0583*EQ
      CD=17.03*(TL/TD)*(1.+.067*(TD/TL)*REY)**.45/REY
      B=F0*H/((1.+F0)*CPM*1500.)
      U=.1
      NC=1
      M=1
5     XU=EXP((B*U-CD-B)/(1.+B))
      PRINT 112,M,XU
      M=M+1
      CALL CONV(U,XU,1,NC)
      GO TO(6,5),NC
6     A4=-(CF/CE)*(1.+B*(1.-U))
      U1=U
      K=100
```

```
      K=100
7     XW1=EXP((B*W1-CD-A472.-B)/(1.+B))
      PRINT 112,K
      K=K+1
      CALL CONV(W1,XW1,2,NC)
      GO TO (8,7),NC
8     P2=(1.-(CF/CE)*(1.+B*(1.-W1)))*P
      DP2=(P-P2)/P
      PRINT 113,DP1,DP2,XW1
      IF(ABS(DP1-DP2).LT..01) GO TO 11
      IF(DP1.LT.DP2) GO TO 9
      IF(J.EQ.1) GO TO 10
      G=G-DG
       GO TO 3
9     J=1
      G=G+DG
      GO TO 3
10    G=G-DG/2
11    T=TO*(1.+B*(1.-W1))
      UA=G*A0*UO/A2
      UT=(T/TO)*(1.-G)*UO*A0/A
      IF(EQ.GT.1.0) GO TO 12
      TF=TO+H*FO/CPH
      GO TO 13
12    TF=TO+H*FO*(2.-EQ)/CPH
13       Y1=1.+3.*UT/UA
      RL=Y1*4.*D2
      SL0=(.10+.342E-5*TO**2)*Q
      SL1=SL0*(1.0-2.625*(EQ-1.0)**2)
      EXCR=D*D2*UO/132.5
      TR=TF
14    XI=(UA*TC/(2.*D*CP0*SL1**2))*EXP(E/(R*TR))/EXP(E/(R*TF))
      PRINT 100,XI
      IF(XI.GT.RL) GO TO 16
      TRC=(EXCR*(CP*TO*XI+CP*TF*(RL-XI))+FRT*CP*T)/(FRT*CP+EXCR*CP*RL)
      IF(ABS(TRC-TR).LT.50.) GO TO 15
      TR=TRC
      GO TO 14
15    XI1=(UA*TC/(2.*D*CP0*SL1**2))*EXP(E/(R*T))/EXP(E/(R*TF))
16          PRINT 105,TO,H,CPH,CP0,Z
      PRINT 106,TF,CV,P,T
      PRINT 107,UO,TD,TL,EQ
      PRINT 108,D1,D2,G,DG
          IF(XI.LT.RL.AND.XI1.GT.RL) GO TO 18
      IF(XI.LT.RL.AND.XI1.LT.RL) GO TO 17
      PRINT 110
      GO TO 20
112   FORMAT(1X,I5,1X,F9.7)
100   FORMAT(1X,F6.4)
17    PRINT 120
      GO TO 20
18        PRINT 130
```

```
C        FORMAT 130
20     PRINT 140,XI,RL,TR,G,DP1
       GO TO 2
110    FORMAT(1X,'BLOW OUT')
120    FORMAT(1X,'FLAME WITHOUT IGNITION')
130    FORMAT(1X,'FLAME REQUIRES IGNITION')
140    FORMAT(1X,'XI=',F6.4,1X,'RL=',F6.4,1X,'TR=',F8.1,1X,'G=',F4.3,1X,'
      1FRAC P LOSS=',F5.4)
113    FORMAT(1X,F5.3,1X,F5.3,1X,F9.7)
105    FORMAT(1X,'TO=',F6.0,1X,'H=',E10.3,1X,'CPH=',E10.3,
      11X,'CPO=',E10.3,1X,'Z=',F6.3)
106    FORMAT(1X,'TF=',F5.0,1X,'CV=',E10.3,1X,'P=',E10.3)
107    FORMAT('UO=',F6.1,1X,'TD=',F5.3,1X,'TL=',F6.3,1X,'EQ=F7.4)
108    FORMAT(1X,'D1=',F5.3,1X,'D2=',F5.3,1X,'G=',F4.3,1X,'DG=',F4.3)
150    STOP
       END
       SUBROUTINE CONV(X,Y,NR,NC)
       DIMENSION XA(10),YA(10)
       IF(ABS(X-Y).LT..01) GO TO 6
       IF(NC.LE.1) GO TO 5
       XT=(XA(NR)*Y-YA(NR)*X)/(XA(NR)-X+Y-YA(NR))
       XA(NR)=X
       YA(NR)=Y
       X=XT
       RETURN
5      XA(NR)=X
       YA(NR)=Y
       X=Y
       NC=2
       RETURN
6      X=Y
       NC=1
       RETURN
       END
EOF:
>
EDIT:
>q

08.38.18 >log
10.28 ARU'S, .21 CONNECT HRS
LOGGED OFF AT 08.38.27 ON  09AUG79
■
```

END

FILMED

1-85

DTIC